AUS DEM LEHRSTUHL
FÜR HUMANGENETIK
PROF. DR. BERNHARD WEBER
DER FAKULTÄT FÜR MEDIZIN
DER UNIVERSITÄT REGENSBURG

CIRCULATING MICRORNA EXPRESSION IN TWO MURINE MODELS OF RETINAL NEOVASCULARIZATION

Inaugural-Dissertation
zur Erlangung des Doktorgrades
der Medizin

der
Fakultät für Medizin
der Universität Regensburg

vorgelegt von
Patricia Berber

2021

Dean:	Prof. Dr. Dirk Hellwig
1. Rapporteur:	Prof. Dr. Bernhard Weber
2. Rapporteur:	Prof. Dr. Gunter Meister
Date of the Oral Exam:	22.06.2021

Table of Contents

0. Foreword

"I think education is a process of self-discovery. When we self-segregate, schools become a reflection of our homogeneity, and an instrument of division. I think of education as a great mechanism of connecting and equalizing."

- Tara Westover in a conversation with Bill Gates

The following text was written with the intention of making the information accessible to persons of many educational backgrounds. While the subject of this work is highly complex, this complexity should not hinder those who wish to understand its meaning. It is my belief that access to an education should not be restricted to an elite minority, but be available to all those who wish to learn about something new and exciting.

1. Introduction

1.1. The Retina

In his seminal book “On the Origin of Species by Means of Natural Selection”, Charles Darwin referred to the eye as an “organ of extreme perfection and complication” (1). Darwin was correct in his assessment that the eye is highly complex, but it is not always perfect. According to a recent systematic review, approximately 67 million Europeans are currently affected by a retinal disorder known as age-related macular degeneration (AMD), and this number is expected to increase to 77 million by 2050 (2). AMD is a complex neurodegenerative eye disease that is characterized by progressive and incurable vision loss and underlies a genetic and environmental predisposition.

In a healthy eye, light is registered and transduced to an electric signal by the retina. The retina is a member of the central nervous system and contains five main types of neurons (from inside to outside): ganglion cells, amacrine cells, bipolar cells, horizontal cells, and photoreceptors. Photoreceptors are highly specialized, postmitotic neurons that consist of a permanent inner segment and a renewable outer segment. Phototransduction, i.e. the transformation of a light signal into an electric impulse, takes place in the outer segments. Humans possess two morphologically and functionally distinct types of photoreceptors, called rods and cones. Cone photoreceptors are imperative for high acuity vision and the perception of color, while rod photoreceptors enable sight at low light levels. Photoreceptors have a unique and specialized support system consisting of the retinal pigment epithelium (RPE), Bruch’s membrane, and the choroidal vasculature (Fig. 1 A, B). The latter supplies the RPE and the photoreceptors with nutrients and oxygen through small, fenestrated capillaries. These blood vessels are separated from the RPE cells by the Bruch’s membrane, a five-layered extracellular matrix of collagen and elastin. The Bruch’s membrane is acellular, so the transport of compounds across the membrane occurs primarily via passive diffusion (3). On the inner side of the membrane, the RPE form a monolayer of pigmented and polarized cells, which shuttle energy sources and waste products between the photoreceptors and the choroidal vasculature. They are equipped with finger-like processes, which envelop the photoreceptor outer segments through which the RPE phagocytize shed photoreceptor outer segments. Importantly, the RPE contain the biochemical machinery required to recycle the photopigments needed for phototransduction.

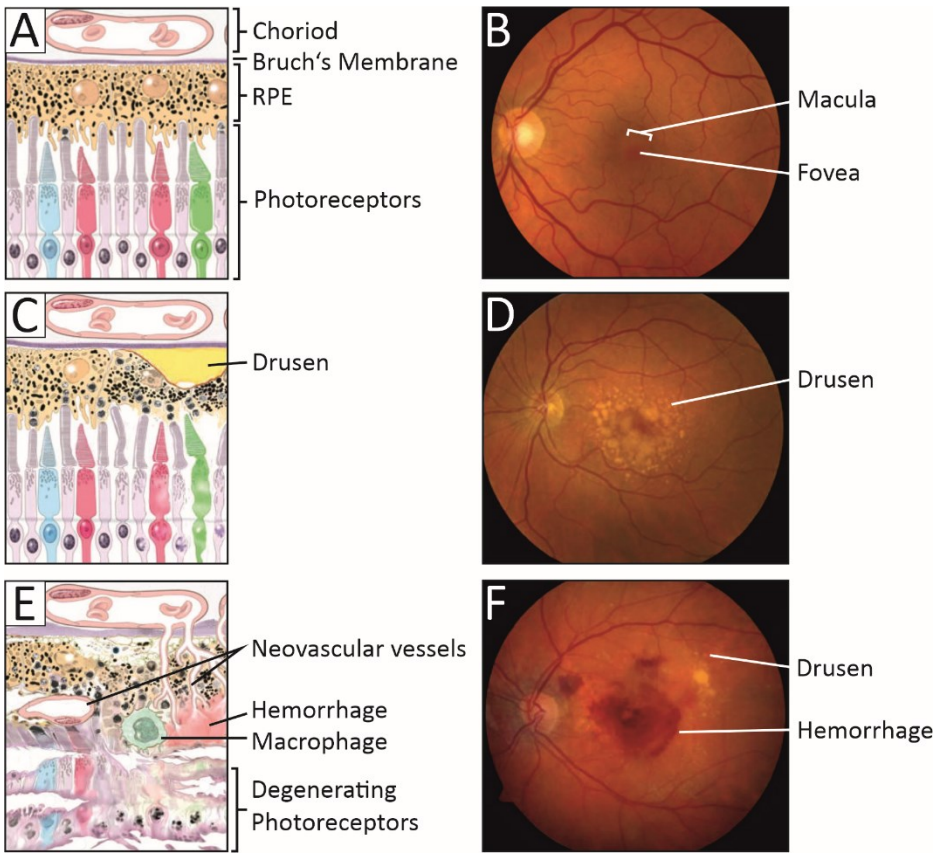

Figure 1: Schematic representation and funduscopic photographs of a healthy retina vs. early AMD and neovascular AMD (nAMD). (A) The retinal layers in a healthy retina. In a healthy retina, the choroidal vasculature is separated from the RPE by the Bruch's membrane. Protrusions from the RPE cells envelop the photoreceptor outer segments. Rod photoreceptors are shown in grey, and cone photoreceptors are shown in blue, red and green. (B) A fundus photograph of a healthy eye, in which the macula and fovea are in good condition. (C) In early AMD, drusen develop between the basolaminar layer of the RPE and the Bruch's membrane. (D) Drusen can be visualized in a funduscopy. (E) In nAMD, the structural integrity of the retina is severely compromised. In a neovascular herd, juvenile blood vessels infiltrate the neural retina, and leak serous fluid and blood into the neural tissue. This is accompanied by the infiltration of inflammatory cells, including macrophages. Over time, the exposed RPE cells atrophy. (F) Severe macular hemorrhages, accompanied by drusen can be observed in a funduscopic photograph. Images adapted from (4,5).

The previously described structures also fulfill a second purpose by forming the blood-retinal barrier. In humans, the central nervous system is separated from the blood stream by a barrier, which protects the neurons from exposure to pathogens, without disturbing the cells' supply of nutrients. In the retina, this barrier is formed by 3 entities: tight junctions between the RPE, the Bruch's membrane, and tight junctions between the choroidal endothelial cells. This sophisticated system allows the diffusion of oxygen and glucose to the retina, while prohibiting the flux of larger particles. Pathologic developments which damage this barrier, obliterate a system which is imperative for a healthy retina.

1.2. Age-Related Macular Degeneration (AMD)

AMD is a complex neurodegenerative disease of the central retina, and is the third leading cause of moderate or severe vision impairment worldwide, after uncorrected refractive error and cataract (6). Although the vision loss caused by AMD is severe and debilitating, the disease progression in its early stages is slow, and usually begins with a fairly mild presentation. Early AMD is characterized by the formation of drusen in the space between the basal lamina of the RPE and the inner collagenous layer of the Bruch's membrane (Fig. 1C, D), and an abnormal RPE pigment distribution in the macula lutea (macula) (5). The macula is an area of the retina which is exclusive to cone photoreceptors, and is capable of high-resolution vision. In a funduscopy, the macula can be visualized, as a yellowish area in the posterior eye (Fig. 1B). The identification of retinal drusen in a funduscopy, is an important diagnostic tool to detect early AMD, although similar structures can result from aging (7). Drusen contain a large portion of lipids (> 40 % of volume) and a variety of proteins including vitronectin, β-amyloid, apolipoproteins, and immune related proteins, specifically from complement cascade as an essential part of the innate immunity (8–10). Early AMD is usually asymptomatic, but may cause a modest decline in visual acuity, resulting in delayed dark adaptation (5).

Early AMD can progress to late-stage AMD, which can be categorized into neovascular AMD (nAMD) and geographic atrophy AMD (gaAMD). The histopathological correlate of gaAMD is RPE atrophy, followed by the degeneration of adjacent photoreceptors (11). Disease progression in gaAMD is usually slow and the visual decline can be relatively minor. However, most cases result in significant visual deficits in reading, night vision, and dark adaptation (12,13). There is currently no approved treatment to prevent the onset or progression of gaAMD (14,15).

The hallmarks of nAMD are retinal inflammation and neovascularization, which usually originates from the choroidal vasculature (16). During choroidal neovascularization (CNV), immature blood vessels infiltrate the subretinal pigment epithelial space and/or the subretinal space, thereby dismantling the blood retinal-barrier (Fig. 1E, F) (17). Rarely, the neovascularization originates from the retinal vascular system, leading to the formation of retinal–choroidal anastomoses (18). In nAMD, the angiogenic vessels are fragile, and leak serous fluid into the neural retina (17). The neovascularization is accompanied by the invasion of inflammatory cells, such as macrophages, which produce proinflammatory and proangiogenic factors (19). The ocular wound-response eventually triggers the shift to an anti-angiogenic state, and the neovascular lesion can become fibrosed, ultimately forming a retinal

scar (17). nAMD patients experience a consistent, steady deterioration in visual acuity over the first few years following CNV onset, with 75% of patients becoming legally blind within 3 years (20).

nAMD can be treated but not cured with inhibitors of a pro-angiogenic factor called vascular endothelial growth factor (VEGF) (reviewed in (21)). VEGF-induced angiogenesis is triggered by hypoxia. When the oxygen demand of a tissue exceeds its supply, increased VEGF expression induces the growth of new blood vessels (22,23). These vessels facilitate blood flow to the tissue, thereby equalizing oxygen supply and demand. VEGF-induced angiogenesis is a critical part of numerous pathologic conditions, such as tumor growth and nAMD development. During the transition from early AMD to nAMD, the RPE cells launch a defensive response against retinal hypoxia, by increasing VEGF expression, resulting in retinal neovascularization (24). The inhibition of VEGF can dramatically reduce CNV formation (25), and is the current standard treatment of nAMD. Although largely effective, monthly injections of VEGF inhibitors are expensive to the health care system and burdensome to patients (26). Additionally, nAMD patients exhibit a great deal of variability in response to anti-VEGF treatments, and some patients even lose visual acuity during treatment (27,28). Whether the visual deterioration is the result of gaAMD that remains once the neovascularization is arrested or a troublesome side effect of the anti-VEGF therapy, is unclear (28).

1.3. AMD Etiology

Although AMD has been studied extensively, the etiology of AMD is complex and to a large part not yet fully understood. The scientific community agrees that the multifactorial etiology is influenced by aging, environmental factors, and genetic predisposition (5,29–32).

At the turn of the 21st century, studies performed in monozygotic twins and first degree siblings validated a genetic component in AMD etiology (33,34). A decade later, a meta-analysis of nine genome-wide linkage studies validated an AMD susceptibility locus on chromosome 10q26 (35). As the efficiency and availability of sequencing technologies improved, researchers were able to perform large-scale genome-wide association studies to further elucidate the genetic AMD risk (36–39). To date, researchers are aware of 52 independent variants in 34 loci which have been significantly linked to AMD, explaining around half of the genomic heritability of the disease (39). The genetic loci which harbor AMD risk variants are enriched in genes involved in the complement pathway, high-density lipoprotein (HDL) transport, and extracellular matrix organization (39).

Beside the genetic risk, the strongest nonmodifiable AMD risk factor is advanced age (31). A meta-analysis of AMD prevalence in Europe by Rudnicka et al., showed that AMD prevalence increases exponentially with age (40). The authors demonstrated that 1.4 % of 70-year-olds have late-stage AMD, which increases to 5.6 % in 80-year-olds, and rises to 20 % at age 90 (40). In industrialized countries, the prevalence of AMD is expected to increase as the overall population ages.

The strongest modifiable AMD risk factor is smoking (reviewed in (30,41)). An association between smoking and AMD was convincingly demonstrated in multiple epidemiological studies from the '90s and early '00s (42–46). More recently, researchers have investigated the risk-altering effect of cigarette smoke in the context of an individuals' genetic background. Interaction analyses between gene and environmental factors, showed that smoking synergistically increased the AMD susceptibility for heterozygotes of certain risk-associated polymorphisms (47–49).

It has been suggested that epigenetic mechanisms may bridge the gap between genetic and environmental AMD risk factors (50,51). 'Epigenetics' describes processes which can alter gene expression, without directly manipulating the genomic sequence (52). One well-known epigenetic mechanism that has been linked to AMD, is DNA methylation. This is a process whereby methyl groups are added to a DNA sequence, thereby generally reducing gene expression. One study, which investigated postmortem RPE/choroid samples from AMD patients found that DNA hypermethylation at the glutathione S-transferase isoform mu1 (*GSTM1)* promoter corresponded to a reduction in the mRNA levels of *GSTM1* and glutathione S-transferase isoform mu5 (*GSTM5)* (29). Furthermore, a genome-wide epigenetic study of nAMD patients found DNA methylation differences near the age-related maculopathy susceptibility 2 (*ARMS2*) locus, which is one of the strongest loci genetically associated with AMD (53). Of note, this effect did not reach genome-wide significance. Other well-known epigenetic mechanisms that have been linked to AMD include histone modification, chromatin remodeling, and microRNA (miRNA) mediated gene silencing (reviewed in (50,54)).

1.4. Animal nAMD Models

Investigations into the etiology and pathogenesis of AMD have been hampered by the inaccessibility of human AMD tissue. Postmortem retinal samples from AMD patients and healthy controls are highly valuable and difficult to acquire. In Germany, the number of postmortem organ donations has fallen from 4,205 organs from 1,296 donors in 2010, to 2,995 organs from 932 donors in 2019 (55). Furthermore, under current German law, the donation of

organs for research purposes requires separate patient consent (56). Many researchers have therefore diverted their research from human post mortem tissue to animal AMD models.

To date, dozens of rodent models have been established which mimic AMD characteristics, with a particular emphasis on recreating the hallmarks of nAMD such as inflammation and neovascularization (reviewed in (57)). In 1998, Tobe et al. debuted a murine model of laser-induced CNV (58), which was refined by Lambert et al. in 2013 (59). In this model, an argon laser is used to perforate the Bruch's membrane, which produces a characteristic ocular response. Three days after mice received the laser treatment, immune cells such as macrophages and neutrophils invade the retina (59). In contrast to the rapid immune response, the angiogenic response is delayed. The neovascular surface area after laser treatment peaks 7 days after treatment, and then gradually decreases (59).

Another reproducible and quantifiable retinal disease model is oxygen-induced retinopathy (OIR) (60–62). Although variations of this model exist, the procedure always includes a hyperoxic and a hypoxic phase. In the standard technique, mouse pups are kept at 75 % oxygen from postnatal day 7 (P7) to P12 (hyperoxic phase). The exposure to hyperoxia inhibits retinal vascular development and obliterates preexisting capillaries (61). After P12 the mice are returned to room air causing the vasoobliterated retina to become hypoxic, which in turn triggers neovascularization (hypoxic phase) (60). The neovascularization peaks at day 17, and resolves around day 25 (61).

Neovascularization after OIR also appears to involve an inflammatory component. Retinopathy was reduced in mice treated with anti-inflammatory medications such as dexamethasone (a corticosteroid) (63), and ibuprofen (a non-steroid anti-inflammatory agent) (64). Furthermore, mice treated with neutralizing antibodies against macrophage inflammatory protein-1α (MIP-1α) and monocyte chemotactic protein-1 (MCP-1) showed an inhibition of retinal neovascularization by 30% (65).

Laser-induced CNV and OIR both mimic the hallmarks of nAMD (inflammation and neovascularization), and have been successfully applied as nAMD models (59,66,67). In a critical advancement, the laser-induced CNV model helped establish the aforementioned anti-VEGF nAMD therapy. In 1992, VEGF emerged as a hypoxia-inducible pro-angiogenic factor (68). In 2000, researches inhibited this factor in the laser-induced CNV model, and observed a dramatic, almost complete inhibition of CNV (25,69). This research eventually led to the approval of anti-VEGF therapeutics as a nAMD treatment (70,71). The effect of VEGF on angiogenesis has also been investigated using the OIR model. Mice treated with an intraocular

injection of a neutralizing antibody against VEGF resulted in a 46 % reduction in the number of nuclei of newly formed vessels (72).

Laser-induced CNV and OIR have been applied as nAMD models because they cause inflammation and neovascularization, but these pathogenic mechanisms are not exclusive to nAMD. Inflammation and neovascularization are also found in retinopathy of prematurity (ROP) ((73), reviewed in (74)), proliferative diabetic retinopathy (75), myopia (76), and rarely, osteogenesis imperfecta (77). Although laser-induced CNV and OIR are not models which specifically emulate nAMD, they are interesting models to investigate the epigenetic context of inflammation and neovascularization. Recently, two studies implemented similar OIR models in mice and rats, to investigate the epigenetic mechanism of miRNA-mediated gene silencing (78,79).

1.5. MiRNA-Mediated Gene Silencing

MiRNA-mediated gene silencing, refers to an epigenetic mechanism where a short RNA molecule negatively regulates gene expression. MiRNAs are single-stranded RNA molecules, which are 20-25 nucleotides (nt) long, and are non-coding. The miRNA integrate with an Argonaute protein to form a RNA-induced silencing complex (RISC), capable of binding to and degrading an mRNA transcript (80). Today, it is known that the negative regulation of protein-encoding genes through miRNA, is imperative for the fine regulation of numerous physiological and pathological cellular processes (81).

In 1993, two publications in the same issue of *Cell*, provided the first concrete evidence of non-coding RNA mediated gene expression regulation (82,83). The study of neural development in *Caenorhabditis elegans* (*C. elegans*), had led to the discovery that worms with mutations in *lin-4* and worms deficient of *lin-14,* have antagonistic developmental timing defects. *C. elegans* have 4 distinct larval stages, with characteristic patterns of cell division. Mutations in *lin-4* were shown to cause cell division patterns, typical for an early larval stage, to reiterate at a later developmental stage (84). In contrast, worms deficient in *lin-14* were shown to skip this developmental stage altogether (85). Four years previously, it had been shown that *lin-14* encodes a nuclear protein whose downregulation initiates the transition to a later developmental stage (86). When researchers investigated the antagonistic developmental timing defects between *lin-4* and *lin-14*, they discovered that *lin-4* encodes a 22 nt non-coding RNA which is partially complementary to the 3'-untranslated region (UTR) of *lin-14* (83). This work showed that an intact copy of *lin-4* was necessary for the successful downregulation of

lin-14 (83), and the scientific field of non-coding RNA mediated gene expression was conceived.

Initially, researchers assumed that miRNA are confined to cell bodies. This assumption was refuted in 2008, when Chim et al. found placental miRNA in maternal blood plasma during pregnancy (87). MiRNAs which travel through the body via the blood stream, are called circulating miRNAs (cmiRNAs). Extracellular cmiRNAs can be released from cell bodies via active transport or passive leakage. The latter is usually a result of cell lysis or apoptosis in pathological conditions involving tissue damage, metastasis, or inflammation (88). In contrast, active transport of the cmiRNA occurs in conjunction with microvesicles (89), apoptotic bodies (90), various multiproteins (91), or HDL (89). Although the term 'cmiRNA' was originally used to refer to extracellular miRNA in serum or plasma (87), it has also been used to describe intracellular miRNA found in peripheral blood nuclear cells (PBNCs) (92,93).

The function of cmiRNA is thought to be based in intercellular communication (94,95). This theory was first proposed by Valadi et al. in 2007, who transferred exosomes derived from a mouse mast cell line to a human mast cell line (95). The exosomes contained mRNA and cmiRNA. After the transfer, mouse proteins were found in the human recipient cells, indicating that the mRNA could be translated after the transfer (95). The authors also proposed that the cmiRNA could be functional in the recipient cells, which sparked a novel line of scientific research. Five years later, a research group founded by Valadi used electroporation to introduce short interfering RNA (siRNA) into human exosomes which were then transferred to human monocytes and lymphocytes where they selectively silenced the target gene (96). Although this study used siRNA, similar effects have been shown with miRNA. Bang et al. showed that cardiac fibroblast-derived exosomes contained miR-21-3p, which were taken up by cardiomyocytes, leading to cellular hypertrophy (97). This study implicates miRNA based cellular cross-talk as a paracrine signaling mediator. MiRNA-based intercellular communication can also occur between organs. In a series of *in vitro* and *in vivo* experiments, Thomou et al showed that exosomal cmiRNA sourced from adipose tissue regulated gene expression in liver cells (98). This series of publications demonstrate, that intercellular cmiRNA-mediated communication, could be involved in physiological and pathological conditions.

1.6. CmiRNA Clinical Applications

Soon after their identification, cmiRNA were proposed as noninvasive diagnostic markers. First, Lawrie et al. reported the detection of several tumor-associated miRNA in serum samples

of diffuse B-cell lymphoma patients (99). Next, Mitchell et al. showed that serum miRNA-141 levels could distinguish between prostate cancer patients and healthy controls (100). Although much of the early research in this field was limited to oncology, the scope widened to include other pathologies. Today, cmiRNA profiles have been linked to a variety of diseases: osteoporosis and osteoporotic fracture (101), heroin and methamphetamine addiction (102), lumbar disc degeneration (103), rheumatoid arthritis (104), chronic kidney disease (105), and genetic generalized epilepsy (106). Multiple studies have also investigated cmiRNA expression in AMD patients, although the results in-between studies have been inconsistent (50,67).

The attraction of cmiRNA as a diagnostic tool is simple. Many of the previously mentioned conditions require burdensome diagnostic procedures, including extensive imaging and invasive biopsies. In contrast, investigations into a persons' cmiRNA status requires a simple blood draw, which can be performed by any general practitioner. The identification of a cmiRNA profile which is robustly linked to a specific pathological condition, could help physicians diagnose their patients. Even if the cmiRNA analysis did not nullify the need for an invasive diagnostic procedure, it could at least help provide the physician with additional information. This additional information is only useful, however, if the cmiRNA profile is robustly linked to a specific trait or disease.

The ability of cmiRNA and other antisense oligonucleotides (ASO) to modulate gene expression, have lead researchers to investigate their therapeutic potential. ASO-based applications have been developed for diseases including spinal muscular atrophy (107), ß-thalassemia (108), cystic fibrosis (109), and Duchenne muscular dystrophy (110). The previously mentioned treatments work by downregulating the transcription of unwanted mutant genes, or changing their splicing profile. All these approaches are challenging, but they are made easier by the fact that they are for monogenetic diseases. In complex disorders such as AMD, a therapeutic application of an ASO or cmiRNA may be more difficult, but not impossible. Prior to the therapeutic application of a cmiRNA to nAMD patients, cmiRNA which are robustly and specifically linked to the disease have to be identified.

1.7. Aim of this Study

The preliminary aim of this study was to conduct a literature analysis of differentially expressed cmiRNA in nAMD patients. This was performed in order to facilitate the identification of cmiRNA which were dysregulated across multiple studies, versus cmiRNA which were identified only in a solitary study.

The subsequent aim of this study, was to analyze the cmiRNA expression profiles of mice in two models of retinal inflammation and neovascularization: laser-induced CNV and OIR. First, we performed an in-depth analysis of cmiRNA dysregulation after laser-induced CNV in a discovery and two-part replication study. In the discovery study, next-generation sequencing (NGS) was used to identify candidate cmiRNA in blood samples of laser treated mice. Consequently, blood samples were analyzed that were extracted at two timepoints after laser treatment: day 3 and day 14. Samples from day 0 (one day prior to laser treatment) and samples from untreated mice, served as controls. Next, we performed a two-part replication study with a second and third set of animals, and investigated the cmiRNA expression via quantitative reverse transcription polymerase chain reaction (qRT-PCR). The time points analyzed in both replication studies were augmented to include blood samples from day 7, in order to improve the temporal resolution of cmiRNA expression. Samples from day 0 and samples from untreated mice, served as controls. The candidate cmiRNA were reduced stepwise in each subsequent analysis, until the top ten dysregulated cmiRNA were identified. The final experiments performed using the laser-induced CNV model, investigated the top ten miRNA in ocular tissue of treated and untreated mice.

The expression of the top ten dysregulated cmiRNA from the laser-induced CNV model were investigated in the second retinal disease model: OIR. For this analysis, blood samples from day 16 after OIR and untreated mice were investigated via qRT-PCR. The overall aim of the study, was to investigate cmiRNA expression in two murine models of retinal inflammation and neovascularization, and crosscheck our results with previous studies of cmiRNA dysregulated in nAMD patients.

2. Materials and Methods

2.1. Chemicals

Table 1: Chemicals used in the Execution of this Study.

Chemicals	Manufacturer
dNTPs (dATP, dGTP, dCTP, dTTP)	Genaxxon Bioscience
Ethanol ≥99,8 p.a, C2H6O	Carl Roth GmbH + Co. KG
Novex® TBE Running Buffer (5X)	Life Technologies
PAXgene Blood RNA Tube	PreAnatytiX
PhiX Control v3	Illumina, Inc.

Power SYBER Green	Invitrogen™
Power SYBR® Green PCR Master Mix	Applied Biosystems
ROTISOLV® HPLC Gradient Grade Water	Carl Roth GmbH + Co. KG
AMPure Beads	Beckman Coulter

2.2. Disposable Material

Table 2: Disposable Material used in the Execution of this Study.

Disposable Materials	**Manufacturer**
10 µl Pipette Tips	Nerbe Plus GmbH
100 µl Filter Tips	Nerbe Plus GmbH
1250 µl SafeSeal-Tips	Biozym Scientific GmbH
30 µl, Matrix™ Pipette Tips	Thermo Fisher Scientific Inc.
8- strip optical clear flat caps	Sarstedt AG & Co.
96-well Plate without skirt	Sarstedt AG & Co.
Corning® Costar® Spin-X® centrifuge tube filters	Sigma-Alderich
DNA Lo Bind Cups 1,5 ml	Eppendorf AG
Eppendorf Cups 0,5 ml SafeSeal	Sarstedt AG & Co.
Eppendorf Cups 1,5 ml SafeSeal	Sarstedt AG & Co.
Greiner centrifuge tubes, 15 ml	Sigma-Aldrich
Greiner centrifuge tubes, 50 ml	Sigma-Aldrich
KIMTECH SCIENCE* GREEN NITRILE Nitril-Gloves	Kimberly-Clark Professional
MicroAmp® Optical 384-Well Reaction Plate with Barcode	Applied Biosystems
MicroAmp® Optical Adhesive Film	Applied Biosystems
Novex® TBE Gels, 6 %, 10 well	Life Technologies
PCR-Cups 0,5 ml	Biozym Scientific GmbH

2.3. Equipment

Table 3: Equipment used in the Execution of this Study.

Device	**Manufacturer**
-80 °C Freezer	Thermo Scientific
Dark Hood DH-30/32	Biostep

Electrophoresis Bioanalyzer System	Agilent Technologies
Ice Machine, AF 100	Scotsman
Matrix™ Equalizer Electronic Multichannel Pipettes	Thermo Scientific
Microcentrifuge 5415R/5415D	Eppendorf
MiSeq Desktop Sequencer	Illumina
Nano Drop ND-1000 Spectrophotometer	Nano Drop
Rotational vacuum concentrators 2-25	Martin Christ Gefriertrocknungsanlagen GmbH
TProfessional Basic PCR Thermocycler 96 well thermal cycler	CORE Life Sciences
Transferpette® S	Brand GmbH + Co KG
ViiA™ 7 System Taqman	Life Technologies
Vortex Genie2	Scientific Industries
XCell SureLock® Mini-Cell	Life Technologies

2.4. Kits

Table 4: Kits used in the Execution of this Study.

Kit	**Manufacturer**
Agilent High Sensitivity DNA Kit	Agilent Technologies
Agilent Small RNA Kit	Agilent Technologies
mirVana™ miRNA Isolation Kit, with phenol	Life Technologies
MiSeq Reagent Kit v3 (150 cycles)	Illumina, Inc.
NEXTflex™ Small RNA Barcodes Primers (Set A)	Bioo Scientific Corporation
NEXTflex™ Small RNA Barcodes Primers (Set B)	Bioo Scientific Corporation
NEXTflex™ Small RNA-Seq Kit v2	Bioo Scientific Corporation
Poly-A Tailing Kit	Ambion®
SuperScript® III Reverse Transcriptase	Invitrogen™

2.5. Primer

Table 5: cmiRNA Primer used in the Execution of this Study.

Primer	Sequence (5' to 3')	Application
mmu-let-7g-3p_RT	ACTGTACAGGCCACTGCC	qRT-PCR
mmu-let-7i-3p_RT	CTGCGCAAGCTACTGCCT	qRT-PCR
mmu-let-7j_RT	TGAGGTATTAGTTTGTGCTGTTAT	qRT-PCR
mmu-mir-15b-3p_RT	CGAATCATTATTTGCTGCTCTA	qRT-PCR
mmu-mir-17-3p_RT	ACTGCAGTGAGGGCACTTG	qRT-PCR
mmu-mir-18a-3p_RT	ACTGCCCTAAGTGCTCCTTCT	qRT-PCR
mmu-mir-20a-5p_RT	TAAAGTGCTTATAGTGCAGGTAG	qRT-PCR
mmu-mir-22-5p_RT	AGTTCTTCAGTGGCAAGCTTTA	qRT-PCR
mmu-mir-25-3p_RT	CATTGCACTTGTCTCGGTCTG	qRT-PCR
mmu-mir-30a-5p_RT	TGTAAACATCCTCGACTGGAAG	qRT-PCR
mmu-mir-30e-5p_RT	TGTAAACATCCTTGACTGGAAG	qRT-PCR
mmu-mir-34a-5p_RT	TGGCAGTGTCTTAGCTGGTT	qRT-PCR
mmu-mir-92a-3p_RT	TATTGCACTTGTCCCGGC	qRT-PCR
mmu-mir-101a-3p_RT	TACAGTACTGTGATAACTGAA	qRT-PCR
mmu-mir-130b-3p_RT	CAGTGCAATGATGAAAGGG	qRT-PCR
mmu-mir-132-3p_RT	TAACAGTCTACAGCCATGGTCG	qRT-PCR
mmu-mir-140-3p_RT	TACCACAGGGTAGAACCAC	qRT-PCR
mmu-mir-148b-3p_RT	TCAGTGCATCACAGAACTTT	qRT-PCR
mmu-mir-148b-5p_RT	GAAGTTCTGTTATACACTCAGGCT	qRT-PCR
mmu-mir-155-5p_RT	TTAATGCTAATTGTGATAGGGGT	qRT-PCR
mmu-mir-191-5p_RT	CAACGGAATCCCAAAAGCAG	qRT-PCR
mmu-mir-298-5p_RT	GGCAGAGGAGGGCTGTTC	qRT-PCR
hsa-mir-301b-3p	CAGTGCAATAGTATTGTCAAAGC	qRT-PCR
mmu-mir-326-3p_RT	CCTCTGGGCCCTTCCTCC	qRT-PCR
hsa-mir-361-5p	TTATCAGAATCTCCAGGGGTA	qRT-PCR
mmu-mir-378a-5p_RT	CTCCTGACTCCAGGTCCTG	qRT-PCR
hsa-mir-424-5p	CAGCAGCAATTCATGTTTTGAA	qRT-PCR
mmu-mir-449a-5p_RT	TGGCAGTGTATTGTTAGCTGGT	qRT-PCR
hsa-mir-451a-5p	AAACCGTTACCATTACTGAGTT	qRT-PCR
mmu-mir-486a-5p_RT	TCCTGTACTGAGCTGCCC	qRT-PCR
mmu-mir-497a-5p_RT	CAGCAGCACACTGTGGTTT	qRT-PCR
mmu-mir-669c-5p_RT	ATAGTTGTGTGTGGATGTGTGT	qRT-PCR
mmu-mir-674-5p_RT	GCACTGAGATGGGAGTGGT	qRT-PCR
mmu-mir-1306-3p_RT	ACGTTGGCTCTGGTGGTG	qRT-PCR
mmu-mir-5126_RT	GCGGGCGGGGCCGGGGGC	qRT-PCR
Universal PCR Primer	AACGAGACGACGACAGACTTT	qRT-PCR

URT Primer	AACGAGACGACGACAGACTTTTTTTTT TTTTTTV	Reverse Transcription

Four miRNA primer (hsa-mir-301b-3p, hsa-mir-361-5p, hsa-mir-424-5p, and hsa-mir-451a-5p), which had been previously designed and used at this institute, could be reused in this project (111). Sequence conservation between the human and mouse miRNA transcripts were confirmed on www.mirbase.org. The universal PCR primer and URT primer were designed according to (112). All other primers were designed using Primer3Plus and purchased from Metabion International AG.

2.6. Software

Table 6: Software used in the Execution of this Study.

Software	Manufacturer
2100 Expert version: B.02.08.SI648	Agilent Technologies
Ape Plasmid Editor	M.Wayne Davis
CorelDRAW 2019	CorelDRAW
DIANA miRPath v.2.0	I. S. Vlachos
Microsoft Office	Microsoft
mirBase	Griffiths-Jones lab
Primer 3 Plus	Andreas Untergasser and Harm Nijveen
R (statistical software)	Ross Ihaka and Robert Gentleman, R Core Team
Surrogate Variable Analysis, Combat	Jeffrey T. Leek
ViiA 7 Software v.1.2.4.	Life Technologies

2.7. Literature Overview of cmiRNA in nAMD Patients

A literature search was conducted in Pubmed in December 2020, using combinations of the key words ‘miRNA’, ‘microRNA’, ‘circulating’, ‘age-related macular degeneration’, and ‘AMD’. In total, 13 published studies have investigated cmiRNA expression in nAMD patients and were considered for inclusion in the literature overview. Exclusion criteria were set in order to eliminate studies which had been performed under anomalous conditions. One study was excluded, because they investigated patients with two ocular pathologies: nAMD and congenital hemochromatosis (113). One study was excluded because it did not specify the mature strand of the cmiRNA they had investigated (114). Finally, two studies were excluded

because they investigated nAMD and gaAMD patients, and did not desegregate their data based on late-stage AMD phenotype (115,116). The remaining 9 studies were used in the literature overview (92,93,111,117–122) (Supp. Table 1).

The literature overview presented in this dissertation was assembled using different exclusion criteria than in the publication which arose from this body of work (67). In the publication, three additional studies were excluded because they investigated intracellular cmiRNA (92,93) or they investigated cmiRNA in exosomes (120). One study was included in the publication but excluded from this dissertation, because it did not specify the mature cmiRNA strand (114). Two studies were excluded from the publication and dissertation because their patient cohort was not desegregated based on the late-stage AMD phenotype (115,116) or congenital hemochromatosis comorbidity (113). Finally, a recent study was published after we submitted our publication, and is therefore only included in this dissertation (122).

2.8. Laser-Induced Choroidal Neovascularization

This animal study conformed to the Association for Research in Vision and Ophthalmology (ARVO) Statement for the Use of Animals in Ophthalmic and Vision Research, and was approved by the local ethics committee of the government of North Rhine-Westphalia (ID: 84-02.04.2015.A413), the authority for animal experiments for our collaborator in Cologne, Prof. Dr. Langmann. The laser treatment and blood sample extraction were performed by Dr. Karlstetter, with assistance from Dr. Aslanidis and Mr. Caramoy (Laboratory for Experimental Immunology of the Eye, Ordinarius Prof. Dr. Langmann, Department of Ophthalmology, University Hospital of Cologne, Germany).

Female drug and test naïve C57Bl/6J mice were used in this study (Table 7). In the discovery study, NGS was performed with samples from 11 mice: 6 laser treated mice, and 5 untreated mice. For the treated mice, NGS was performed with samples from three timepoints: day 0 (as a baseline control), day 3 and day 14. For the untreated mice, NGS was performed with samples that were age-matched to the day 14 samples, although RNA was also extracted from samples age-matched to day 0 and 3. In the first replication study, 6 additional laser treated mice and 6 additional untreated mice were analyzed. For the treated mice, samples from four timepoints were analyzed: day 0 (as a baseline control), day 3, day 7 and day 14. For the untreated mice, samples were age-matched to the day 14 samples. Mice from the discovery study, and first replication study were handled simultaneously, and were 78 days old on day 0.

In the second replication study, samples from 6 additional laser treated mice were analyzed. Samples from four timepoints were analyzed: day 0 (as a baseline control), day 3, day 7 and day 14. In the tissue study, samples from 11 laser treated mice were analyzed: samples from the same mice used in the second replication study (6 mice) plus 5 additional mice. In the tissue study, samples from one timepoint were analyzed: day 14. Samples from 12 untreated mice, age-matched to the day 14 samples, were used as controls. Mice from the second replication study and tissue study were handled simultaneously, and were 56 days old on day 0. One mouse which had a unilateral idiopathic cataract, was excluded from our study.

Table 7: Overview of the Mice used in the Laser-induced CNV Model.

Study	Treated Mice (#)	Timepoints (day)	Untreated Mice (#)
Discovery Study[†]	6	0, 3, 14	5
Replication Study 1[‡]	6	0, 3, 7, 14	6
Replication Study 2[§]	6	0, 3, 7, 14	-
Tissue Study[**]	6 + 5	14	12

[†] In the discovery study, blood samples were analyzed from six treated mice taken at three timepoints: day 0, day 3, and day 14. RNA was also isolated from the blood samples of five untreated mice age-matched to the samples from all three timepoints, although only the samples age-matched to day 14 were analyzed.
[‡] In replication study 1, blood samples were analyzed from six treated mice taken at four timepoints: day 0, day 3, day 7, and day 14. Blood samples were also analyzed from six untreated mice, age-matched to the day 14 samples.
[§] In replication study 2, blood samples were analyzed from six treated mice as per replication study 1.
[**] The tissue study was performed with retinal tissue and tissue from the RPE and choroid. Samples from eleven laser treated mice were analyzed: samples from the same mice used in the second replication study (six mice) plus five additional mice. Samples were taken from the treated mice on day 14. Samples from twelve untreated mice were age-matched to the day 14 samples.

Mice received laser treatment on day 1. First, narcosis was induced with Rompun (6 mg/kg) and Ketavet (100 mg/kg), and pupils were dilated using a drop of Phenylephrine HCl (0.25 %-Tropicamide (0.05 %) (59). Treated mice received laser burns in 6 spots per eye in both eyes. The untreated mice were handled identically, except for the laser-treatment.

Blood was taken from each mouse at four time points: day 0 (one day prior to laser-treatment), day 3, day 7, and day 14. A ~40 µl blood sample was taken by puncturing the facial vein dorsocaudal of the mandible. The blood was mixed with 160 µl stabilizing solution (PaxGene Blood RNA Tube Solution) to slow the enzymatic digestion of the cmiRNA by RNAses.

After the blood samples had been obtained on day 14, narcosis was induced, and the choroidal neovascularization was confirmed in the laser treated mice using angiography and spectral domain Optical Coherence Tomography (SD-OCT). The control mice received the

same diagnostic procedures, but no neovascularization was observed. For the tissue samples, the eyes were enucleated and the retina and RPE/choroid was extracted. The blood and tissue samples were shipped to Regensburg on dry ice, where they were stored at -80 ºC.

2.9. RNA Isolation

2.9.1. RNA Isolation from Blood and Tissue Samples

Prior to RNA isolation, the blood and tissue samples were prepared for the extraction procedure. For the blood samples, the blood-stabilization solution mixture was thawed on ice, centrifuged at 2,800 g at 4 ^{0}C for 10 min, and approximately 150 µl of the supernatant was collected. For the tissue samples, the tissue was roughly homogenized with a pestle, and then further homogenized by forcing the sample through 18G, 20G, and 23G needles.

RNA from the blood and tissue samples was isolated using the mirVana™ miRNA Isolation Kit (Life Technologies), with some modifications. The protocol for organic extraction was performed for a lysate volume of 600 µl. The centrifugation time was increased to 30 min and 16,000 g at 4 ^{0}C during the final step. After the organic extraction was completed, the total RNA isolation was performed according to manufacturer's instructions. The RNA was eluted in 50 µl RNAse-free water and stored at -80 ^{0}C.

2.9.2. RNA Quality Control and Analysis

Two methods of quality control were performed to confirm that the RNA isolations were successful, and to investigate the size distribution of the RNA. First, the amount of total RNA in the sample was measured using a Nano Drop ND-1000 Spectrophotometer (Nano Drop). In addition to the Nano Drop, an Electrophoresis Bioanalyzer System (Agilent Technologies) was used to assess the small RNA and cmiRNA concentration in the blood samples. For this analysis, the Small RNA Analysis Kit (Agilent Technologies) was used according to manufacturer's instructions.

The RNA size distribution and RNA concentration of the isolated blood samples were investigated in the laser treated and untreated mice. The proportion of large RNA, small RNA, and cmiRNA were calculated for all samples. The proportion of small RNA out of total RNA were calculated for the samples from laser treated and untreated mice for each time point. Normal distribution was evaluated using the Kolmogorow-Smirnow test, and a student t-test was used to test for significance. A p-value <0.05 was considered statistically significant.

Finally the cmiRNA concentration and total RNA concentration of each sample was investigated. A regression analysis of the pooled samples was performed.

The RNA concentration of the isolated tissue samples were investigated in the laser treated and untreated mice. Normal distribution was evaluated using the Kolmogorow-Smirnow test, and a student t-test was used to test for significance. A p-value <0.05 was considered statistically significant.

2.10. NGS (Discovery Study)

2.10.1. Library Preparation and NGS

cDNA libraries were prepared in batches, and samples from laser treated mice were handled simultaneously with control samples to reduce batch dependent discrepancies. Prior to library preparation, 40 µl of the isolated RNA was heated in a centrifugal evaporator set to 37 ^{0}C for 75-85 minutes, to increase the RNA concentration. The NEXTflex™ Illumina Small RNA Sequencing Kit v2 (Life Technologies), was used to create the libraries with a starting volume of 4 µl, with one modification. Nineteen cycles were used during the PCR, instead of the recommended 12-18, to ensure a higher product yield. The NEXTflex™ Small RNA Barcode Primers kit, Set A and B (Bioo Scientific Corporation) served to barcode the samples. The samples were purified using AMPure beads (Beckman Coulter). The size distribution and concentration of the final library was evaluated using a Bioanalyzer High Sensitivity DNA Assay (Agilent Technologies).

The cDNA libraries were diluted to a concentration of 2 nM, and 10 µl of each sample was pooled. The pooled libraries were reheated in the centrifugal evaporator, to a final concentration of 4 nM. The pooled libraries were denatured using freshly diluted 1 mM NaOH (pH 12.8), according to the protocol "Preparing Libraries for Sequencing" on the MiSeq® (Illumina), resulting in a 20 pM DNA solution. Prior to sequencing, 120 µl of the denatured Phix control, was added to 480 µl of the denatured library pool. This concentration of Phix was applied to ameliorate sequencing problems associated with low diversity libraries, as shown in human studies (111).

Sequencing was performed on the Miseq Desktop Sequencer (Illumina) using MiSeq Reagent Kit v3 with 150 cycles (Illumina). The samples were sequenced paired end, using 35 cycles. The cluster density was ~5,700K cluster per mm^2.

2.10.2. Analysis

The analysis of NGS data was performed by Dr. Grassmann, former employee of the Institute of Human Genetics, Director Prof. Dr. Weber, University of Regensburg, Germany, according to (111). The sequencing data were analyzed using the mirDEEP2 package (123) in the statistical software R (124). All reads were mapped to the mouse genome (mm10) using BowTie2 (125), and reads that failed to align were excluded. Reads were then mapped to pre-miRNA and mature miRNA sequences from mirbase.org (released June 21st, 2014), and quantified. The data were normalized, using the trimmed mean of M-values (TMM) algorithm implemented in the edge R package (126), which adjusts for variance between samples. The normalized data were transformed with the binary logarithm. The ComBat algorithm (127), was used to adjust for batch effects. All cmiRNA which had a read count < 90 were discarded, and the log2 value was taken of all remaining data.

The analysis of cmiRNA expression data from several time points, was performed with a linear mixed effects model, implemented in the nlme package (128). First, the miRNA profiles of laser treated mice on day 0 were compared with day 3. In this analysis, the day 0 samples served as a control. Up or down regulated cmiRNA with a p-value (uncorrected) <0.1 were further analyzed in a second comparison with the samples from the untreated mice. This was performed using a linear fixed effects model, implemented in R. The cmiRNA which did not show an effect in the second analysis, or showed an effect in the opposite direction, were excluded from further analysis.

Next, the cmiRNA profiles of laser treated mice on day 0 were compared with day 14, as described previously for the samples from day 3. Finally, the cmiRNA profiles of laser treated mice on day 0 were compared with the samples from the untreated mice using a Firth's bias-reduced logistic regression model, which is implemented in the logistf package (129). CmiRNA with a p-value (uncorrected) <0.1 were excluded from further analyses. In total, 34 cmiRNA met the inclusion criteria set in the discovery study, and were investigated in the replication studies.

2.11. qRT-PCR (Replication Studies, Tissue Study)

2.11.1. cDNA Synthesis and Reverse Transcription

cDNA synthesis was performed using the RNA isolated from the blood and tissue samples. Prior to reverse transcription, half the water volume was evaporated from the RNA samples using a centrifugal evaporator, set to 37 ^{0}C for 30-35 minutes. The isolated RNA from each

sample was reverse transcribed according to Hurteau et al. (112). Briefly, a polyA tail was added to the RNA in each sample by *E. coli* Poly-A Polymerase I, using the Poly-A Tailing Kit (Ambion®) with a starting volume of 12.2 µl. The modified RNA was reverse transcribed to cDNA using the SuperScript® III Reverse Transcriptase (Invitrogen™). Reverse transcription was performed with a universal RT oligonucleotide primer, which contains a polyT that binds to the newly synthesized polyA tail.

2.11.2. qRT-PCR

Oligonucleotide primers for qRT-PCR were designed using Primer3Plus (130). The corresponding cDNA sequence of each miRNA was analyzed using Primer3Plus, to evaluate its suitability as a primer. If the predicted annealing temperature exceeded 58 ºC, the primer was shortened, to a minimum of 18 bases. Primers are listed in Table 5.

To evaluate the suitability of the qRT-PCR primers, melt curve profiles were generated for each primer. To this end, a qRT-PCR reaction was performed for each target, using cDNA from an unrelated experiment, in triplicates according to Table 8. Primers were deemed suitable if the melt curve showed a solitary peak, at the same position in each sample. The melt curve profiles of the primers in ocular tissue were evaluated in collaboration with Christina Kiel (Institute of Human Genetics, Director Prof. Dr. Weber, University of Regensburg, Germany).

Table 8: Reagents for one qRT-PCR Reaction

Component	Volume
cDNA	4µl
miRNA Primer diluted 1:10	0,5µl
URT Primer diluted 1:5	0,5µl
Power SYBR® Green PCR Master Mix	5µl

Candidate cmiRNA which were investigated in the replication studies were evaluated using the ViiA™ 7 System Taqman (Life Technologies). Candidate miRNA which were investigated in the tissue studies were evaluated using the QuantStudio5 (Applied Biosystems). Prior to qRT-PCR, cDNA samples were diluted 1:40 with RNAse free water. Samples were assayed in triplicates. One negative control reaction per miRNA target and 384 well plate was performed, which comprised of the same reagents as in Table 8 with water instead of cDNA.

2.11.3. Analysis

In replication study 1, the 34 cmiRNA from the discovery study were investigated in the samples taken from the laser treated mice on day 0, day 3, day 7, and day 14. If samples had a standard deviation >0.4 Ct, the outlier were removed, at most one per triplicate. The expression was normalized to the mean expression on day 0. The quantified expression of the target miRNA was expressed as $2^{\Delta Ct}$. Normal distribution was evaluated using the Kolmogorow-Smirnow test. In this analysis, the expression data were not normally distributed, so a Wilcoxon-Mann-Whitney-U-Test (U-test) was used to test for significance. A p-value <0.05 was considered statistically significant.

In replication study 1, 18 cmiRNA were investigated in the samples taken from laser treated mice on day 14, in comparison to the samples taken from the age-matched untreated mice. The expression of the target cmiRNA was analyzed as described previously, with minor modifications. The expression was normalized to the mean expression of the untreated samples. The expression data were normally distributed, so a student t-test was used to test for significance.

In replication study 1, a cmiRNA which had been used as a housekeeper in a similar study using human samples (111), was evaluated. The expression was investigated in the samples from the laser treated mice on day 0, day 3, day 7, and day 14, and in a second comparison between the samples from day 14 in the treated and untreated mice, as described previously.

In replication study 2, 21 cmiRNA were investigated in the samples taken from the laser treated mice on day 0, day 3, day 7, and day 14. The expression was analyzed as described previously.

Finally, ten dysregulated cmiRNA were analyzed in the pooled data from both replication studies. Here, the data from each study were normalized separately. The expression was analyzed as described previously.

In the replication studies, cmiRNA were selected for each analysis by Dr. Grassmann (former employee of the Institute of Human Genetics, Director Prof. Dr. Weber) according to (111). Briefly, the outliers from samples with a standard deviation >0.4 Ct were removed from each triplicate, at most one per triplicate. The program for TMM normalization was implemented in the edgeR package (126). CmiRNA expression was normalized to the median of day 0 expression.

2.12. Oxygen-Induced Retinopathy

The expression of the top ten dysregulated cmiRNA from the laser-induced CNV model were investigated in the second retinal disease model: OIR. This animal study conformed to the Association for Research in Vision and Ophthalmology (ARVO) Statement for the Use of Animals in Ophthalmic and Vision Research, and was approved by the local ethics committee of the government of Lower Franconia (ID: DMS 2532-2-273, Applicant: PD Dr. Ohlmann). OIR was performed by PD Dr. Ohlmann and colleagues at the Institute of Human Anatomy and Embryology, Director Prof. Dr. Tamm, University of Regensburg, Germany, according to (61).

Drug and test naïve C57Bl/6J mice were used in this study. Briefly, on P7 mouse pups were transferred to a 75 % oxygen environment with their mother for 5 days (until P12). The mice were then returned to room air, where they were kept until P16. On P16, mice were anaesthetized with 100 mg/kg bodyweight Ketamine (Ketavet) and 10 mg/kg bodyweight Xylazin (Rompun). A ~40 µl blood sample was taken by puncturing the tail vein. This was performed by Dr. Grassmann (former employee of the Institute of Human Genetics, Director Prof. Dr. Weber). The eyes were extracted and retinal whole mounts were prepared for FITC-labeled dextran staining. The mice were euthanized via manual cervical dislocation while under anesthesia. The untreated siblings were used as controls. The control mice were handled identically, except for the OIR treatment, during which time they were kept with a foster mouse. In total, 16 OIR treated and 19 untreated mice were investigated during this study.

RNA was isolated according to section 2.9, cDNA synthesis and reverse transcription was performed according to section 2.11.1, qRT-PCR was performed according to section 2.11.2 and the analysis was performed according to section 2.11.3. The expression of the target cmiRNA was normalized to the mean expression in the control mice.

3. Results

3.1. Dysregulated cmiRNA in nAMD Patients

Several research groups have investigated cmiRNA expression in nAMD patients vs controls. In order to establish an overview of previous research, a Pubmed literature search was performed in March 2020, using combinations of the key words ‘miRNA’, ‘microRNA’, ‘circulating’, ‘age-related macular degeneration’, and ‘AMD’. In total, 13 published studies have investigated cmiRNA expression in nAMD patients and were considered for inclusion in the literature overview. Exclusion criteria were defined in order to eliminate publications

performed under incompatible conditions (92,93,111,117–121). Therefore, one study which investigated patients with nAMD and congenital hemochromatosis (115), two studies which investigated nAMD and gaAMD patients jointly (117,118), and one study which did not specify the mature strand of the cmiRNA they had investigated (116), were excluded. Nine publications passed the exclusion criteria, and were analyzed in the literature overview.

The first aim of this literature overview was to assess the scope of cmiRNA dysregulation in nAMD patients (Fig. 2; Supp. Table 1). Our analysis revealed 54 different cmiRNA across 9 independent publications, which were differentially expressed in nAMD patients in comparison to controls. We further sought to distinguish between cmiRNA which were dysregulated in a single study vs. cmiRNA which have been independently replicated. We observed that the majority of cmiRNA (47/54 = 87 %) have not been replicated by an independent research group. In total, four cmiRNA were independently replicated in the same direction: mir-16-5p (93,122), mir-25-3p (117,122), mir-126-3p (121,122) and mir-223-3p (93,117). Three out of four replicated cmiRNA were dysregulated in the most recent study, which investigated cmiRNA expression in nAMD patient serum samples (mir-16-5p, mir-25-3p, and mir-126-3p) (122). The three dysregulated cmiRNA from this publication, were replicated across three previous publications which also investigated nAMD patient serum samples (93,117,121). The final cmiRNA which was independently replicated in the same effect direction is mir-223-3p. This cmiRNA was upregulated in blood plasma (117) and PBNCs (93). Of note, the latter publication also performed a multivariate analysis, which adjusted for age, sex, and smoking status. In this analysis, nAMD was not independently associated with a higher expression of mir-223-3p (93).

Two cmiRNA were also dysregulated in two independent studies, but in opposite effect directions. Mir-150-5p was upregulated in PBNCs (92) and downregulated in PBNCs (93) in two studies which were published 18 months apart. The latter publication performed the same multivariate analysis mentioned previously, which showed that nAMD was an independent factor associated with a lower expression of mir-150-5p (p-value = 0.01) (93). Of note, the recent study which replicated three cmiRNA in the same effect direction, also replicated one cmiRNA in the opposite direction: mir-146a-5p, which was downregulated in serum samples (117) and upregulated in plasma in a previous study (118).

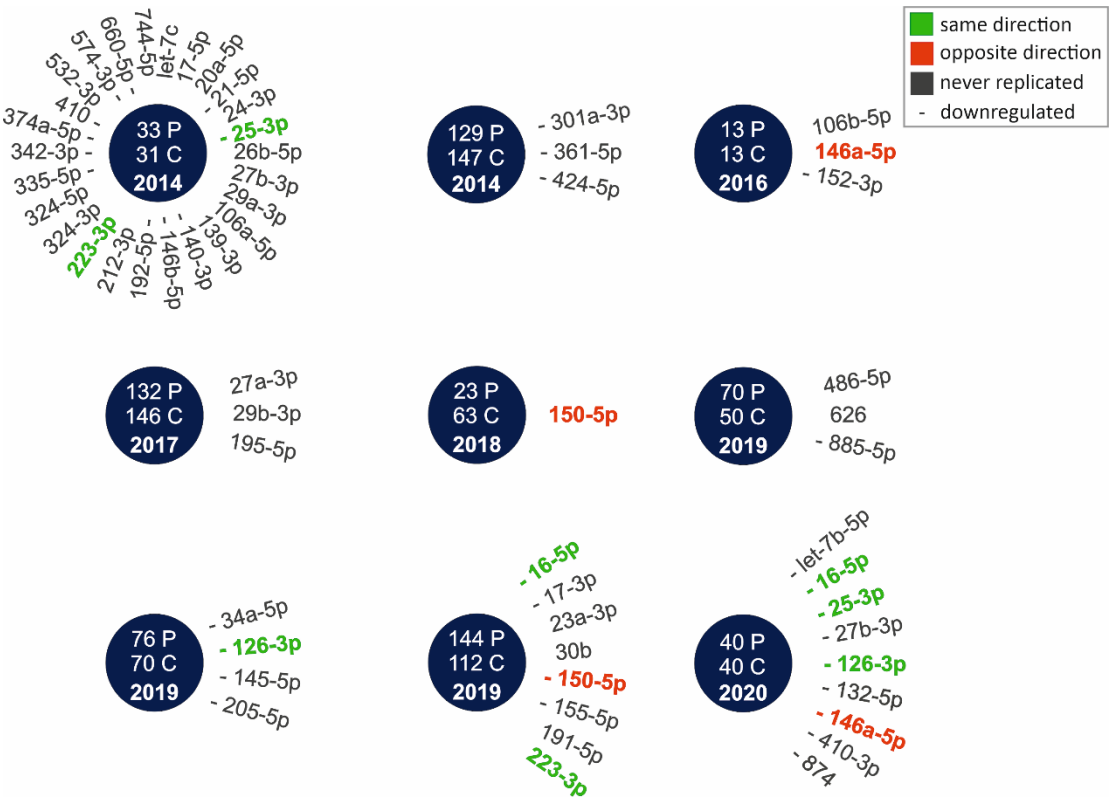

Figure 2: CmiRNA differentially expressed in nAMD patients, summarized from literature data. Each publication that investigated cmiRNA in nAMD patients and passed the exclusion criteria, is represented by a circle. The year of publication is denoted in each circle, along with the number of participants ("P" represents nAMD patients, and "C" represents controls). The cmiRNA identified in each study are listed around the circle, and downregulated cmiRNA are marked with a dash. Four cmiRNA were dysregulated in the same direction in two studies: mir-16-5p, mir-25-3p, mir-126-3p and mir-223-3p (highlighted in green). Two cmiRNA were dysregulated in opposite directions in two studies: mir-146a-5p and mir-150-5p (highlighted in red). The majority of cmiRNA (47/54 = 87 %) differentially regulated in nAMD patients have not been replicated in independent studies (in grey). The prefix of each cmiRNA is hsa-mir-, except for hsa-let-7c and hsa-let-7b-5p.The corresponding references from top left to bottom right, are: (117)(111)(118); (119)(92)(120); (121)(93)(122).

3.2. Dysregulated cmiRNA in Laser-Induced CNV

The aim of the following work was to identify dysregulated cmiRNA in a murine model of laser-induced CNV. In this model, an argon laser is used to perforate the Bruch's membrane, and the subsequent healing process generates inflammation and neovascularization. The laser treatment and blood sample acquisition was performed by Dr. Karlstetter and colleagues (Laboratory for Experimental Immunology of the Eye, Ordinarius Prof. Dr. Langmann).

We performed an in-depth analysis of differential cmiRNA expression after laser-induced CNV in a discovery and two-part replication study. An overview of the steps involved in each analysis is presented (Fig. 3). In the discovery study, next-generation sequencing (NGS) was used to identify candidate cmiRNA in blood samples of laser treated mice. For this study,

we analyzed blood samples that were extracted on day 3 and day 14 after laser treatment. Samples from day 0 (one day prior to laser treatment) and samples from untreated mice age-matched to the day 14 samples, served as controls. RNA was also isolated from samples taken from the untreated mice age-matched to day 0 and day 3, but these samples were not sequenced. In this study, RNA were extracted from the blood samples, the concentration and purity of the cmiRNA fraction were determined, and reverse transcription was performed. Libraries were prepared from the samples, and the purity of the cmiRNA fraction pre- and post-library preparation were investigated. The samples were sequenced, and the sequencing data were analyzed by Dr. Grassmann (former employee of the Institute of Human Genetics, Director Prof. Dr. Weber), according to (111). Briefly, the cmiRNA expression data from the laser treated mice on day 3 were compared to day 0, and to the samples from the untreated mice. The following inclusion criteria were used to identify cmiRNA for downstream replication: uniform effect directions in comparison to the samples from day 0 and untreated mice, and a p-value (uncorrected <0.1). The same procedure was followed for the samples from laser treated mice on day 14. In total, 34 cmiRNA met the inclusion criteria set in the discovery study, and were investigated in the replication studies.

Next, we investigated the expression of the cmiRNA candidates via qRT-PCR in the replication studies. In replication study 1, the expression of the 34 cmiRNA candidates from the discovery study were investigated in 6 laser treated and 6 control mice. Blood samples from laser treated mice were analyzed at four timepoints: day 0, day 3, day 7, and day 14. In contrast to the discovery study, the replication studies were amended to include samples from day 7, in order to gain more refined insight into cmiRNA expression over time. Samples from untreated mice age-matched to the day 14 samples, were also analyzed. In this study RNA was isolated from the blood samples and reverse transcribed to cDNA. In preparation for qRT-PCR the primer quality was investigated by analyzing the melt curve profile of each target cmiRNA. The expression of a potential cmiRNA housekeeper was also investigated. qRT-PCR was performed with all 34 cmiRNA candidates, using the samples from the laser treated mice. In this analysis, the samples from day 0 served as a control. A selection of cmiRNA was also investigated in the samples from laser treated mice on day 14, in comparison to the samples from untreated mice.

In replication study 2, the expression of 21 cmiRNA candidates were investigated in samples from 6 additional laser treated mice, at four timepoints: day 0, day 3, day 7, and day 14. RNA from the blood samples were isolated and reverse transcribed to cDNA, followed by qRT-PCR. Here, samples from day 0 served as a control.

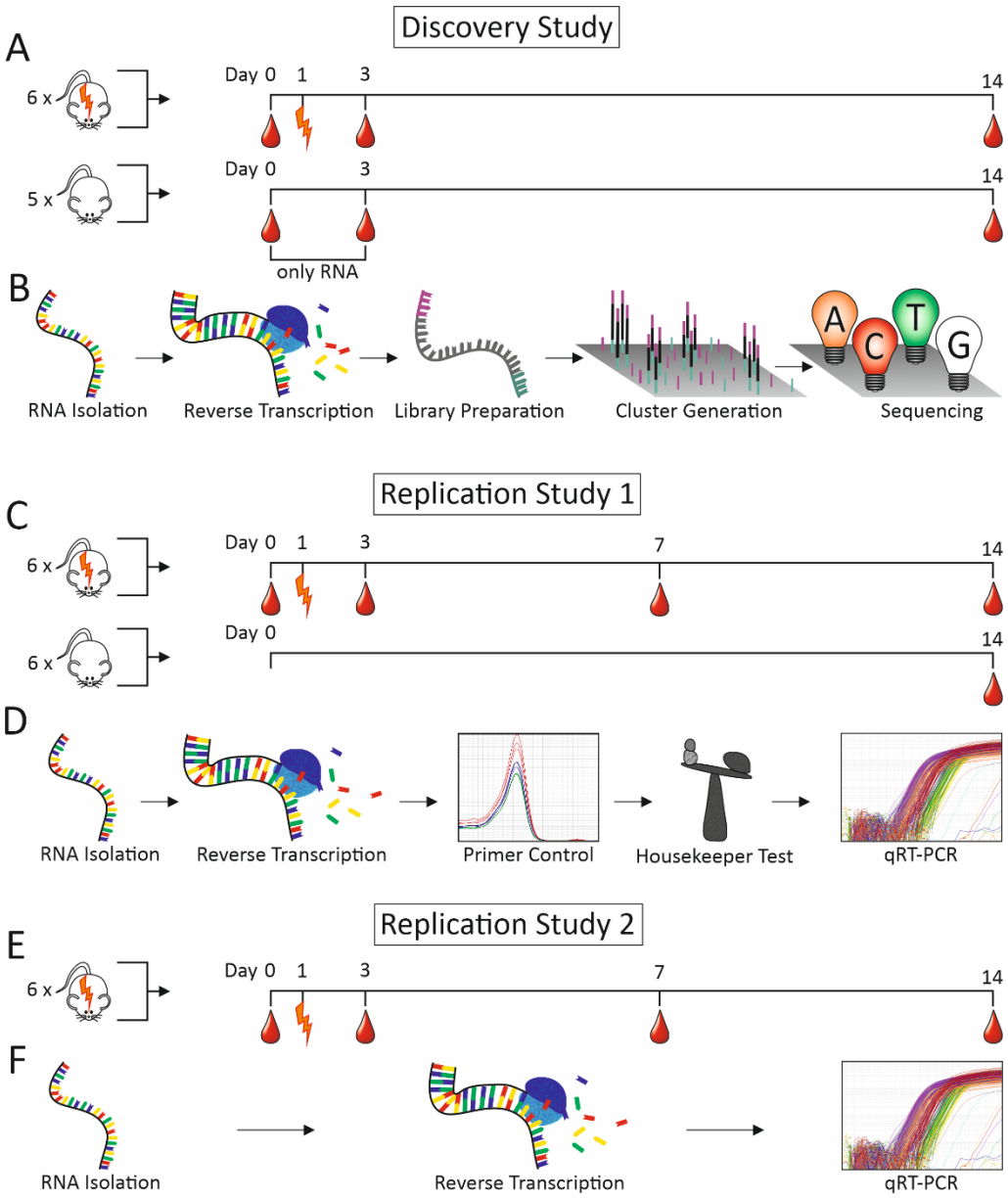

Figure 3: Dysregulated cmiRNA in Laser-Induced Choroidal Neovascularization Workflow Overview. NGS and qRT-PCR were used to investigate dysregulated cmiRNA in a murine model of laser-induced CNV. (A) In the discovery study, blood samples from laser treated mice on day 0, day 3, and day 14 were analyzed. RNA was also extracted from the blood samples of five untreated mice age-matched to each timepoint, but only the samples age-matched to day 14 were sequenced. (B) RNA was isolated from the blood samples and reverse transcribed, followed by library preparation. Samples were sequenced, and the NGS data were analyzed by Dr. Grassmann (former employee of the Institute of Human Genetics, Director Prof. Dr. Weber). Dr. Grassmann selected cmiRNA candidates for downstream replication. (C) In replication study 1, blood samples were investigated from six laser treated mice at four timepoints: day 0, day 3, day 7, and day 14, and six untreated mice age-matched with the day 14 samples. (D) RNA was isolated from the blood samples and reverse transcribed. Quality control was performed for oligonucleotide qRT-PCR primers, and the expression of a potential cmiRNA housekeeper was investigated. qRT-PCR was performed, and the expression of each target cmiRNA was analyzed. Dr. Grassmann (former employee of the Institute of Human Genetics, Director Prof. Dr. Weber) independently analyzed the expression data and selected cmiRNA candidates for downstream replication. (E) In replication study 2, blood samples were

investigated from 6 additional laser treated mice at four timepoints: day 0, day 3, day 7, and day 14. (F) RNA was isolated from the blood samples and reverse transcribed. qRT-PCR was performed, and the expression of each target cmiRNA was analyzed. Dr. Grassmann independently investigated the qRT-PCR data, and selected the top ten dysregulated cmiRNA candidates for replication in a second murine model system. I created the images in this figure from scratch for this dissertation.

3.2.1. Discovery Study

RNA was isolated from the blood samples of the laser treated and untreated mice. Two methods of quality control were performed to ensure RNA integrity. The total RNA concentration was measured using a Nano Drop ND-1000 Spectrophotometer, and an Electrophoresis Bioanalyzer System was used to assess the concentration of the small RNA and cmiRNA fractions (Supp. Table 2). The data from both investigations were used to gain insight into the distribution of the size gradient in each sample. Overall, the samples contained mostly large RNAs (11.7 ng/µl ± 6), and a small portion of cmiRNA (0.12 ng/µl ± 0.05) (Fig. 4A). Next, the proportion of small RNA out of total RNA in samples from laser treated and age-matched control samples was investigated, which revealed no significant differences (Fig. 4B). Finally, the cmiRNA concentration out of total RNA concentration was investigated in the samples which were used for NGS (Fig. 4C). A regression analysis did not show a correlation between cmiRNA and total RNA concentration ($R^2 = 0.05$).

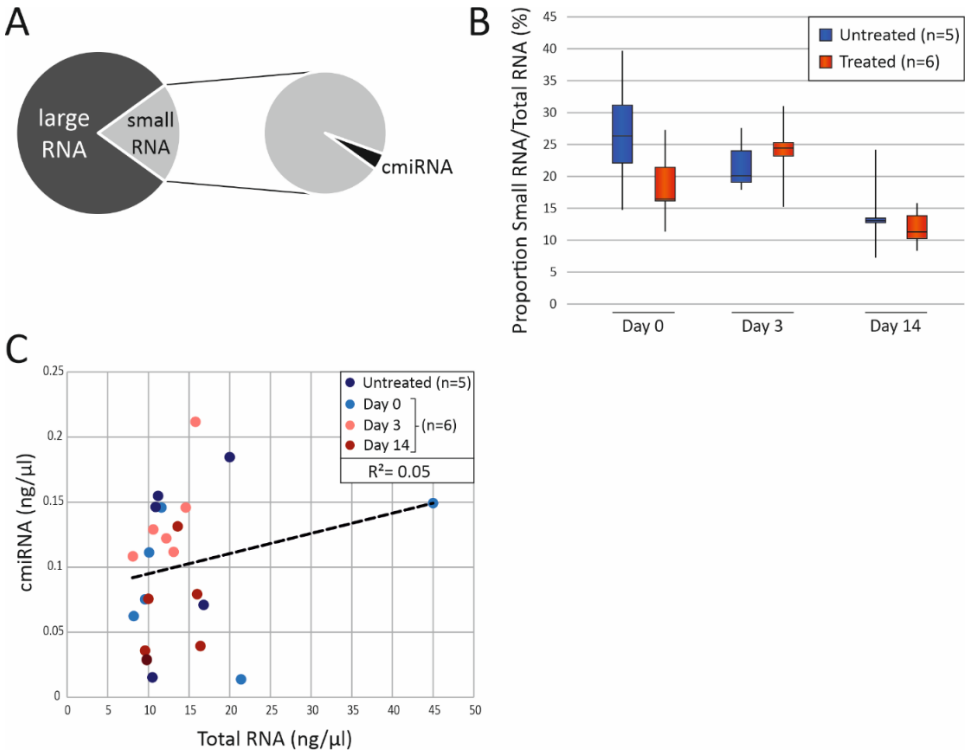

Figure 4: Discovery Study RNA Isolation. (A) The average proportion of large, small, and cmiRNA across all samples are shown. Overall, the RNA samples contained mostly large RNAs, and a small portion of cmiRNA (n = 23). (B) The proportion of small RNA out of the

total RNA is shown. No significant differences between the laser treated and untreated mice were observed (student t-test, n = 6 treated, 5 untreated). (C) CmiRNA concentration vs. total RNA concentration is shown in the samples which were used for NGS. A regression analysis did not show a correlation between cmiRNA and total RNA concentration ($R^2 = 0.05$).

In preparation for sequencing, the RNA samples were reverse transcribed to cDNA, and libraries were prepped from each sample. One aim of the library preparation, was to purify the cmiRNA fraction in each sample. To investigate the cmiRNA purity, samples were analyzed pre and post library preparation using the Electrophoresis Bioanalyzer System (8 exemplary samples shown in Fig. 5). In the images pre library preparation, the cmiRNA fraction corresponds to a very subtle peak between 20-40 nt. The cmiRNA fraction is accompanied by a marker peak (4 nt), and a very prominent fraction of non-cmiRNA small RNAs (40-150 nt). Post library preparation, the cmiRNA fraction corresponds to the prominent peak at ~180 base pairs (bp). The size increase is a result of the addition of a poly-A tail prior to reverse transcription, and adaptors and a barcode sequence during library preparation. In the images acquired post library preparation, the cmiRNA peaks are accompanied by two marker peaks (lower marker at 35 bp and upper marker at 10,380 bp). The purity of the cmiRNA fractions was greatly improved during library preparation, and the libraries were mostly free from non-cmiRNA small RNAs.

After confirming successful library preparation and cmiRNA fraction purity, the libraries were pooled and sequenced. The sequencing data from the discovery study were analyzed by Dr. Grassmann, (former employee of the Institute of Human Genetics, Director Prof. Dr. Weber) according to (111). In total, 34 cmiRNA met the inclusion criteria set in the discovery study, and were investigated in replication study 1.

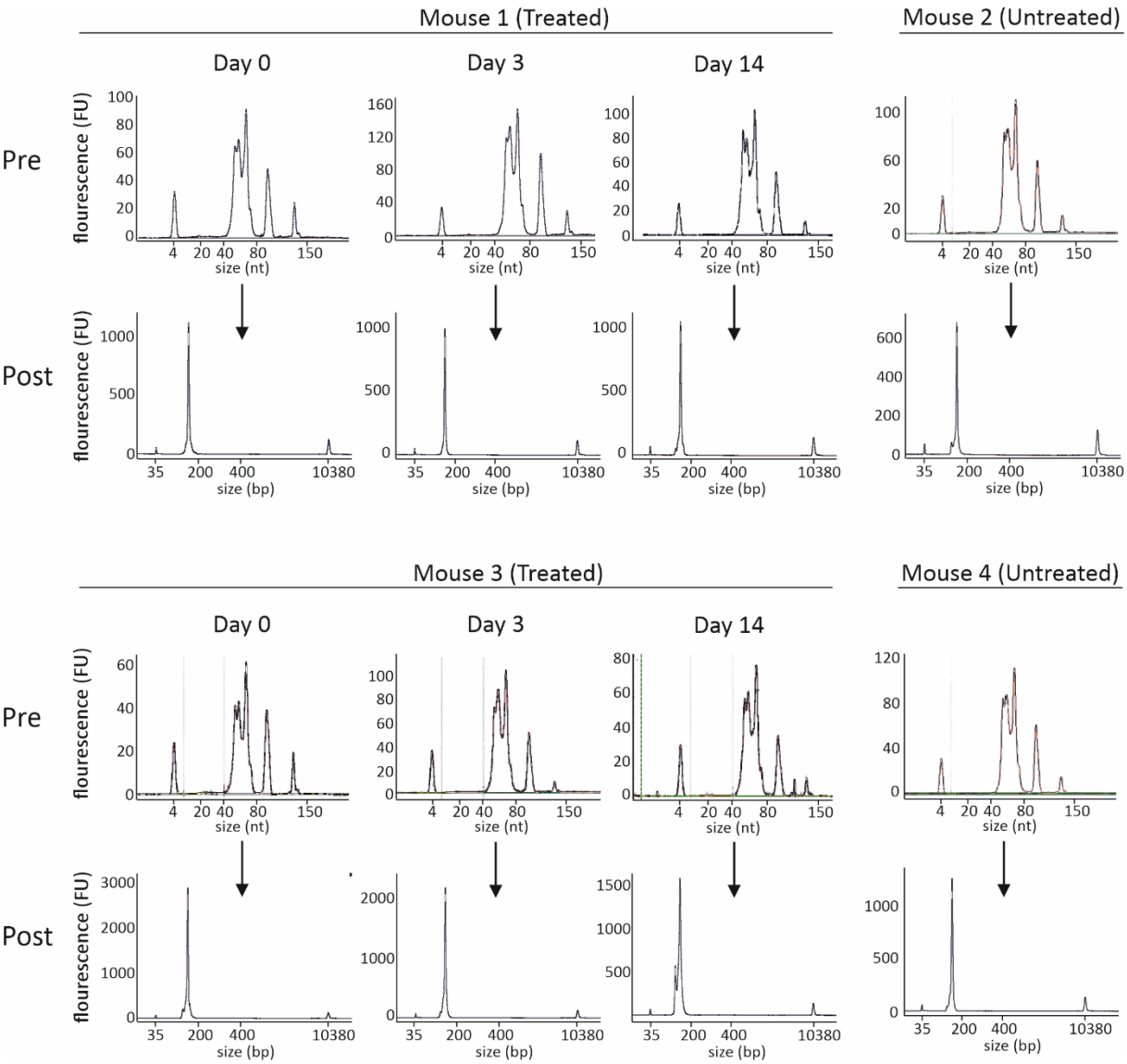

Figure 5: Discovery Study Library Preparation. The size distribution of 8 exemplary samples pre and post library preparation from two laser treated and two untreated mice are shown. In the images pre library preparation (labeled 'Pre') a marker peak is located at 4 nt, the cmiRNA fraction is located between 20-40 nt, and the non-cmiRNA small RNAs are located between 40-150 nt. In the images post library preparation (labeled 'Post') two marker peaks are located at 35 bp and 10,380 bp, and the cmiRNA fraction is located at 180 bp. No surplus non-cmiRNA small RNAs were seen in the samples post library preparation. Samples were analyzed using an Electrophoresis Bioanalyzer System (Agilent Technologies). Nt = nucleotides, bp = base pairs

3.2.2. Replication Study 1

RNA was isolated from the blood samples of treated and untreated mice. The total RNA concentration of the samples was estimated using a Nano Drop ND-1000 Spectrophotometer, and the size distribution of the small RNAs was measured using an Electrophoresis Bioanalyzer System (Supp. Table 3). As in the discovery study the samples contained mostly large RNAs and a small portion of cmiRNA, and a regression analysis showed a weak correlation between

the cmiRNA and total RNA concentration (Supp. Fig. 1). No significant differences were observed between the samples from the laser treated and untreated mice. The RNA samples were subsequently reverse transcribed.

In preparation for qRT-PCR, primers were designed for each of the 34 cmiRNA targets. Primer quality was investigated by analyzing the primer melt curve profiles in a series of preliminary qRT-PCR experiments, in triplicate (6 exemplary melt curve profiles are shown in Supp. Fig. 2). All primers had a single melt curve peak at the same position in all triplicates, and were considered to be sufficient quality for the qRT-PCR experiments.

The expression of a potential housekeeping cmiRNA (mir-451a-5p) was investigated. This cmiRNA was previously used as a housekeeping cmiRNA in a similar study at this institute (111). The expression of mir-451a-5p was investigated in samples from laser treated mice taken at four timepoints: day 0, day 3, day 7, and day 14 (Supp. Fig. 3A; Supp. Table 4). In this analysis, the expression was significantly decreased on day 7. In a second analysis between the day 14 samples from the laser treated mice and the untreated controls, the cmiRNA was also significantly decreased (Supp. Fig. 3A; Supp. Table 5). Our analyses revealed that the cmiRNA was affected by the laser treatment, so it was not used as a housekeeping cmiRNA. Instead, the cmiRNA expression was normalized to the mean expression on day 0 or in untreated mice.

qRT-PCR was performed with all 34 cmiRNA candidates identified in the discovery study (Fig. 6A-C; Supp. Table 6). For this analysis, samples were investigated from the laser treated mice taken at four timepoints: day 0, day 3, day 7, and day 14. The expression of each target cmiRNA was normalized to the mean expression on day 0. Normal distribution was evaluated using the Kolmogorow-Smirnow test. In this analysis, the expression data were not normally distributed, so a U-test was used to test for significance. The statistical analysis performed in this dissertation is in line with the analyses performed in similar projects (120,131). In the publication which arose from this body of work, the qRT-PCR data were independently analyzed by Christina Kiel (Ph.D. student, Institute of Human Genetics Regensburg) using the TMM normalization algorithm (67).

Multiple cmiRNA showed prominent fluctuations on day 0: mir-140-3p, mir-191-5p, mir-361-5p, and mir-424-5p. Interestingly, the cmiRNA expression at the other timepoints showed more moderate fluctuations. Nevertheless, three cmiRNA were significantly dysregulated after laser treatment: mir-7g-3p, mir-155-5p, and mir-20a-5p. Mir-7g-3p was downregulated on day 7, and mir-155-5p was upregulated on day 14. Mir-20a-5p was upregulated at all three timepoints post laser treatment: day 3, day 7, and day 14.

The expression of a portion of the cmiRNA candidates, was investigated in a second comparison between the day 14 samples from the laser treated mice and untreated mice (Supp. Fig. 4; Supp. Table 7). The expression of the target cmiRNA was analyzed as described previously with one modification: the expression was normalized to the mean expression of the untreated samples. The expression data were normally distributed, so a student t-test was used to test for significance.

Again, the expression of some cmiRNA exhibited fluctuations in the control samples. Five cmiRNA were significantly downregulated in the samples taken from the laser treated mice: mir-15b-3p, mir-25-3p, mir-101a-3p, mir-140-3p, and mir-191-5p. Two of the cmiRNA which were significantly dysregulated in the previous comparison (mir-7g-3p and mir-20a-5p) were investigated in the second comparison, but were not significantly dysregulated.

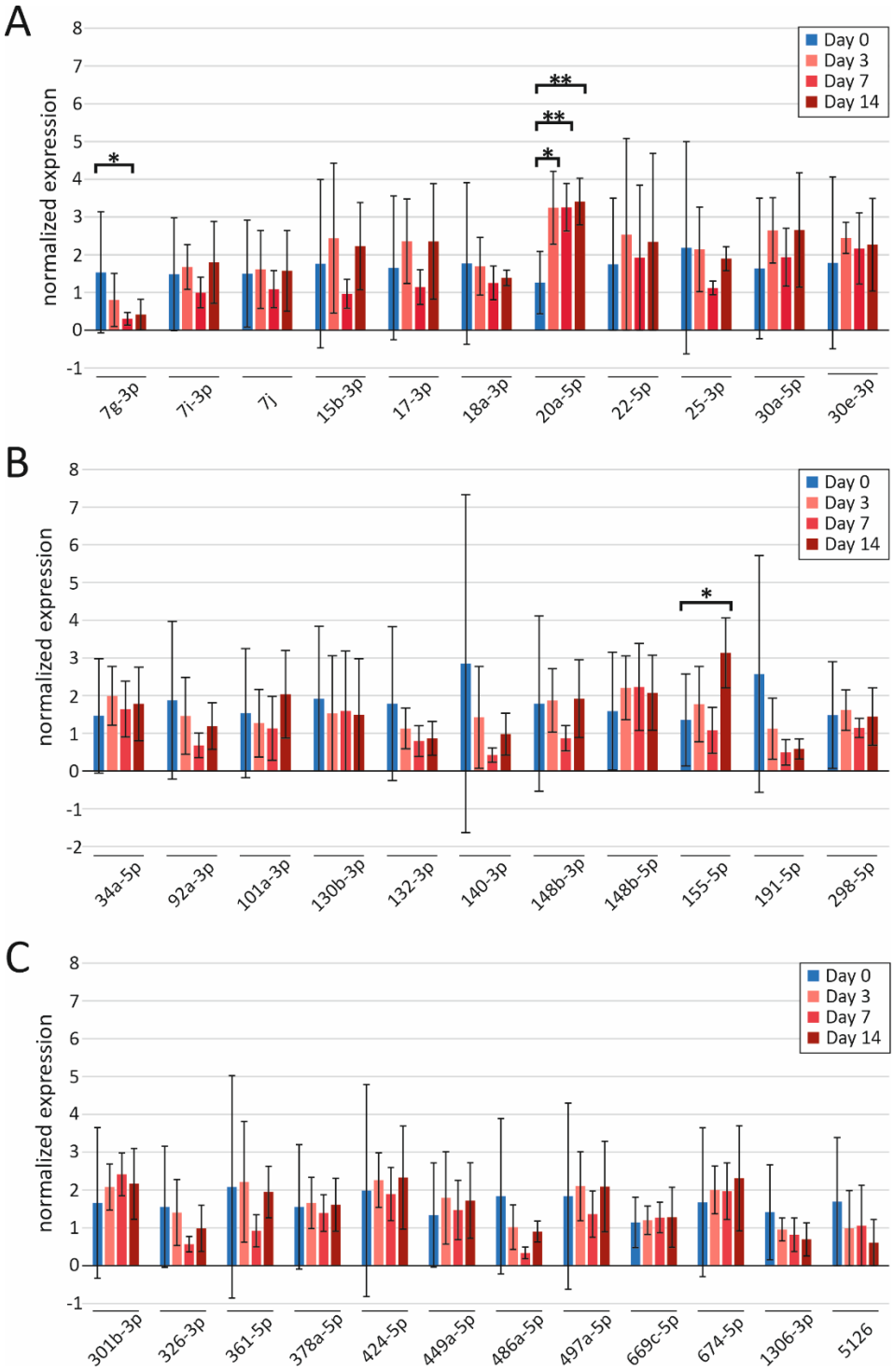

Figure 6: Replication Study 1 Expression of 34 cmiRNA Candidates. The expression of 34 cmiRNA, normalized to the mean expression on day 0 are shown. (A) The expression of mmu-let-7g-3p through mmu-mir-30e-3p are shown. The expression of mmu-let-7g-3p was significantly downregulated on day 7 (p-value = 0.01), and mmu-mir-20a-5p was upregulated on day 3 (p-value = 0.016), day 7 (p-value = 0.004), and day 14 (p-value = 0.004). (B) The expression of mmu-mir-34-5p through mmu-mir-298-5p are shown. The expression of mmu-mir-155-5p was significantly upregulated on day 14 (p-value = 0.047). (C) The expression of mmu-mir-301-3p through mmu-mir-5126 are shown. The prefix of each cmiRNA is mmu-mir, except mmu-let-7g-3p, mmu-let-7i-3p, mmu-let-7j. n = 6 per timepoint, * p-value < 0.05, ** p-value < 0.01 (U-Test).

3.2.3. Replication Study 2

RNA was isolated from the blood samples of treated mice. The total RNA concentration of the samples was estimated using a Nano Drop ND-1000 Spectrophotometer (Supp. Table 8). No significant differences in the total RNA concentration between the samples pre (day 0) and post laser treatment (day 3, day 7, and day 14) were observed (Supp. Fig. 5). The samples were subsequently reverse transcribed and qRT-PCR was performed.

In the replication study 2, the expression of 21 cmiRNA candidates were investigated (Supp. Fig. 6; Supp. Table 9). The expression was analyzed as described previously. In this data set, eleven cmiRNA were upregulated on day 14 (let-7i-, mir-17-3p, mir-20a-5p, mir-30a-5p, mir-30e-5p, mir-301b-3p, mir-322-5p, mir-326-3p, mir-449a-5p, mir-497a-5p and mir-674-5p). One of these cmiRNA was also significantly upregulated on day 14 in replication study 1 (mir-20a-5p). No cmiRNA were significantly downregulated on day 14, or were dysregulated in either direction on day 3 or day 7.

The qRT-PCR data from replication study 1 and 2 were analyzed using the TMM normalization method by Dr. Grassmann (former employee of the Institute of Human Genetics, Director Prof. Dr. Weber) (126), and the top ten dysregulated cmiRNA with the strongest effect sizes were identified. For this dissertation, the expression of the top ten cmiRNA was independently analyzed in the combined data sets from replication study 1 and 2 (Fig. 7; Supp. Table 10). In this analysis, the data from replication study 1 and 2 were normalized separately to the mean expression on day 0.

The expression on day 0 fluctuated strongly for some cmiRNA (mir-140-3p and mir-191-5p), while others showed a fairly moderate variation (mir-20a-5p and mir-298-5p). Out of the top ten cmiRNA, seven were significantly dysregulated on at least one timepoint. Five cmiRNA were upregulated on day 14: mir-20a-5p, mir-30a-5p, mir-30e-5p, mir-449-5p, and mir-674-5p. Two cmiRNA were downregulated on day 7: mir-191-5p and mir-486a-5p. One cmiRNA was upregulated at two timepoints: mir-449-5p on day 3, and day 14. In total, at least one cmiRNA was significantly dysregulated at each timepoint, and the majority were dysregulated on day 14.

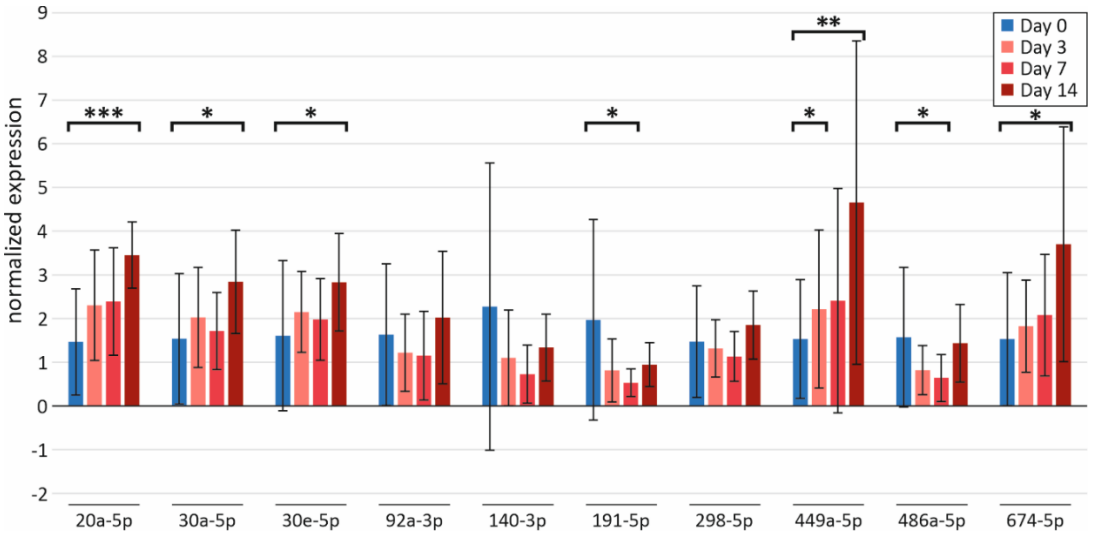

Figure 7: Top Ten Differentially Expressed cmiRNA in Replication Study 1 & 2. The expression of the top ten cmiRNA in laser treated mice is shown. Mmu-mir-20a-5p was upregulated on day 14 (p-value = 0.001), mmu-mir-30a-5p was upregulated on day 14 (p-value = 0.02), mmu-mir-30e-5p was upregulated on day 14 (p-value = 0.01), mmu-mir-191-5p was downregulated on day 7 (p-value = 0.03), mmu-mir-449-5p was upregulated on day 3 (p-value = 0.01) and day 14 (p-value = 0.005), mmu-mir-486a-5p was downregulated on day 7 (p-value = 0.02), and mmu-mir-674-5p was upregulated on day 14 (p-value = 0.02).The prefix of each cmiRNA is mmu-mir- except for mmu-let-7i-3p. Expression levels from replication study 1 & 2 were normalized separately. N = 12 per timepoint, * *p*-value < 0.05, ** *p*-value < 0.01 (U-Test).

3.2.4. Tissue Study

In the tissue study, we aimed to analyze ocular tissue for the top ten dysregulated cmiRNA, which had been identified in the discovery study and corroborated in the replication studies 1 and 2. Therefore, retinal and RPE/choroid tissue samples were acquired from eleven laser treated and twelve untreated mice (Fig. 8A).

RNA was extracted from the tissue samples, reverse transcribed, and evaluated for quality of RNA (Fig. 8B). The qRT-PCR primers from the replication studies were tested in the ocular tissue samples, with assistance from Christina Kiel (Ph.D. student, Institute of Human Genetics Regensburg).

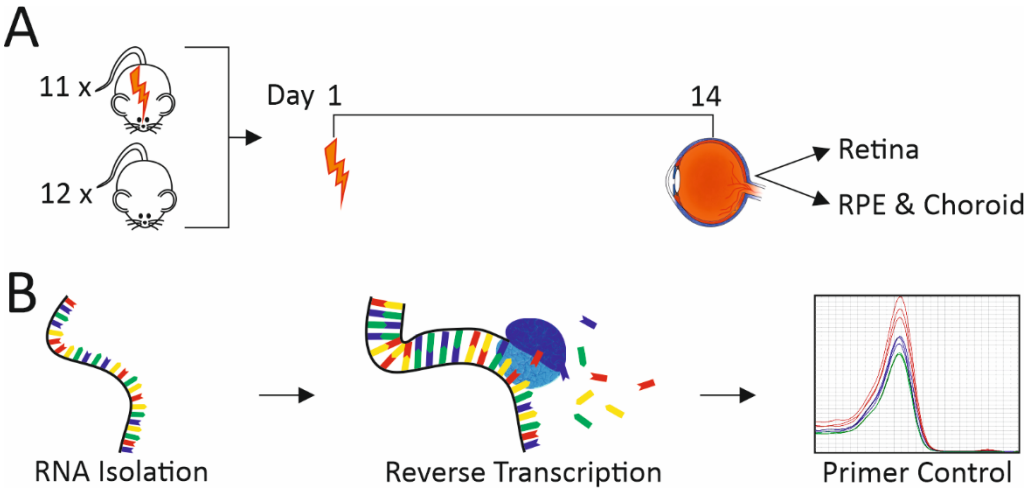

Figure 8: Ocular cmiRNA Expression Workflow Overview. We aimed to investigate the expression of the top ten dysregulated cmiRNA in ocular tissue. (A) Eleven mice received laser treatment on day 1. On day 14, retinal and RPE/choroid tissue samples were extracted from the laser treated and untreated animals. (B) RNA was isolated from the ocular tissue samples, and reverse transcribed. In preparation for the qRT-PCR the quality of the qRT-PCR oligonucleotide primers were evaluated based on their melting curve profiles.

First, RNA was isolated from the tissue samples of treated and untreated mice, and the total RNA concentration was estimated using a Nano Drop ND-1000 Spectrophotometer (Supp. Table 11). No significant differences were observed between the treated and untreated samples (Supp. Fig. 7). The samples were subsequently reverse transcribed to cDNA.

The qRT-PCR primers which were validated in the replication studies using blood samples, were retested for specificity in the tissue samples (Fig. 9). In contrast to the replication studies, where all primers passed this quality control step, multiple primers performed very poorly in the tissue samples. Some primers showed a poorly defined peak (mir-92a-3p in RPE/choroid), or multiple peaks (mir-92a-3p in retina, and mir-298-5p in retina and RPE/choroid). There were some primers which performed well in the ocular tissue samples (mir-30a-5p). Regardless, many primers had to be modified prior to the expression analysis. This modification and reevaluation was performed by Christina Kiel, and was not conducted as part of this dissertation.

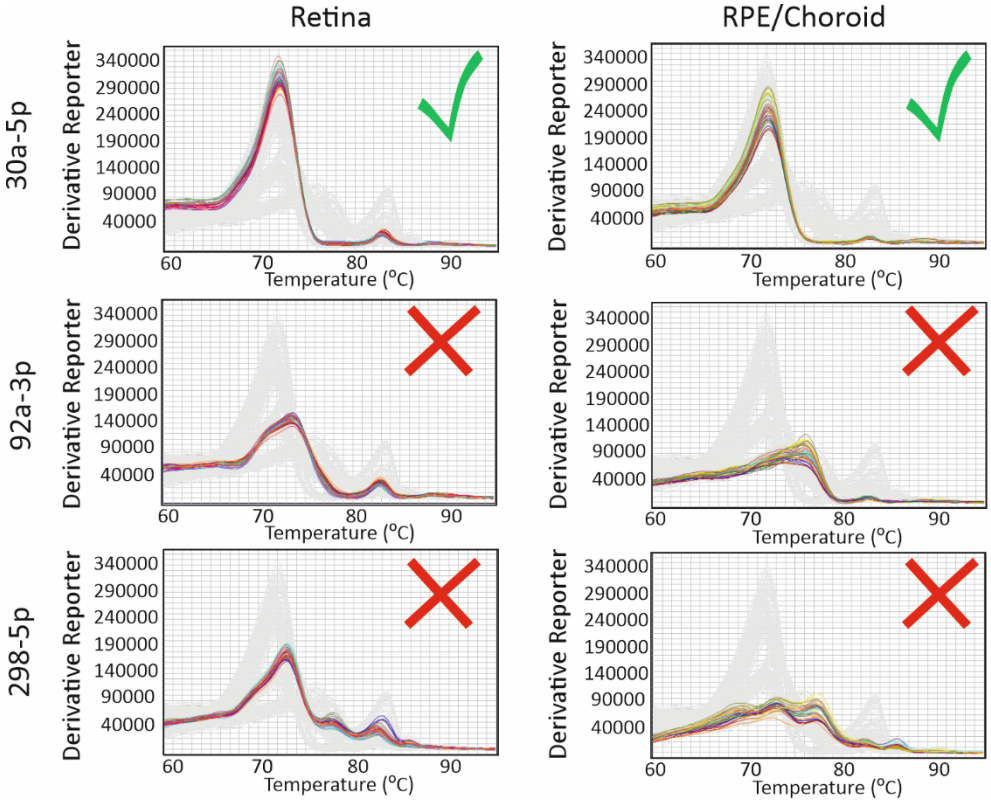

Figure 9: Primer Quality Control in Ocular Tissue. Melt curve profiles of three exemplary qRT-PCR primers in retina and RPE/choroid samples are shown. Primers which showed a single peak in the melt curve profile, were considered of sufficient quality for qRT-PCR (mir-30a-5p, green checkmark). Primers which showed multiple or poorly defined peaks were considered of insufficient quality for qRT-PCR experiments (mir-92a-3p and mir-298-5p, red X). The prefix of each miRNA is mmu-mir-.

3.3. Dysregulated cmiRNA in OIR

The aim of the following work was to investigate the expression of the top ten dysregulated cmiRNA identified and corroborated in laser-induced CNV mouse model, in a second murine model of retinal neovascularization and inflammation, namely OIR. In OIR, preretinal neovascularization is induced by exposing 7 day old mouse pups to hyperoxia for 5 days, followed by the return to room air for 4 days (Fig. 10A). The exposure to hyperoxia inhibits retinal vascular development and obliterates preexisting capillaries (61). After P12 the mice are returned to room air causing the vasoobliterated retina to become hypoxic, which in turn triggers neovascularization (hypoxic phase) (60). OIR was performed by PD Dr. Ohlmann and colleagues (Institute of Human Anatomy and Embryology, Director Prof. Dr. Tamm).

As in the laser-induced CNV study, RNA was isolated from the blood samples and reverse transcribed followed by qRT-PCR (Fig. 10B). CmiRNA expression was investigated in the treated mice in comparison to the controls, in order to identify cmiRNA which were dysregulated as a result of OIR treatment.

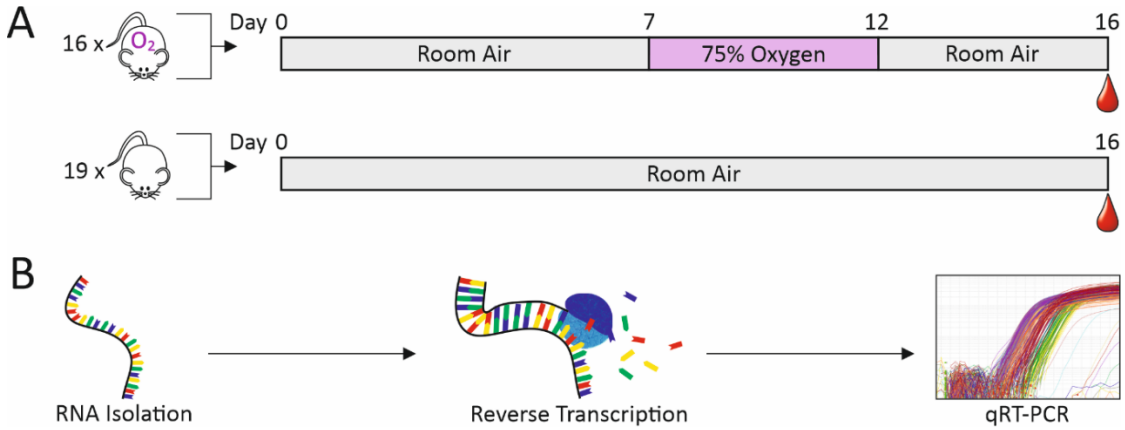

Figure 10: OIR Workflow. Investigation of the top ten dysregulated cmiRNA from the laser-induced CNV mouse model, in a second murine model of retinal neovascularization and inflammation: OIR. (A) Sixteen mice were transferred from room air to 75% oxygen on p7. After 5 days at 75% oxygen, the mice were returned to room air for 4 days. Blood samples were extracted from the OIR mice, and 19 control mice, on p16. (B) RNA was isolated from the blood samples and reverse transcribed. qRT-PCR was performed to investigate the cmiRNA expression.

RNA was isolated from the blood samples of OIR treated and untreated mice. The total RNA concentration was measured using a Nano Drop ND-1000 Spectrophotometer, and the size distribution of the small RNAs was measured using an Electrophoresis Bioanalyzer System (Supp. Table 12). As in the laser-induced CNV study, the samples contained mostly large RNAs and a moderate portion of cmiRNA, and a regression analysis showed a weak correlation between cmiRNA and total RNA concentration (Supp. Fig. 8). No significant differences were observed between the samples from treated and untreated mice, so the samples were reverse transcribed.

qRT-PCR was performed to investigate the expression of the top ten cmiRNA identified in the laser-induced CNV model (Fig. 11; Supp. Table 13). The expression was normalized to the mean expression of the samples from untreated mice. In total, nine out of ten cmiRNA were significantly dysregulated in the treated mice: mir-20a-, mir-30a-5p, mir-30e-5p, mir-92a-3p, mir-191-5p, mir-298-5p, mir-449a-5p, mir-486a-5p, and mir-674-5p. Curiously, each cmiRNA was significantly downregulated in the treated mice, whereas none were upregulated. The only cmiRNA which was not significantly dysregulated in the OIR study was mir-140-3p.

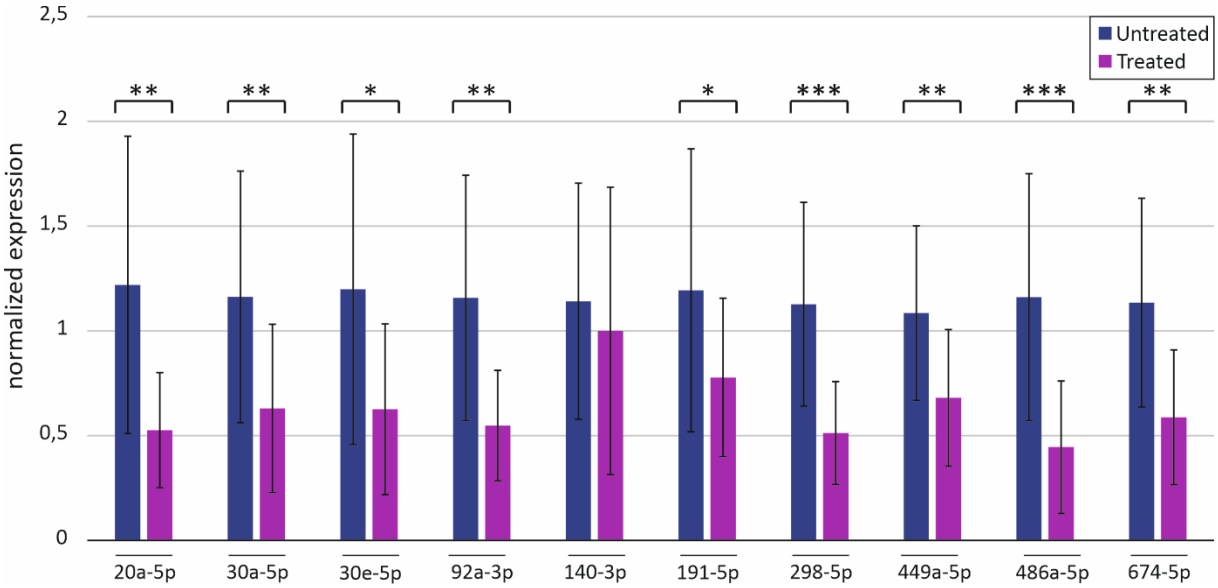

Figure 11: cmiRNA Expression in OIR Mice. The expression of the top ten dysregulated cmiRNA identified in the laser-induced CNV model was investigated in OIR treated mice. The expression, normalized to the mean expression of the controls, is shown. Nine cmiRNA were significantly downregulated in the treated mice: mir-20a-5p (p-value = 0.002), mir-30a-5p (p-value = 0.007), mir-30e-5p (p-value = 0.014), mir-92a-3p (p-value = 0.001), mir-191-5p (p-value = 0.047), mir-298-5p (p-value = 1.8 x 10^{-04}), mir-449a-5p (p-value = 0.005), mir-486a-5p (p-value = 2.6 x 10^{-04}), and mir-674-5p (p-value = 0.001). The prefix of each cmiRNA is mmu-mir-. n = 16 treated and 19 untreated mice, * p-value < 0.05, ** p-value < 0.01, *** p-value < 0.001 (student t-test).

4. Discussion

The aim of this study was to conduct a literature analysis of differentially expressed cmiRNA in nAMD patients, and to identify cmiRNA which are dysregulated in two murine models of retinal neovascularization and inflammation: laser-induced CNV and OIR. In the laser-induced CNV model, cmiRNA dysregulation was investigated in three successive experiments, in a discovery study and two replication studies. In the discovery study, 34 candidate cmiRNA were identified via NGS. The cmiRNA candidates were then reduced stepwise in two replication studies, via qRT-PCR. In replication study 1 the expression of all 34 candidates was investigated, whereas in replication study 2 the expression of 21 cmiRNA candidates was investigated. The top ten cmiRNA candidates were analyzed in the pooled data from both replication studies, which ultimately revealed seven significantly dysregulated cmiRNA. The top ten cmiRNA were further investigated in the OIR treated mice, which revealed nine significantly dysregulated cmiRNA. When the results from both models are compared, two cmiRNA were dysregulated in the same direction in both models (mir-191-5p and mir-486a-5p), two cmiRNA were exclusively dysregulated in OIR treated mice (mir-92a-3p and mir-298-5p), and five cmiRNA were dysregulated in opposite directions (mir-20a-5p, mir-30a-5p, mir-30e-5p, mir-449a-5p, mir-674-5p) (Fig. 12). These results are intriguing,

because when the models are regarded separately, each provides a straightforward narrative of cmiRNA dysregulation. When the results are taken together, the narrative is dismantled to reveal a higher order of complexity. This complexity encourages further deliberation about the source and implication of these findings, as well as their place in the context of previous research.

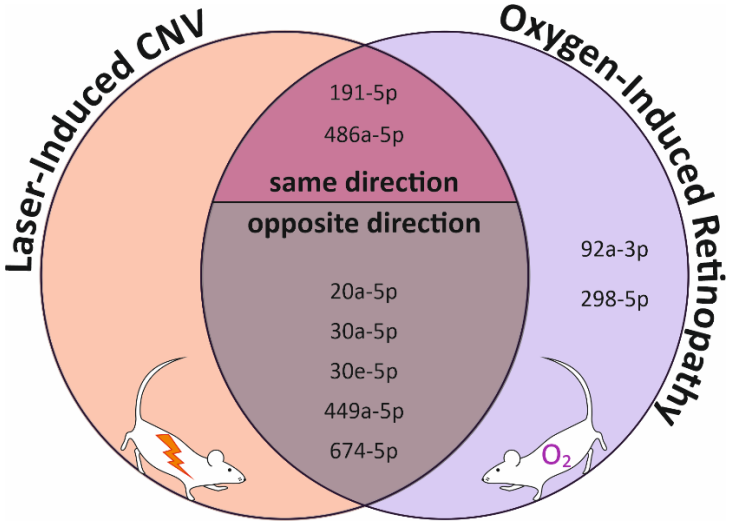

Figure 12: Differentially Expressed cmiRNA in Two Murine Models of Retinal Neovascularization and Inflammation. CmiRNA expression was investigated in mice treated with laser-induced CNV (orange circle) or OIR (purple circle). The cmiRNA which were significantly dysregulated in each model are shown. Two cmiRNA were upregulated in both models: mir-191-5p and mir-486a-5p (red sector, labeled 'same direction'). Five cmiRNA were upregulated in the laser-induced CNV model and downregulated in the OIR model: mir-20a-5p, mir-30a-5p, mir-30e-5p, mir-449a-5p and mir-674-5p (grey sector, labeled 'opposite direction'). Two cmiRNA were downregulated exclusively in the OIR treated mice: mir-92a-3p and mir-298-5p (purple sector).

Over the past few years, multiple research groups have investigated cmiRNA expression directly in nAMD patients (92,93,111,113–121). CmiRNA are the focus of multiple studies, since they are accessible by a simple blood draw, allowing researchers a practicable means of procurement. In this dissertation, an overview of the differentially expressed cmiRNA in these studies was compiled. Publications which had prominent differences in their study design, such as the inclusion of patients with other retinal comorbidities (113–116), were excluded from the compilation. Although the remaining studies were performed under similar conditions, they show very little consensus as to which cmiRNA are truly dysregulated in nAMD.

Across all 9 included studies, 54 cmiRNA were significantly dysregulated in the patient cohorts, which the authors concluded to mean that these cmiRNA are associated with nAMD (92,93,111,117–122). That interpretation loses merit, when the results from each study were compared to one other. The majority of cmiRNA (47/54 = 87 %) have not been replicated by

an independent research group. Only four cmiRNA were dysregulated in the same direction in two independent studies: mir-16-5p (93,122), mir-25-3p (117,122), mir-126-3p (121,122) and mir-223-3p (93,117). Furthermore, two cmiRNA were also dysregulated in two independent studies, but in opposite effect directions: mir-150-5p (92,93) and mir-146a-5p (117,118).

One of the fundamental principles of scientific discovery is the importance of reproducibility, i.e. if two people perform the same experiment, under the same conditions, they should achieve the same result. Nine independent groups have investigated cmiRNA expression in nAMD patients, but their results are largely irreconcilable with each other. Although some discrepancies are to be expected, the abundance of irreproducible results should inspire deliberation about the source of these inconsistencies, before correlating them to the results of the current study.

One explanation for the inconsistent cmiRNA profiles is aberrant patient inclusion criteria. nAMD is a chronic disease, which develops over the course of several years, if not decades. It is plausible that cmiRNA profiles vary according to disease status, and that a certain set of cmiRNA may be associated with disease onset, while others may be associated with long-term disease. Two studies only included patients which were “newly diagnosed” with nAMD (93,117), implying the pathology had recently progressed from early AMD to nAMD. Another publication focused on “previously diagnosed” patients, which could have included patients that had been diagnosed with nAMD years earlier. For the most part, the patient inclusion and exclusion are described very generally in each study, making it difficult to draw conclusions about their similarities.

The identification of a suitable control population presents another challenge. Ideally, researchers would compare the cmiRNA profiles of persons solely affected by nAMD, with age-matched, sex-matched healthy controls. This is an immense challenge because nAMD predominantly affects the elderly, and it can be very difficult to recruit healthy controls at this age. In 2014, 86 % of Italians over the age of 65 had at least one chronic condition (132), and 76 % of Americans over the age of 75 had at least one of the four following chronic conditions: cardiovascular disease, cancer, diabetes and/or chronic respiratory disease (133). Since healthy controls are scarce, the next best approach would be to compare nAMD patients to controls with a comparable spectrum of illnesses. In this endeavor, the studies on nAMD-related cmiRNA profiles have left considerable room for improvement. Many publications claim their control groups had no retinal diseases, but do not exclude patients who have a systemic disease which are known to cause retinal damage such as hypertension and diabetes (92,93,119).

Hypertensive retinopathy and diabetic retinopathy can impact retinal health before they are apparent funduscopically, and thereby potentially confound the cmiRNA profile. The control population from another publication had an ocular pathology which required a surgical intervention, such as a macular hole or an epiretinal membrane (118). Interestingly, one publication performed an analysis which demonstrated that two out of three significantly dysregulated cmiRNA were strongly confounded by glaucoma disease status (111). This analysis demonstrates that the selection of the control cohort is essential for the successful identification of a nAMD-related cmiRNA profile. Furthermore, the effects of suboptimal recruiting conditions could be mitigated with a sufficient sample size, but most studies have investigated fewer than 150 individuals (92,117,118,120,121).

Another source of discrepancy could be methodological differences between the studies. For example, different strategies were used to identify cmiRNA for investigation. One group chose cmiRNA from literature (93), another study performed NGS (111), and many performed a miRNA array or used a commercially available primer set (117,119–122). Furthermore, while almost all studies performed RT-PCR during their investigations, most groups normalized their values differently. Five studies used a reference gene as a housekeeper, but they all chose different ones: mir-93 (93), mir-451a-5p (111), mir-423-5p and mir-425-5p (121), mir-16 (118), 18S RNA (119), or mir-323-3p and mir-324-3p (122). A housekeeping gene can differ between publications without confounding the results, but it should be properly validated. In this study, we investigated the expression of mir-451a-5p with the intention of using it as a housekeeper, as per (111). We observed, however, that this cmiRNA was significantly dysregulated in the samples from mice which were exposed to laser treatment, thereby invalidating it as a standard to equilibrate gene expression. In contrast, a previous study diligently investigated the same cmiRNA in their samples, and found that it was a suitable housekeeper for their application (111). This demonstrates that housekeeping genes should be routinely tested, even if they passed quality control standard in previous publications.

The previously mentioned criteria (participant selection, normalization strategy, and sample size) could be used to assess the quality of each individual study. Here, it is interesting to take a closer look at the most recent publication, since it replicated four cmiRNA from previous studies (122). First of all, this was the first study which deliberately excluded patients and controls with coexisting ocular pathologies and systemic diseases which can cause retinal damage. The authors' prudence is commendable, but it was presumably detrimental to the study size. Only 40 patients and 40 controls were included, whereas the previous average was 77,5 patients and 79 controls per study. Nevertheless, the authors demonstrated further discretion in

the selection of a suitable housekeeping cmiRNA which was consistently expressed in their samples. Whether these decisions were the reason why they were able to replicate four cmiRNA is difficult to determine, and it should be noted that one of the cmiRNA was replicated in the opposite effect direction. Still, the findings imply that methodological acumen could be essential in further investigations.

Overall, the high variability of nAMD-related cmiRNA expression in literature, implies that miRNA expression is subject to fluctuations. This hypothesis is strengthened by considering miRNA function. MiRNA buffer against changes in gene expression due to cellular stress, in order to maintain homeostasis (134). It is therefore plausible that many factors can influence miRNA expression, which should be taken into account when designing a study. In this study, we investigated cmiRNA dysregulation in two murine models: laser-induced CNV and OIR. We also investigated samples from four sets of mice: one set in the discovery study, two in the replication studies, and one in the OIR study. By choosing two murine models which utilize different triggers to produce the same retinal endpoint, we aimed to identify cmiRNA which are robustly associated with retinal inflammation and neovascularization. We successfully identified two cmiRNA which were dysregulated in the same direction in both models, although we were surprised to discover that five cmiRNA were dysregulated in opposite directions and two were dysregulated exclusively in OIR mice. A possible explanation for the divergent results is that cmiRNA dysregulation is heavily influenced by the disease trigger, in this case laser treatment or oxygen manipulation.

To understand how different disease triggers may impact cmiRNA dysregulation, it is worthwhile to garner a deeper understanding of the disease models, especially OIR. The OIR model is a widely used approach to model neovascular phenotypes, which implements transient hyperoxia to induce a retinal insult. It has previously been used to model nAMD (66), but it was originally established as a model for a different disease: ROP ((135), reviewed in (136)). When an infant is born prior to 31 weeks gestation (37-42 weeks are considered full-term) the retinal vessels may not be sufficiently developed to supply the entire retina with oxygen and nutrients. After birth, metabolically active but poorly vascularized regions become hypoxic, which triggers a feedback loop that ultimately induces retinal neovascularization. As in nAMD, these friable vessels are prone to bleeding, which causes retinal scarring and can lead to retinal detachment. This pathology is known as ROP (reviewed in (74)).

In the OIR mouse, seven day-old pups are exposed to very high oxygen levels (usually 75 %) for 5 days, which causes retinal vessels to obliterate (hyperoxic phase). When the pups are

returned to room air, the retina becomes hypoxic, which triggers retinal neovascularization (hypoxic phase). The retinal neovascularization can be quantified by analyzing FITC dextran-perfused retinal whole-mounts. Many research groups have used this model for its reliability, since it generally produces characteristic results. A drawback of this model, however, is that even though it is called “oxygen-induced retinopathy”, the pathologic repercussions of the oxygen treatment are not limited to the retina. In fact, a very similar method is used to model bronchopulmonary dysplasia (BPD) (137,138).

In the murine BPD model, three day old mouse pups are exposed to hyperoxia (many variations exist, but usually around 60-65 % oxygen) for a few days or weeks (reviewed in (137)). Researches then investigate the toxic effects of oxygen treatment on the lung tissue. One publication showed that hyperoxia-exposed mice exhibited a dramatic decrease of alveolarization and significantly increased granulocyte infiltration in the lung tissue (138). Another study which exposed rat lung slices to 85 % oxygen, showed that hyperoxia increased the pulmonary production of oxygen radicals (139). On a cellular level, hyperoxia was shown to inhibit proliferation and activate cell death mediators, in human lung epithelial cells and fetal rat lung fibroblasts (140).

In our study, we sought to identify a cmiRNA profile which is robustly linked to retinal neovascularization and inflammation in mice independent of a pathologic trigger, and to draw parallels to cmiRNA dysregulation in nAMD patients. Although the OIR model consistently and reliably produces the desired retinal phenotype, the hyperoxic conditions implemented in this model likely have pathologic effects on other organ systems. Hyperoxia is known to produce a pulmonary phenotype, but it is a reasonable hypothesis that the detrimental effects of oxygen manipulation may extend well beyond the lung, to the entire organism. A well-known side effect of the OIR model, is that mice exhibit a growth retardation in comparison to normoxic controls (141). Of course, this measurement is fairly imprecise, and cannot be used to gain insight into the pathomechanism underlying the weight loss. Nevertheless, it demonstrates that oxygen treatment has far reaching consequences beyond retina. It is likely that the cmiRNA dysregulation which we observed in OIR treated mice was influenced by pathogenic developments in extra-retinal organs.

In our study, two cmiRNA were significantly dysregulated in the OIR treated mice but not the laser treated mice (mir-92a-3p and mir-298-5p were downregulated). A possible explanation for this finding, is that the downregulation of these cmiRNA was caused by an

extra-retinal hyperoxia response. To test this theory, a literature search for investigations into the function of these miRNA was conducted.

Multiple previous investigations have suggested that the expression of one of the cmiRNA exclusively dysregulated in OIR, mir-92a-3p, regulates neovascularization (142–144). One of the earliest studies on *in vivo* miRNA function administered a mir-92a antagomir in murine models of limb ischemia and myocardial infarction, and demonstrated improved blood vessel growth (145). These results inspired more studies which aimed to further characterize the proangiogenic effect of mir-92a downregulation. A synthetic mir-92a inhibitor was shown to accelerate angiogenesis in diabetic and nondiabetic mice with cutaneous wounds (146). Furthermore, mir-92a inhibition enhanced angiogenesis and bone healing in mice with femur fractures (147). Taken together, these studies suggest that mir-92a downregulation promotes angiogenesis. Of note, an antiangiogenic effect of mir-92a overexpression has been observed (145), although this was not reproducible in downstream studies (67,143).

In contrast to mir-92a-3p which has been linked to neovascularization by multiple groups, little is known about the function of mir-298-5p. Of the few studies which have investigated this miRNA, the strongest known association is to tissue ischemia. One study showed that mir-298 was downregulated after myocardial infarction in a rat model (148), while another study showed it was downregulated after ischemic stroke in mice (149). Both studies investigated a possible relationship of mir-298 to apoptosis, but observed contradictory results. One of the studies observed that mir-298 upregulation inhibited the expression of apoptosis-related proteins (148), while the other study showed enhanced apoptosis (149).

In our study, mir-92a-3p and mir-298-5p were downregulated in OIR treated mice. Placing these findings in the context of other publications corroborates the theory that these effects were caused by the extra-retinal response to OIR. It is plausible that mir-92a-3p downregulation was caused by neovascularization and mir-298-5p downregulation was triggered by tissue ischemia. One question which remains is why mir-92a-3p downregulation was not observed in the laser-induced CNV model, which also causes neovascularization. Here, the answer may be an insufficient sample size. In one of the publications which arose from this dissertation, the cmiRNA expression of six additional mice was investigated. In this sample cohort, mir-92a-3p was significantly downregulated after laser treatment.

In contrast to the OIR model, the second disease model used in this study selectively targets the retina. In laser-induced CNV, an argon laser perforates the Bruch's membrane, which triggers an inflammatory and neovascular ocular response. Three days after laser treatment,

immune cells invade the retina, and seven days after treatment the neovascular surface area peaks (59). Although it is possible that the laser treatment produces a response in an unintended organ, it is fairly unlikely, since the insult is directed specifically to the Bruch's membrane.

No cmiRNA were exclusively dysregulated in the laser-induced CNV model, but two cmiRNA were dysregulated in both models: mir-191-5p and mir-486a-5p. We hypothesize that the downregulation of these two cmiRNA was caused by retinal inflammation and neovascularization. Interestingly, previous investigations have already linked both cmiRNA to nAMD. Mir-486a-5p was upregulated in serum exosomes from nAMD patients (120), and mir-191-5p was upregulated in plasma samples from nAMD patients (93). In contrast, both cmiRNA were downregulated in our samples. In the laser-induced CNV model, mir-191-5p and mir-486a-5p were significantly downregulated at one of the three investigated timepoints: day 7. At this timepoint, previous studies have shown that the neovascular surface area reaches its maximum (59). In contrast to the laser-induced CNV model, one timepoint of prominent neovascularization was investigated in the OIR model (61). Both cmiRNA were downregulated at this timepoint, but it is unclear whether this downregulation was constant over time, or if by chance the dysregulated timepoint was selected. It is possible that mir-191-5p and mir-486a-5p expression fluctuates over the course of disease progression, and are not constantly dysregulated in either direction. For example, if these cmiRNA are downregulated during acute neovascularization but increase as a compensatory mechanism during chronic disease, this could explain the divergent results in our murine models vs. the nAMD patient studies.

Another explanation for the divergent results, is that cmiRNA expression is influenced by the disease trigger. To this end, our results indicate that mir-191-5p and mir-486a-5p are downregulated as a result of an external insult: laser treatment or oxygen manipulation. Although nAMD has a similar retinal endpoint of neovascularization and inflammation, in nAMD retinal disease progresses from early AMD. Similar phenomena, where a chronic disease develops an acute component, are referred to as 'acute-on-chronic' disease progression. Although the term is not commonly used in the context of AMD, one could argue that the progression of nAMD from early AMD, fits the description of acute-on-chronic. If the direction of cmiRNA dysregulation is influenced by the disease trigger, it is plausible that an external insult such as laser treatment or oxygen manipulation, and an acute-on-chronic disease progression produce diverging results.

To take it one step further, we also observed that the type of external insult, i.e. laser treatment or oxygen manipulation, produced antagonistic results. Five cmiRNA were

dysregulated in opposite directions in the two models: mir-20a-5p, mir-30a-5p, mir-30e-5p, mir-449a-5p, and mir-674-5p. All five cmiRNA were upregulated on day 14 in laser treated mice (mir-449a-5p was also upregulated on day 3), and downregulated in OIR treated mice. If only one or two cmiRNA were dysregulated in opposite directions, one could theorize that the oxygen manipulation and laser treatment produce antagonistic side effects, which are not directly related to the retinal phenotype. Out of the ten investigated cmiRNA however, half were dysregulated in opposite directions. Admittedly, it is not unheard of that cmiRNA are unexpectedly dysregulated in opposite directions in similar projects. As mentioned previously, two cmiRNA were upregulated in one study of nAMD patient samples, and downregulated in another (mir-146a-5p and mir-150-5p). Every meaningful scientific undertaking has outliers which have the potential to cloud the path of scientific discovery. A prominent example of this are investigations into the efficacy of homeopathic treatments. Sporadic publications indicate an improvement in clinical endpoints relative to a placebo, whereas extensive meta-analyses do not observe a reproducible effect (150–154).

Contrary to the investigations into homeopathy, where the bulk of scientific evidence does not substantiate a therapeutic effect, cmiRNA dysregulation shows a much more heterogeneous picture. In the case of cmiRNA dysregulation in laser-induced CNV, OIR, and nAMD patients it would be negligent to call the observed discrepancies a scientific outlier. Instead, a logical and probable conclusion is that cmiRNA expression is heavily influenced by a disease trigger, and inherently prone to fluctuations.

Our theory that miRNA expression is inherently prone to fluctuations, is underscored by the variability we observed in untreated mice. In our study, we investigated cmiRNA expression in three sets of untreated mice during the laser-induced CNV study: the day 0 and day 14 samples in replication study 1, and day 0 samples in replication study 2. The cmiRNA expression in these samples exhibited prominent fluctuations, especially in the day 0 samples from replication study 1. The samples from untreated mice which were acquired and analyzed during the OIR study were also fairly heterogeneous. This demonstrates that baseline cmiRNA expression vacillates even without any external intervention. Interestingly, the variability appeared to decrease in the samples after laser treatment. This could indicate that the laser treatment harnessed the cmiRNA profile and directed it to a certain expression motif. Nevertheless, the fluctuation we observed in untreated mice underscores the need for a comprehensive and thoroughly validated normalization method when investigating cmiRNA expression.

The fluctuations we observed in the untreated samples could explain some of the discrepancies in our two murine models of neovascularization. It is unlikely, however, that these fluctuations were the underlying reason why five cmiRNA were dysregulated in opposite directions. Instead, this effect appears to be more closely related to the disease trigger. Therefore, it may be worthwhile to replicate nAMD more closely in mice. In this study, we used drug and test naïve mice. Samples from OIR treated mice were acquired when the mice were 16 days old, and samples from laser treated mice were around 3 months old. These conditions could be manipulated, in order to more closely mimic acute-on-chronic nAMD pathogenesis, by emulating environmental AMD risk factors.

Previous studies have simulated environmental AMD risk factors in mice, by providing the mice with a high fat diet, exposing them to cigarette smoke, and by investigating mice near the middle to end of their natural lifespan (156,157). These mice sporadically showed some signs of a retinal pathology, such as the development of nodular basal laminar deposits and a thickening of the Bruch's membrane (156,157). Although these conditions do not replicate nAMD, they can be layered with a second intervention. Laser-induced CNV performed with the aged mice fed a high fat diet and exposed to cigarette smoke, could emulate an acute-on-chronic disease progression. Interestingly, laser-induced CNV performed in aged mice (158) and middle-aged mice exposed to nicotine (159) showed that age and nicotine exposure was associated with larger CNV lesions. To take this a step further, young mice which received a bone marrow transplant from older mice before laser treatment, showed an increased susceptibility to laser treatment (160). This indicates that mobile elements in the blood stream can influence the development of a retinal pathology, despite the shielding effect of the blood-retinal barrier. Serial investigations into cmiRNA expression in the aged mice, fed a high fat diet and exposed to cigarette smoke before and after laser treatment, could help identify cmiRNA which are related to an nAMD-like pathology in mice. In regards to the previously discussed variability, appropriate controls would have to be diligently selected in order to decrease the likelihood of identifying false hits. Ideally, an equal number of control mice would be assigned to every layer of the intervention (diet, cigarette smoke exposure, and laser treatment). Nevertheless, if cmiRNA expression is largely dependent on a disease trigger, mimicking acute-on-chronic disease progression could be a highly worthwhile endeavor.

Even the most ideal mouse model will not be enough to directly transfer knowledge of cmiRNA dysregulation from a laboratory to a clinical setting, without additional investigations with nAMD patient samples. Before a cmiRNA-based nAMD diagnostic test can be developed, we need consistent and reliable data about cmiRNA dysregulation in nAMD patients. Even

though mouse models do not negate the need for investigations in humans, they can help provide constructive insight. The importance of this study is that it assigns a value to something which was previously intangible: the extent to which a disease trigger influences the incurring cmiRNA profile. Five cmiRNA were dysregulated in opposite directions in two murine models of neovascularization, whereas two were dysregulated in the same direction. Ultimately, the main objective of this project was realized. We used two model systems to diminish the number of aberrant findings, and help us hone in on cmiRNA which were dysregulated in conjunction with a common retinal endpoint. Both cmiRNA which we found are strong candidates for a true association with retinal neovascularization and inflammation, especially since they have already been linked to nAMD in patients. Regardless of the remaining challenges, our theory that cmiRNA expression is heavily influenced by a disease trigger, implies that a diagnostic application of a nAMD-related cmiRNA profile may one day be possible.

5. Summary

Choroidal neovascularization (CNV) is a pathologic process where blood vessels invade the retina, and is one of the hallmarks of neovascular age-related macular degeneration (nAMD). Emerging evidence suggests that epigenetic mechanisms such as microRNA regulation of gene expression, are relevant to nAMD and provide an exciting avenue of research. In this study, we performed a literature search of nAMD-related dysregulation of blood derived circulating microRNA (cmiRNA), and found that the results in between studies are largely irreconcilable. Only four cmiRNA were dysregulated in the same direction in two studies, two cmiRNA were dysregulated in opposite directions, and the majority of cmiRNA were never replicated by an independent study.

We investigated cmiRNA expression in two established murine models of retinal neovascularization and inflammation: laser-induced CNV and oxygen-induced retinopathy (OIR). We theorized that two models with different external triggers and the same retinal endpoint would help identify cmiRNA which are robustly associated with retinal nAMD hallmarks. In the laser-induced CNV model, cmiRNA dysregulation was investigated in three successive experiments, and the top ten cmiRNA candidates were identified. These cmiRNA were further tested in the OIR model. Overall, two cmiRNA were dysregulated in the same direction in both models, implying that they were dysregulated in conjunction with retinal neovascularization and inflammation. Surprisingly, five cmiRNA were dysregulated in opposite directions in the murine models. We theorize that this finding indicates that cmiRNA

dysregulation is strongly influenced by a disease trigger, which could be conducive for a future diagnostic application.

6. Zusammenfassung

Choroidale Neovaskularisation (CNV) ist ein pathologischer Prozess, bei welchem Blutgefäße in die Retina einwandern und stellt ein klassisches Merkmal der neovaskulären altersabhängigen Makuladegeneration (nAMD) dar. Neue Forschungsergebnisse lassen vermuten, dass epigenetische Mechanismen, wie z. B. die Regulation der Genexpression durch mikroRNA, relevant für nAMD sind. In dieser Arbeit wurde eine Literaturrecherche über die Expression von zirkulierender mikroRNA (cmiRNA) bei nAMD-Patienten durchgeführt. Insgesamt wurden in neun vergleichbaren Studien cmiRNA Expression in nAMD-Patienten untersucht, die Ergebnisse sind jedoch nur schlecht reproduzierbar. Nur vier cmiRNAs zeigten in zwei Studien eine Regulation in die gleiche Richtung, während zwei andere cmiRNAs in zwei Studien eine Regulation in unterschiedliche Richtungen aufwies. Der Großteil der cmiRNAs konnte nicht unabhängig reproduziert werden.

Das Ziel dieser Dissertationsarbeit war es, die Expression von cmiRNA in zwei etablierten Mausmodellen zu untersuchen: der laserinduzierten CNV und der sauerstoffinduzierten Retinopathie (OIR). Anhand dieser zwei Modelle, mit unterschiedlichen Interventionen und einem vergleichbaren retinalen Ergebnis, sollen cmiRNAs identifiziert werden, die beständig mit der CNV und der einhergehenden Entzündungsreaktion assoziiert sind. Hierfür wurden zunächst zehn potenziell fehlregulierte cmiRNAs in einem mehrstufigen Versuchsaufbau in Proben des laserinduzierten CNV Modells identifiziert. Der Vergleich der Ergebnisse der zwei Modelle hat gezeigt, dass zwei der zehn cmiRNAs in beiden Modellen eine signifikante Expressionsveränderung in derselben Richtung aufweisen, welches eine Assoziation mit der retinalen Entzündungsreaktion vermuten lässt. Unerwarteterweise wiesen fünf cmiRNAs aber eine signifikante Expressionsveränderung in unterschiedliche Richtungen auf. Wir theoretisieren, dass die Expressionsänderung der cmiRNA stark von dem vorausgegangenen pathologischen Auslöser abhängt. Sollte sich diese Theorie als wahrheitsgetreu erweisen, vermuten wir weitreichende Konsequenzen für die Etablierung einer diagnostischen Anwendung der cmiRNA.

7. Publications

Two original articles were published in conjunction with this dissertation: one review and one research article (Table 9). The review was published in 2016, and provides an overview of ocular miRNA and cmiRNA dysregulation in AMD patients and murine AMD models (50). This article was published in the journal "Molecular Diagnosis and Therapy", which has an impact factor of 3.18 (as of December 2020). According to www.pubmed.com, it has been cited by 22 publications (as of December 2020).

The second article published in conjunction with this dissertation, is an original research article. In this publication, miRNA dysregulation in the laser-induced CNV model was investigated in blood and ocular tissue samples, as well as the *in vitro* functional characterization of the miRNA (67). The results shown in the publication are based in part on the NGS and qRT-PCR data I generated, and presented in this medical dissertation. The NGS and qRT-PCR raw data was analyzed using different normalization strategies than were applied in this dissertation, by Dr. Grassmann and Ms. Kiel, for presentation in the publication (former and current employee, respectively, of the Institute of Human Genetics, Director Prof. Dr. Weber. The laser treatment and blood/ocular tissue sample acquisition were performed by Dr. Karlstetter and colleagues (Laboratory for Experimental Immunology of the Eye, Ordinarius Prof. Dr. Langmann). I performed a literature analysis of cmiRNA dysregulated in nAMD patients for the publication and dissertation, using different inclusion and exclusion criteria. Detailed descriptions of my contribution and the contributions of others to this project are documented in the methods section of this dissertation (Section 2.7 - 2.12).

Table 9: Publications. Two original articles were published in conjunction with this dissertation: one review and one original research article. The title of each article and pertinent information are shown. The impact factor of Molecular Diagnosis and Therapy was derived from www.academic-accelerator.com, and the impact factor of the International Journal of Molecular Sciences was derived from www.mdpi.com/journal/ijms in December 2020. The number of citations was viewed on www.pubmed.com in December 2020. IF: Impact Factor.

An Eye on Age-Related Macular Degeneration: The Role of MicroRNAs in Disease Pathology

Authors	**Berber, Patricia**; Grassmann, Felix; Kiel, Christina; Weber, Bernhard H.F.
Type	Review
Publication Date	23 September 2016

Journal (IF)	Molecular Diagnosis and Therapy (**3.18**)
Citations	22

A Circulating MicroRNA Profile in a Laser-Induced Mouse Model of Choroidal Neovascularization

Authors	Kiel, Christina*; **Berber, Patricia***; Karlstetter, Marcus*; Aslanidis, Alexander; Strunz, Tobias; Langmann, Thomas; Grassmann, Felix‡; Weber, Bernhard H. F‡. * These authors contributed equally to this work. ‡ These authors are joint senior authors.
Type	Research Article
Publication Date	13 April 2020
Journal (IF)	International Journal of Molecular Sciences (**4.556**)
Citations	2

8. Appendix

8.1. Supplementary Figures

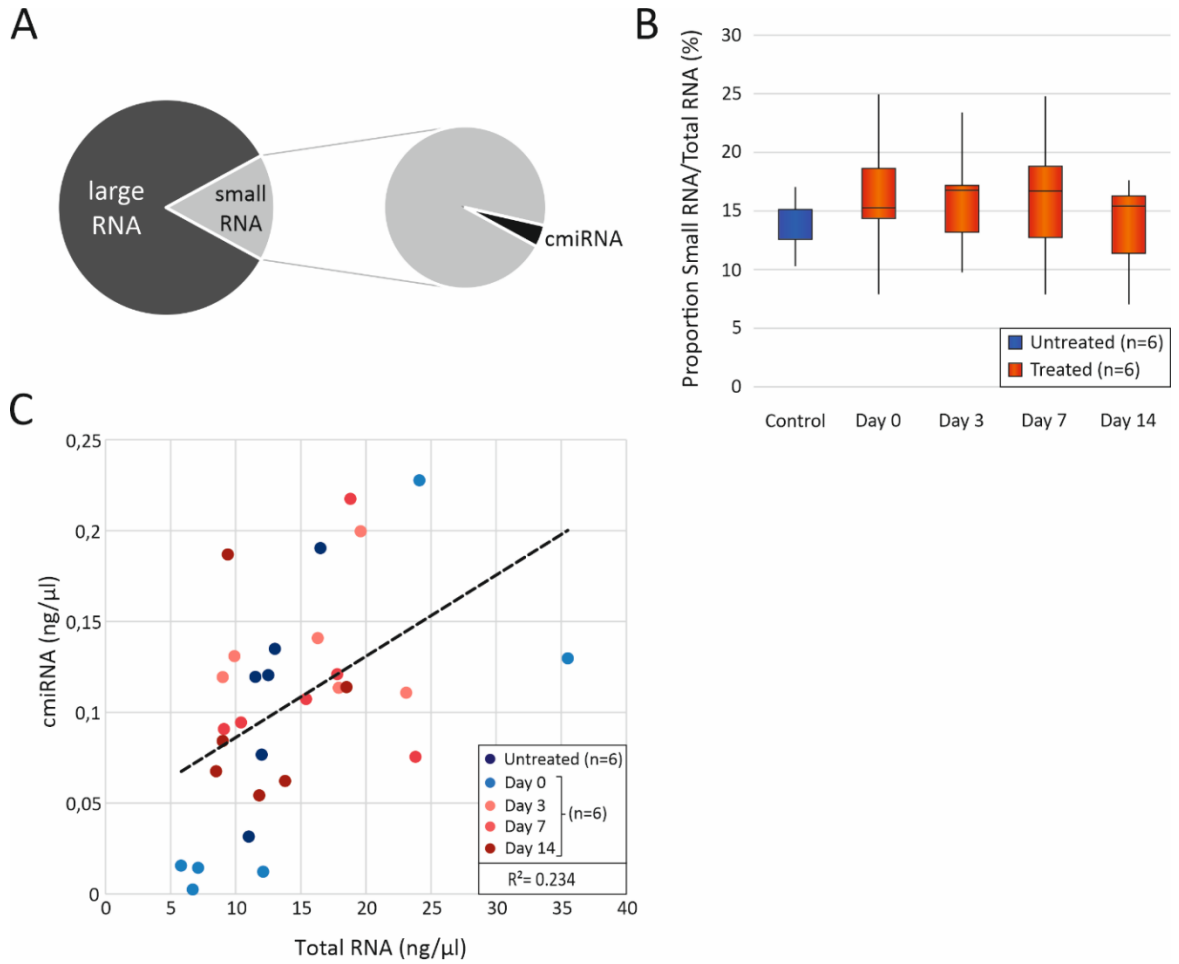

Supp. Figure 1: Replication Study 1 RNA Isolation. (A) The average proportion of large, small, and cmiRNA across all samples are shown. Overall, the RNA samples contained mostly large RNAs (12.2 ng/µl ± 5.6), and a small portion of cmiRNAs (0.1 ng/µl ± 0.06) (n = 30). (B) The proportion of small RNA out of the total RNA is shown. No significant differences between the laser treated and untreated mice were observed (student t-test, n = 6 treated, 6 untreated). Furthermore, no significant differences between the samples pre and post laser treatment were observed (student t-test). Of note, the proportion showed strong fluctuations in the samples acquired from laser treated mice: day 0 (16 % ± 6), day 3 (16 % ± 5), day 7 (16 % ± 6), and day 14 (14 % ± 4). The samples from the untreated mice, showed less prominent fluctuations (14 % ± 3). (C) CmiRNA concentration vs. total RNA concentration is shown. A weak correlation between the cmiRNA and total RNA concentration was observed ($R^2 = 0.234$).

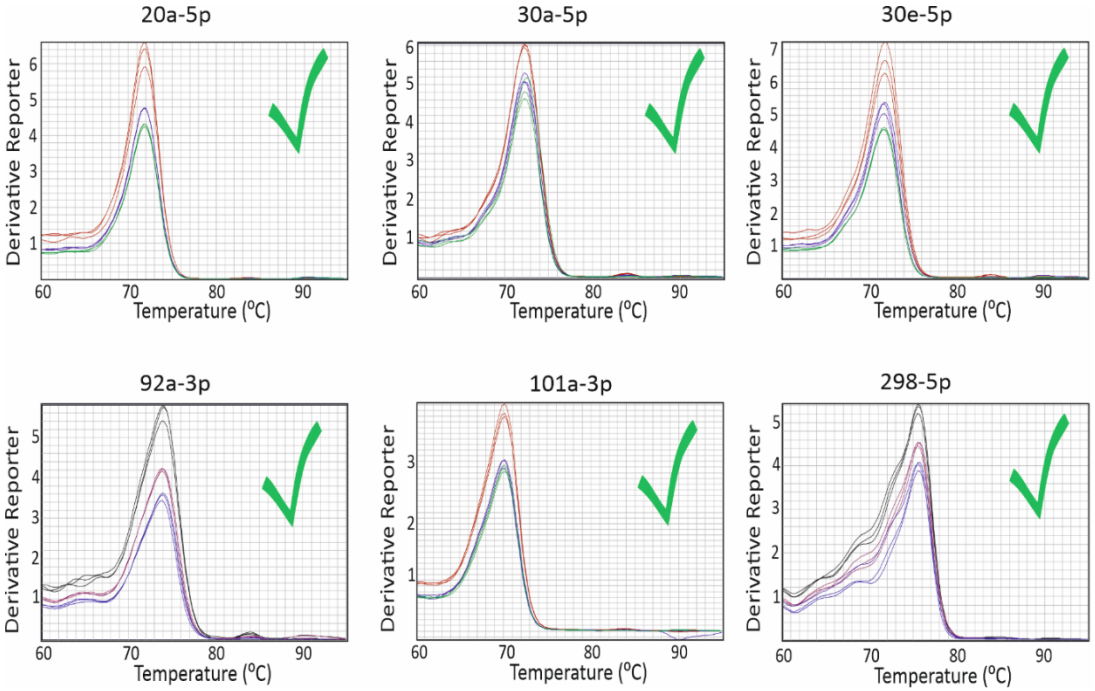

Supp. Figure 2: Replication Study 1 Primer Quality Control. Melt curve profiles of six exemplary qRT-PCR primers are shown. All primers showed a single peak in the melt curve profile, and were considered of sufficient quality for qRT-PCR (green checkmark). The prefix of each cmiRNA target is mmu-mir-.

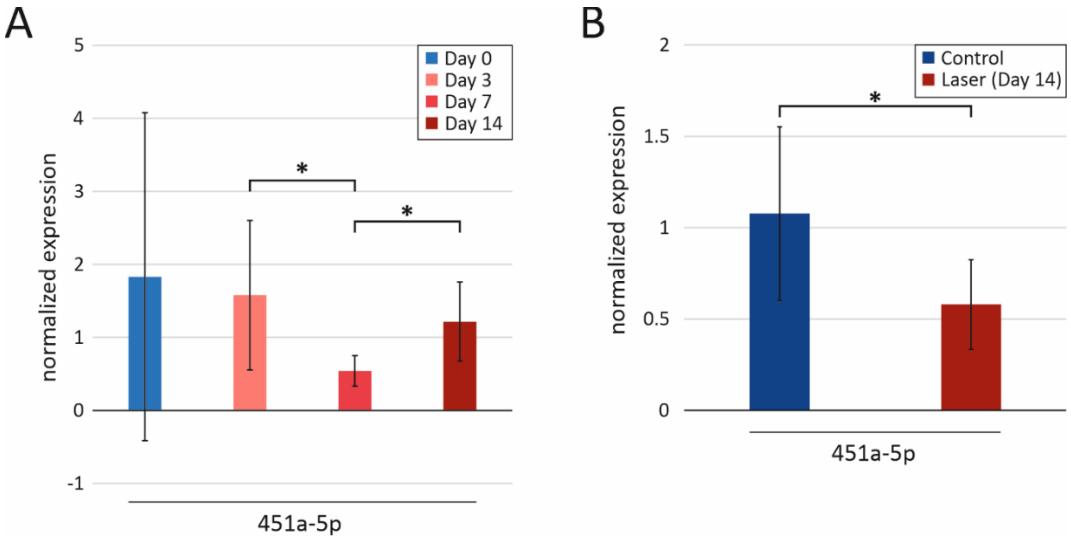

Supp. Figure 3: Replication Study 1 Potential Housekeeper Evaluation. (A) The expression of mir-451a-5p on day 0 (pre laser treatment) and day 3, 7, and 14 (post laser treatment) is shown. Expression was normalized to the mean expression on day 0. The expression on day 7 was significantly lower than on day 3 (p-value = 0.035) and day 14 (p-value = 0.017). n = 6 per timepoint. Three qRT-PCR experiments were investigated. Each experiment was normalized separately. (B) The expression of mir-451a-5p in laser treated and control mice is shown. Expression was normalized to the mean expression of the control mice. The expression in the laser treated mice was significantly lower than the control mice (p-value = 0.045). The prefix of mir-451a-5p is mmu-. n = 6 per condition, * p-value < 0.05 (student t-test).

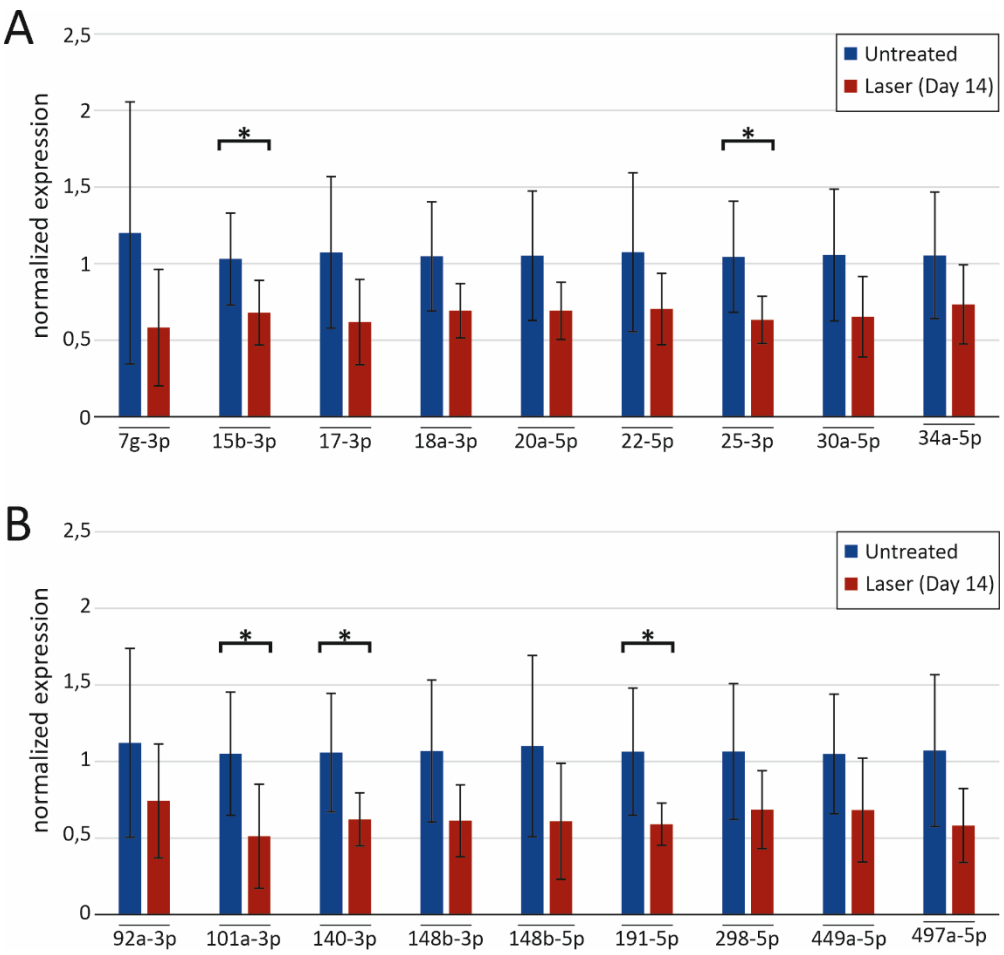

Supp. Figure 4: Replication Study 1 cmiRNA Expression of cmiRNA in Laser Treated and Untreated Mice. Expression of 18 cmiRNA, normalized to the mean expression of the control mice are shown. (A) Expression of let-7g-3p through mir-34a-5p. Mir-15b-3p and mir-25-3p were significantly downregulated in the laser treated mice (p-value = 0.041 and p-value = 0.028, respectively). (B) Expression of mir-92a-3p through mir-497a-5p. Mir-101a-3p, mir-140-3p, and mir-191-5p were significantly downregulated in the laser treated mice (p-value = 0.031, p-value = 0.03 and p-value = 0.024, respectively). The prefix of each cmiRNA is mmu-mir, except mmu-let-7g-3p. n = 6 per condition, * p-value < 0.05 (student t-test).

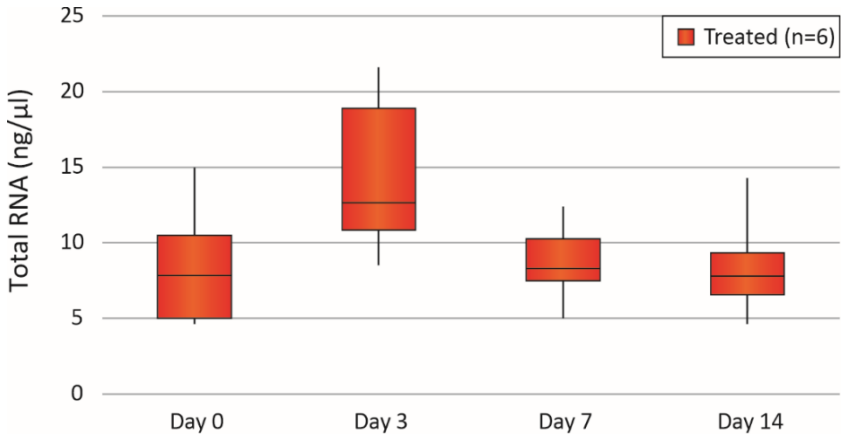

Supp. Figure 5: Replication Study 2 RNA Isolation. The total RNA concentration in the samples taken from laser treated mice at four timepoints, is shown. No significant differences between the samples pre laser (day 0) and post laser (day 3, day 7, and day 14) were observed (p-value > 0.05, student t-test).

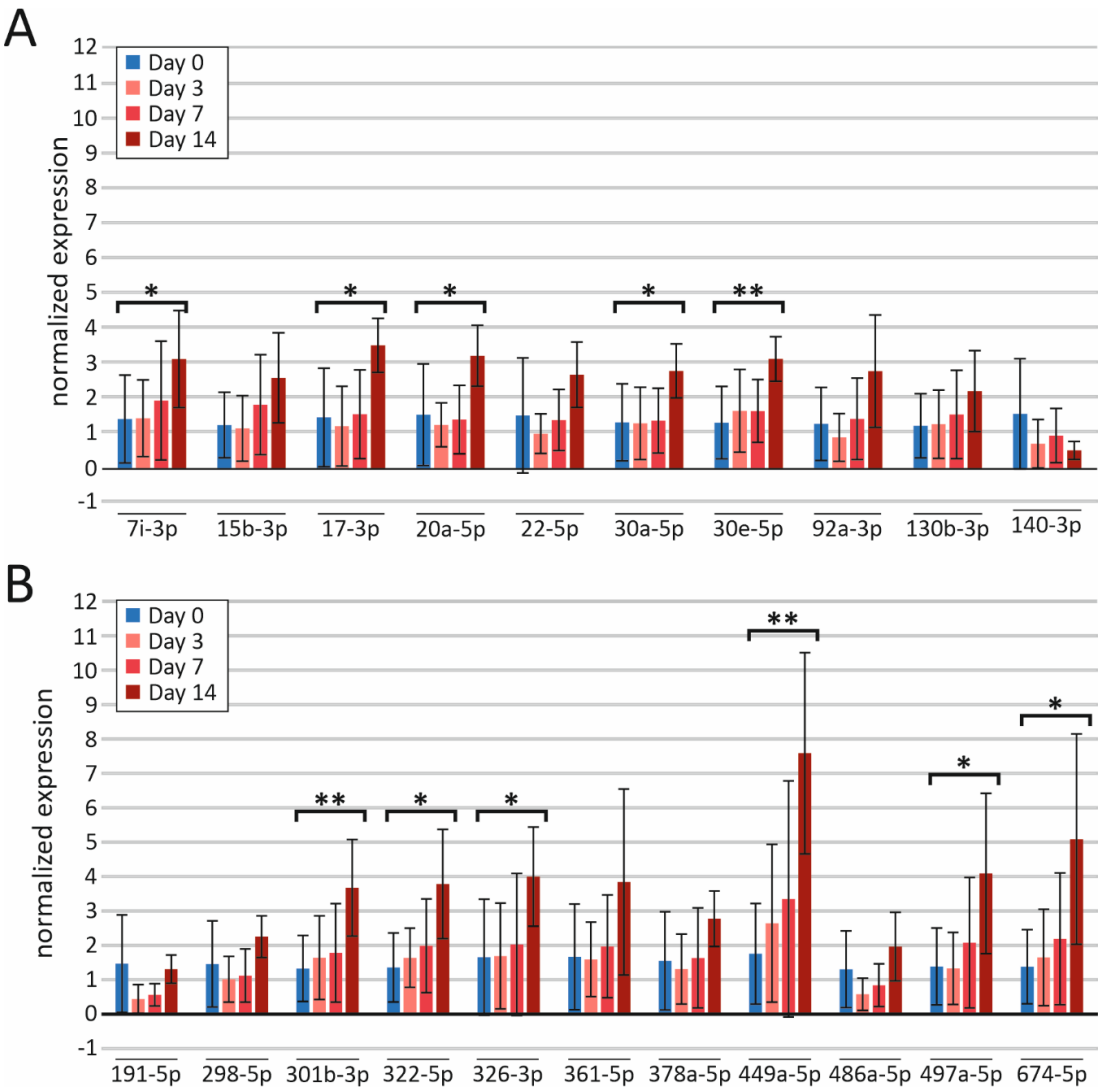

Supp. Figure 6: Replication Study 2 cmiRNA Expression in Mice Pre and Post Laser Treatment. Expression of 21 cmiRNA, normalized to the mean expression on day 0 are shown. (A) Expression of let-7i-3p through mir-140-3p are shown. Let-7i-3p, mir-17-3p, mir-20a-5p, mir-30a-5p, mir-30e-5p were significantly upregulated on day 14 (p-value = 0.049, p-value = 0.01, p-value = 0.035, p-value = 0.023, p-value = 0.004, respectively) (B) Expression of mmu-mir-191-5p through mmu-mir-674-5p are shown. Mmu-mir 301b-3p, mmu-mir-322-5p, mmu-mir-326-3p, mmu-mir-449a-5p, mmu-mir-497a-5p and mmu-mir-674-5p were significantly upregulated on day 14 (p-value = 0.007, p-value = 0.01, p-value = 0.027, p-value = 0.003, p-value = 0.028 and p-value = 0.019, respectively). The prefix of each cmiRNA is mmu-mir-, except for mmu-let-7i-3p. N = 6 per timepoint, * p-value < 0.05, ** p-value < 0.01 (student t-test).

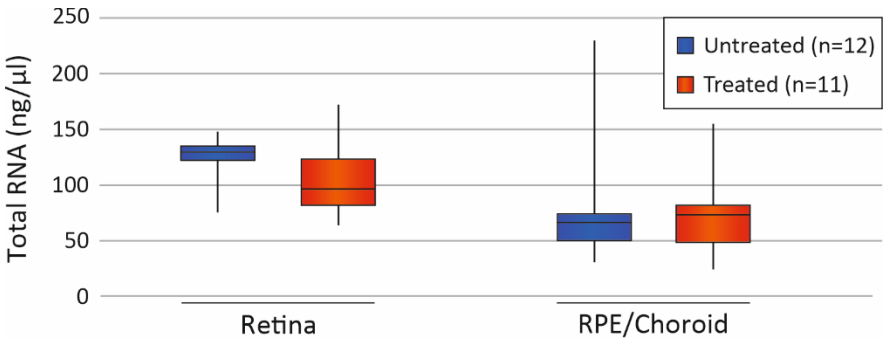

Supp. Figure 7: RNA Isolation from Ocular Tissue. The concentration of total RNA in retinal and RPE/choroid samples from laser treated and untreated mice, are shown. No significant differences in total RNA concentration between laser treated and untreated samples, were observed (n = 11 treated and 12 untreated, student t-test).

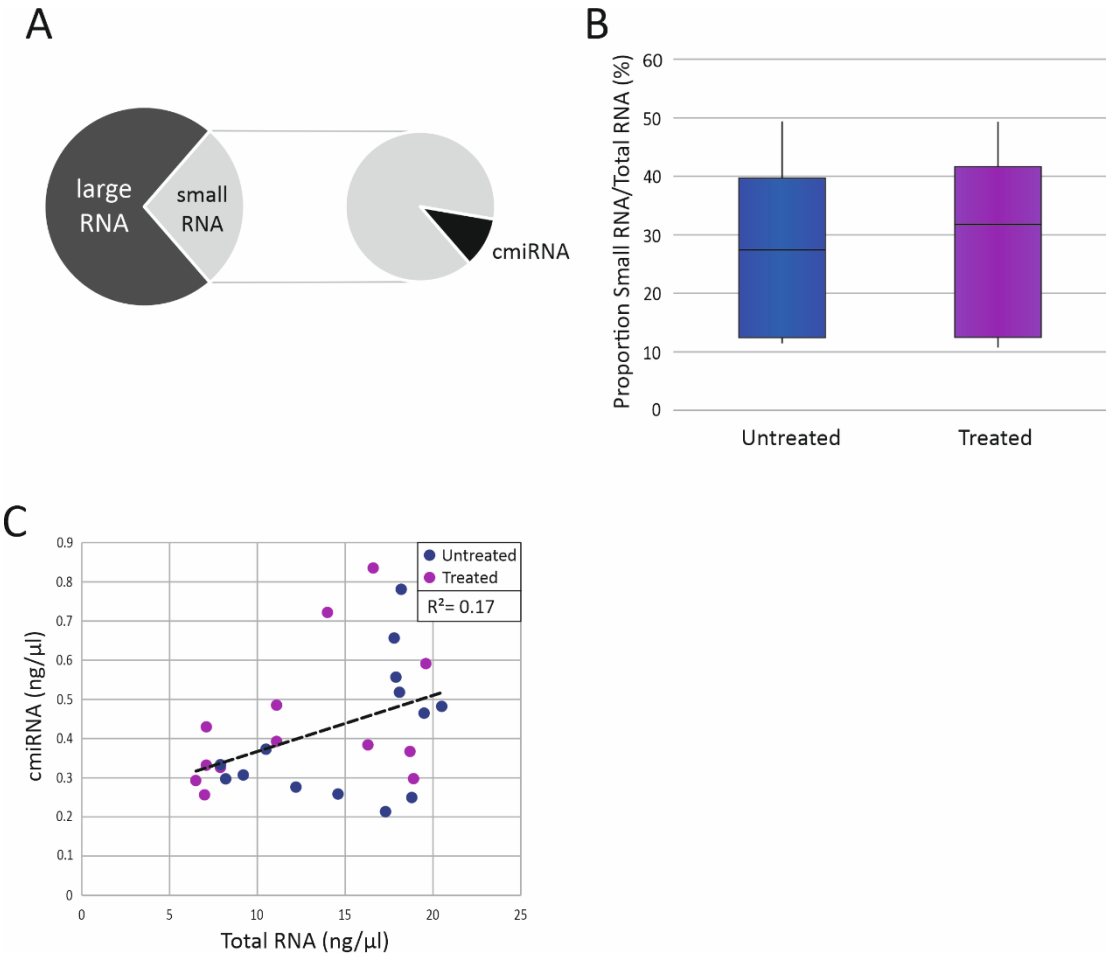

Supp. Figure 8: OIR RNA Isolation. (A) The average proportion of large, small, and cmiRNA are shown. The RNA samples were comprised of mostly large RNA, and a small portion of cmiRNA. (B) The proportion of small RNA out of the total RNA is shown. No significant difference was observed between the untreated and control mice (student t-test, n = 13 treated and 12 control mice). (C) MiRNA concentration vs. total RNA concentration is shown. A weak correlation between the miRNA and total RNA concentration was observed (n = 16 treated and 19 control, $R^2 = 0.17$).

8.2. Supplementary Tables

Supp. Table 1: Literature Analysis of Differentially Expressed cmiRNA in nAMD Patients. CmiRNA differentially expressed in nAMD patients are listed by the publication. Replication indicates whether a cmiRNA was replicated by an independent study. CmiRNA which were never replicated are indicated with "N", cmiRNA replicated in the same direction are indicated with "S", and cmiRNA which were differentially expressed in an intendent study with a different effect direction are indicated with "D". CmiRNA which were upregulated in nAMD patients are indicated with "+", downregulated cmiRNA are indicated with "-", and cmiRNA which were only expressed in patients are indicated with "P". The number of participants included in each study are listed. Patients are indicated with “nAMD” and controls are indicated with “C”. Publications are listed chronologically, and consecutive studies are separated by a bold line. “Peripheral blood mononuclear cells” are abbreviated as “PBMC” and “Peripheral blood nuclear cells” are abbreviated as “PBNC”. The literature search was performed in Pubmed in December 2020.

cmiRNA	Replication	Direction	Tissue	Participants	Year	Reference
hsa-let-7c	N	P	plasma	33 nAMD 31 C	2014	(117)
hsa-mir-17-5p	N	+				
hsa-mir-20a-5p	N	+				
hsa-mir-21-5p	N	-				
hsa-mir-24-3p	N	+				
hsa-mir-25-3p	**S**	-				
hsa-mir-26b-5p	N	P				
hsa-mir-27b-3p	N	P				
hsa-mir-29a-3p	N	P				
hsa-mir-106a-5p	N	+				
hsa-mir-139-3p	N	P				
hsa-mir-140-3p	N	-				
hsa-mir-146b-5p	N	-				
hsa-mir-192-5p	N	-				
hsa-mir-212-3p	N	P				
hsa-mir-223-3p	**S**	+				
hsa-mir-324-3p	N	P				
hsa-mir-324-5p	N	P				
hsa-mir-335-5p	N	-				
hsa-mir-342-3p	N	-				
hsa-mir-374a-5p	N	-				
hsa-mir-410	N	-				
hsa-mir-532-3p	N	P				
hsa-mir-574-3p	N	-				
hsa-mir-660-5p	N	-				
hsa-mir-744-5p	N	P				
hsa-mir-301a-3p	N	-	plasma	129 nAMD 147 C	2014	(111)
hsa-mir-361-5p	N	-				
hsa-mir-424-5p	N	-				
hsa-mir-106b-5p	N	-	plasma		2016	(118)

hsa-mir-146a-5p	**D**	+	13 nAMD 13 C			
hsa-mir-152-3p	N	-				
hsa-mir-27a-3p	N	+	whole blood	132 nAMD 146 C	2017	(119)
hsa-mir-29b-3p	N	+				
hsa-mir-195-5p	N	+				
hsa-mir-150-5p	**D**	+	PBMC	23nAMD 63C	2018	(92)
hsa-mir-486-5p	N	+	serum	70 nAMD 50 C	2019	(120)
hsa-mir-626	N	+				
hsa-mir-885-5p	N	-				
hsa-mir-34a-5p	N	-	serum	76 nAMD 70 C	2019	(121)
hsa-mir-126-3p	**S**	-				
hsa-mir-145-5p	N	-				
hsa-mir-205-5p	N	-				
hsa-mir-16-5p	**S**	-	PBNC	144 nAMD 112 C	2019	(93)
hsa-mir-17-3p	N	-				
hsa-mir-23a-3p	N	+				
hsa-mir-30b	N	+				
hsa-mir-150-5p	**D**	-				
hsa-mir-155-5p	N	-				
hsa-mir-191-5p	N	+				
hsa-mir-223-3p	**S**	+				
hsa-let-7b-5p	N	-	serum	40 nAMD 40 C	2020	(122)
hsa-mir-16-5p	S	-				
hsa-mir-25-3p	**S**	-				
hsa-mir-27b-3p	N	-				
hsa-mir-126-3p	**S**	-				
Hsa-mir-132-5p	N	-				
hsa-mir-146-5p	**D**	-				
hsa-mir-410-3p	N	-				
hsa-mir-874	N	-				

Supp. Table 2: Discovery Study RNA Isolation. The RNA concentration of samples used in the discovery study are shown. Total RNA was measured using a Nano Drop ND-1000 Spectrophotometer, and the small RNA and cmiRNA concentrations were measured using an Electrophoresis Bioanalyzer System. All values are shown as ng/µl.

		Day 0			Day 3			Day 14		
ID	**Condition**	**Total RNA (ng/µl)**	**Small RNA (ng/µl)**	**cmiRNA (ng/µl)**	**Total RNA (ng/µl)**	**Small RNA (ng/µl)**	**cmiRNA (ng/µl)**	**Total RNA (ng/µl)**	**Small RNA (ng/µl)**	**cmiRNA (ng/µl)**
354	Laser	9.600	1.089	0.075	8.100	2.513	0.108	13.600	1.137	0.131
355	Laser	10.100	1.667	0.111	12.200	1.857	0.122	9.600	1.138	0.036

359	Laser	11.600	1.863	0.146	13.100	3.016	0.112	16.400	1.761	0.039
360	Laser	8.200	2.237	0.062	14.600	3.449	0.146	10.000	1.447	0.076
374	Laser	21.400	3.500	0.014	15.800	4.000	0.212	16.000	2.527	0.079
365	Laser	45.000	10.373	0.149	10.600	2.679	0.129	9.800	0.990	0.029
369	Control	14.800	3.272	0.058	13.600	2.433	0.167	11.200	1.460	0.155
371	Control	11.000	3.428	0.086	10.500	2.898	0.179	20.000	2.551	0.185
375	Control	17.900	2.639	0.074	9.000	1.806	0.127	10.500	1.411	0.015
395	Control	9.400	3.731	0.076	10.200	2.448	0.135	10.900	2.638	0.146
364	Control	19.200	5.060	0.177	11.400	2.174	0.353	16.800	1.218	0.071

Supp. Table 3: Replication Study 1 RNA Isolation. The RNA concentration of samples used in the first replication study are shown. Total RNA was measured using a Nano Drop ND-1000 Spectrophotometer, and the small RNA and cmiRNA concentrations were measured using an Electrophoresis Bioanalyzer System. In the first replication study, RNA was only isolated from samples which were age-matched to the day 14 laser treated animals.

		Day 0			Day 3			Day 7			Day 14		
ID	**Condition**	**Total RNA (ng/µl)**	**Small RNA (ng/µl)**	**cmiRNA (ng/µl)**	**Total RNA (ng/µl)**	**Small RNA (ng/µl)**	**cmiRNA (ng/µl)**	**Total RNA (ng/µl)**	**Small RNA (ng/µl)**	**cmiRNA (ng/µl)**	**Total RNA (ng/µl)**	**Small RNA (ng/µl)**	**cmiRNA (ng/µl)**
356	Laser	6.700	0.530	0.003	9.000	2.106	0.119	9.100	2.256	0.091	9.400	1.657	0.187
357	Laser	5.800	0.822	0.016	16.300	2.809	0.141	15.400	2.590	0.107	13.800	2.219	0.062
358	Laser	7.100	1.062	0.015	9.900	1.685	0.131	10.400	1.727	0.095	11.800	0.831	0.054
362	Laser	24.100	6.014	0.228	19.600	3.234	0.200	18.800	3.662	0.218	8.500	1.258	0.068
368	Laser	35.500	5.523	0.130	23.100	2.257	0.111	23.800	1.877	0.076	18.500	1.895	0.114
393	Laser	12.100	2.380	0.012	17.900	2.163	0.114	17.800	2.040	0.121	9.000	1.472	0.084
394	Control										11.000	1.877	0.032
397	Control										12.000	1.951	0.077
370	Control										11.500	1.353	0.120
373	Control										13.000	1.958	0.135
366	Control										12.500	1.893	0.121
367	Control										16.500	1.699	0.190

Supp. Table 4: Replication Study 1 Potential Housekeeper Evaluation of Samples Over Time. The qRT-PCR expression of mmu-mir-451-5p in the samples from laser treated mice at four timepoints are shown. Three qRT-PCR experiments were investigated, and each experiment was normalized separately. Expression was normalized to the mean expression on day 0. The expression on day 7 was significantly lower than on day 3 (p-value = 0.035) and day 14 (p-value = 0.017). The expression at the other timepoints was not significantly altered: day 0 vs. day 3 p-value = 0.808, day 0 vs. day 7 p-value = 0.191, day 0 vs. day 14 p-value = 0.519, day 3 vs. day 14 p-value = 0.459. The mean expression and standard deviation are shown. The standard deviation is abbreviated as SD.

	Day 0	Day 3	Day 7	Day 14
mean	1.831	1.580	0.540	1.216
SD	2.245	1.023	0.207	0.541

Supp. Table 5: Replication Study 1 Potential Housekeeper Evaluation of Laser Treated versus Control Samples. The qRT-PCR expression of mmu-mir-451-5p in the samples from laser treated mice on day 14 and age-matched controls are shown. Expression was normalized to the mean expression on day 0. The expression in the laser treated mice was significantly lower than in the untreated mice: p-value = 0.045. The mean expression and standard deviation are shown. The standard deviation is abbreviated as SD.

	Laser	Control
mean	0.580	1.077
SD	0.245	0.474

Supp. Table 6: Replication Study 1 Expression of 34 cmiRNA. The qRT-PCR expression of the 34 cmiRNA candidates which were identified in the discovery study are shown in the samples investigated in the replication study 1. The expression was normalized to the mean expression on day 0. Significance was investigated using a U-Test. Significantly dysregulated cmiRNA, and the corresponding p-values are shown in bold. The prefix of each cmiRNA is mmu-mir, except mmu-let-7g-3p, mmu-let-7i-3p, mmu-let-7j. The mean expression and standard deviation are shown. The standard deviation is abbreviated as SD.

cmiRNA	Day 0		Day 3			Day 7			Day 14		
	mean	SD	mean	SD	p-value	mean	SD	p-value	mean	SD	p-value
let-7g-3p	1.534	1.604	0.803	0.701	0.361	0.306	0.165	**0.010**	0.416	0.404	0.109
let-7i-3p	1.483	1.493	1.678	0.591	0.262	0.999	0.405	1.000	1.797	1.084	0.631
let-7j	1.501	1.415	1.613	1.032	1.000	1.090	0.492	0.855	1.575	1.069	0.749
mir-15b-3p	1.763	2.233	2.440	1.983	0.200	0.966	0.383	0.855	2.229	1.151	0.262
mir-17-3p	1.654	1.907	2.359	1.117	0.200	1.143	0.459	1.000	2.353	1.528	0.337
mir-18a-3p	1.771	2.141	1.698	0.764	1.535	1.255	0.448	0.522	1.387	0.205	0.337
mir-20a-5p	1.261	0.827	3.246	0.965	**0.016**	3.258	0.628	**0.004**	3.409	0.618	**0.004**
mir-22-5p	1.750	1.750	2.539	2.539	0.078	1.922	1.922	0.150	2.344	2.344	0.150
mir-25-3p	2.187	2.811	2.142	1.119	0.337	1.121	0.182	0.749	1.900	0.316	0.337
mir-30a-5p	1.639	1.863	2.646	0.866	0.584	1.937	0.766	0.200	2.657	1.512	0.200
mir-30e-3p	1.786	2.277	2.447	0.414	0.055	2.167	0.944	0.150	2.266	1.229	0.150
mir-34a-5p	1.463	1.515	1.993	0.778	0.150	1.643	0.740	0.337	1.781	0.973	0.337
mir-92a-3p	1.876	2.092	1.462	1.019	0.855	0.679	0.325	0.465	1.192	0.617	0.873
mir-101a-3p	1.537	1.711	1.267	0.894	1.416	1.131	0.847	0.873	2.036	1.161	0.855
mir-130b-3p	1.919	1.919	1.527	1.527	0.522	1.592	1.592	0.631	1.490	1.490	0.873
mir-132-3p	1.788	2.042	1.129	0.539	0.873	0.793	0.407	0.631	0.865	0.447	0.631
mir-140-3p	2.848	4.484	1.424	1.352	0.749	0.424	0.192	0.150	0.979	0.554	0.873
mir-148b-3p	1.786	2.325	1.872	0.843	0.262	0.870	0.336	0.749	1.918	1.032	0.262
mir-148b-5p	1.587	1.564	2.208	0.844	0.337	2.230	1.156	0.200	2.076	0.993	0.262
mir-155-5p	1.355	1.221	1.773	0.999	0.465	1.078	0.612	0.917	3.137	0.929	**0.047**
mir-191-5p	2.573	3.141	1.122	0.809	0.361	0.497	0.339	0.361	0.583	0.268	0.584

mir-298-5p	1.483	1.417	1.616	0.539	0.423	1.143	0.255	1.145	1.445	0.764	0.631
mir-301b-3p	1.659	1.991	2.081	0.607	0.109	2.417	0.565	0.078	2.166	0.935	0.200
mir-326-3p	1.558	1.601	1.407	0.869	0.749	0.568	0.205	0.262	0.989	0.612	0.749
mir-361-5p	2.084	2.939	2.217	1.597	0.337	0.924	0.425	0.873	1.949	0.682	0.715
mir-378a-5p	1.557	1.645	1.662	0.676	1.285	1.394	0.485	0.855	1.612	0.700	1.145
mir-424-5p	1.985	2.803	2.263	0.722	0.150	1.896	0.702	0.262	2.330	1.363	0.337
mir-449a-5p	1.341	1.378	1.794	1.221	0.855	1.473	0.786	0.855	1.724	0.998	0.522
mir-486a-5p	1.839	2.054	1.021	0.589	0.873	0.339	0.154	0.088	0.905	0.274	0.873
mir-497a-5p	1.840	2.460	2.103	0.914	0.200	1.366	0.609	0.337	2.095	1.198	0.262
mir-669c-5p	1.145	0.666	1.202	0.376	0.749	1.274	0.405	0.423	1.282	0.793	0.873
mir-674-5p	1.679	1.969	2.004	0.633	0.200	1.970	0.746	0.200	2.312	1.390	0.423
mir-1306-3p	1.414	1.256	0.960	0.303	0.749	0.818	0.444	0.749	0.698	0.436	0.423
mir-5126	1.694	1.694	0.993	0.993	0.749	1.062	1.062	0.749	0.611	0.611	0.631

Supp. Table 7: Replication Study 1 Expression of 18 cmiRNA in Laser v. Controls. The qRT-PCR expression of the 18 cmiRNA candidates which were identified in the discovery study are shown in the samples from laser treated mice on day 14 and age-matched untreated mice. The expression was normalized to the mean expression on day 0. Significance was investigated using a student t-test. Significantly dysregulated cmiRNA, and the corresponding p-values are shown in bold. The prefix of each cmiRNA is mmu-mir, except mmu-let-7g-3p. The mean expression and standard deviation are shown. The standard deviation is abbreviated as SD.

cmiRNA	**Control**		**Laser**		**p-value**
	mean	**SD**	**mean**	**SD**	
mir-7g-3p	1.200	0.856	0.582	0.381	0.137
mir-15b-3p	1.031	0.300	0.681	0.211	**0.041**
mir-17-3p	1.073	0.495	0.618	0.279	0.078
mir-18a-3p	1.047	0.357	0.693	0.177	0.054
mir-20a-5p	1.052	0.422	0.692	0.187	0.085
mir-22-5p	1.075	0.518	0.704	0.233	0.141
mir-25-3p	1.045	0.363	0.633	0.154	**0.028**
mir-30a-5p	1.056	0.430	0.653	0.263	0.078
mir-34a-5p	1.054	0.413	0.733	0.259	0.138
mir-92a-3p	1.122	0.617	0.743	0.371	0.226
mir-101a-3p	1.051	0.403	0.513	0.339	**0.031**
mir-140-3p	1.059	0.387	0.622	0.173	**0.030**
mir-148b-3p	1.069	0.463	0.614	0.235	0.057
mir-148b-5p	1.101	0.591	0.610	0.379	0.118
mir-191-5p	1.065	0.415	0.591	0.138	**0.024**
mir-298-5p	1.066	0.443	0.686	0.255	0.098
mir-449a-5p	1.050	0.390	0.683	0.339	0.113
mir-497a-5p	1.072	0.495	0.582	0.241	0.055

Supp. Table 8: Replication Study 2 RNA Isolation. The RNA concentration of samples used in the second replication study are shown. Total RNA was measured using a Nano Drop ND-1000 Spectrophotometer, and are shown in ng/µl. Significance was measured using the student t-test. In the analysis day 0 vs. day 3 p-value = 0.059, day 0 vs. day 7 p-value = 0.911, day 0 vs. day 14 p-value = 0.989.

ID	Treatment	Day 0	Day 3	Day 7	Day 14
466	Laser	4,6	10,8	7,3	8,6
453	Laser	5,2	20,4	10,8	7
457	Laser	4,9	21,6	8,6	6,4
458	Laser	10,5	8,5	5	4,6
454	Laser	15	14,3	12,4	9,6
460	Laser	10,5	11	8	14,3

Supp. Table 9: Replication Study 2 Expression of 21 cmiRNA Over Time. The qRT-PCR expression of 21 cmiRNA candidates are shown in the samples from laser treated mice on four timepoints: day 0, day 3, day 7 and day 14. The expression was normalized to the mean expression on day 0. Significance was investigated using a U-test. Significantly dysregulated cmiRNA, and the corresponding p-values are shown in bold. The prefix of each cmiRNA is mmu-mir, except mmu-let-7i-3p. The mean expression and standard deviation are shown. The standard deviation is abbreviated as SD.

cmiRNA	Day 0		Day 3			Day 7			Day 14		
	mean	SD	mean	SD	p-value	mean	SD	p-value	mean	SD	p-value
let-7i-3p	1.540	1.357	1.562	1.184	0.976	2.110	1.836	0.554	3.392	1.498	**0.049**
mir-15b-3p	1.356	1.013	1.251	1.011	0.861	1.982	1.545	0.426	2.810	1.391	0.065
mir-17-3p	1.589	1.520	1.318	1.233	0.742	1.688	1.372	0.908	3.815	0.835	**0.010**
mir-20a-5p	1.670	1.571	1.360	0.678	0.666	1.520	1.058	0.850	3.494	0.941	**0.035**
mir-22-5p	1.649	1.776	1.088	0.610	0.481	1.510	0.944	0.869	2.906	1.009	0.163
mir-30a-5p	1.437	1.191	1.405	1.115	0.964	1.490	0.999	0.936	3.026	0.834	**0.023**
mir-30e-5p	1.428	1.117	1.792	1.277	0.626	1.787	0.971	0.566	3.394	0.687	**0.004**
mir-92a-3p	1.388	1.128	0.969	0.735	0.464	1.544	1.256	0.825	3.018	1.735	0.092
mir-130b-3p	1.330	0.989	1.380	1.055	0.935	1.678	1.366	0.636	2.400	1.250	0.131
mir-140-3p	1.699	1.703	0.775	0.749	0.251	1.028	0.840	0.407	0.568	0.277	0.139
mir-191-5p	1.467	1.415	0.440	0.414	0.154	0.562	0.323	0.158	1.309	0.409	0.798
mir-298-5p	1.460	1.252	1.014	0.668	0.460	1.122	0.773	0.586	2.252	0.604	0.193
mir-301b-3p	1.326	0.959	1.639	1.216	0.631	1.780	1.433	0.533	3.673	1.403	**0.007**
mir-322-5p	1.356	1.002	1.638	0.859	0.612	1.985	1.362	0.383	3.782	1.588	**0.010**
mir-326-3p	1.654	1.686	1.690	1.537	0.970	2.025	2.067	0.741	3.999	1.442	**0.027**
mir-361-5p	1.661	1.537	1.592	1.083	0.940	1.969	1.494	0.762	3.843	2.703	0.126
mir-378a-5p	1.549	1.427	1.312	1.018	0.747	1.634	1.453	0.921	2.771	0.806	0.098
mir-449a-5p	1.755	1.461	2.642	2.296	0.476	3.347	3.431	0.362	7.585	2.926	**0.003**
mir-486a-5p	1.304	1.113	0.577	0.468	0.209	0.840	0.620	0.394	1.964	0.998	0.305
mir-497a-5p	1.386	1.117	1.328	1.046	0.928	2.077	1.894	0.459	4.089	2.332	**0.028**
mir-674-5p	1.379	1.079	1.649	1.402	0.716	2.187	1.917	0.390	5.087	3.058	**0.019**

Supp. Table 10: Replication Study 1 & 2 Top Ten Dysregulated CmiRNA. The qRT-PCR expression of the top 10 cmiRNA candidates are shown. For this analysis, the data from replication studies 1 & 2 were pooled. The expression was normalized to the mean expression on day 0, the data from separate experiments were normalized separately. Significance was investigated using a U-test. Significantly dysregulated cmiRNA, and the corresponding p-values are shown in bold. The prefix of each cmiRNA is mmu-mir. The mean expression and standard deviation are shown. The standard deviation is abbreviated as SD.

cmiRNA	Day 0		Day 3			Day 7			Day 14		
	mean	SD	mean	SD	p-value	mean	SD	p-value	mean	SD	p-value
miR-20a-5p	1.466	1.216	2.303	1.266	0.094	2.389	1.230	0.083	3.452	0.760	**0.001**
miR-30a-5p	1.538	1.495	2.026	1.146	1.053	1.713	0.880	0.326	2.842	1.180	**0.021**
mir-30e-5p	1.607	1.720	2.149	0.925	0.325	1.977	0.935	0.119	2.830	1.117	**0.011**
miR-92a-3p	1.632	1.623	1.216	0.885	0.954	1.151	1.018	0.806	2.022	1.518	0.712
mir-140-3p	2.274	3.289	1.099	1.096	0.644	0.726	0.661	0.204	1.335	0.766	0.862
mir-191-5p	1.970	2.298	0.812	0.723	0.053	0.529	0.318	0.027	0.946	0.502	0.268
mir-298-5p	1.471	1.275	1.315	0.658	0.453	1.131	0.570	0.498	1.848	0.780	0.273
mir-449a-5p	1.529	1.360	2.218	1.808	0.012	2.410	2.567	0.670	4.654	3.703	**0.005**
mir-486a-5p	1.572	1.600	0.819	0.561	0.097	0.640	0.537	0.021	1.434	0.890	0.488
mir-674-5p	1.529	1.522	1.827	1.053	0.248	2.079	1.391	0.149	3.700	2.689	**0.021**

Supp. Table 11: Ocular Tissue RNA Expression. The RNA concentration of samples used in the ocular tissue study are shown. Total RNA was measured using a Nano Drop ND-1000 Spectrophotometer. Significance was measured using the student t-test. In the comparison between the retinal RNA concentration of laser treated and untreated mice, the p-value = 0.0961, whereas in the RPE/choroid samples the p-value = 0.808. All values are shown as ng/µl.

ID	Treatment	Retina	RPE/Choroid	ID	Treatment	Retina	RPE/Choroid
454	Laser	172.3	24.3	463	Control	129.4	48.5
455	Laser	83.8	82.3	464	Control	136.9	71.7
456	Laser	126.4	77	465	Control	75.4	30.7
460	Laser	136.3	73.3	451	Control	114.9	50.8
461	Laser	79.6	55.6	467	Control	134.4	229.8
462	Laser	93.9	35.3	468	Control	148	68.1
466	Laser	96.5	81.7	469	Control	129.8	47.9
453	Laser	63.8	104.2	470	Control	129.5	81.4
457	Laser	120.2	47.2	471	Control	131.3	95.3
458	Laser	110.3	49.8	472	Control	124.7	55.7
459	Laser	80.1	155	473	Control	102.3	64.9
				474	Control	136.9	67.6

Supp. Table 12: OIR Study RNA Isolation. The RNA concentration of samples used in the OIR study are shown. Total RNA was measured using a Nano Drop ND-1000 Spectrophotometer, and the small RNA and cmiRNA concentrations were measured using an

Electrophoresis Bioanalyzer System. Significance was measured using the student t-test, and the p-value = 0.702.

Condition	Total (ng/µl)	Small (ng/µl)	miRNA (ng/µl)	Condition	Total (ng/µl)	Small (ng/µl)	miRNA (ng/µl)
Treated 1	14.000	3.806	0.721	Control 1	17.300	2.008	0.213
Treated 2	16.300	2.036	0.383	Control 2	20.500	2.459	0.482
Treated 3	18.900	2.168	0.297	Control 3	18.100	2.077	0.518
Treated 4	18.700	2.003	0.367	Control 4	18.800	2.156	0.249
Treated 5	19.600	2.149	0.591	Control 5	19.500	2.647	0.465
Treated 6	16.600	3.440	0.835	Control 6	18.200	4.369	0.780
Treated 7	11.100	5.477	0.485	Control 7	17.900	8.365	0.556
Treated 8	7.100	2.889	0.429	Control 8	14.600	5.993	0.258
Treated 9	7.100	2.256	0.332	Control 9	10.500	5.184	0.372
Treated 10	6.500	3.025	0.292	Control 10	8.200	3.781	0.297
Treated 11	7.900	3.287	0.326	Control 11	9.200	2.854	0.307
Treated 12	7.000	2.435	0.256	Control 12	17.800	5.501	0.656
Treated 13	11.100	5.478	0.392	Control 13	5.247	2.357	0.273
Treated 14	6.039	1.682	0.314	Control 14	5.995	1.844	0.312
Treated 15	4.363	1.602	0.227	Control 15	7.900	2.812	0.333
				Control 16	12.200	2.643	0.276
				Control 17	5.631	2.410	0.293
				Control 18	9.470	3.623	0.493
				Control 19	9.980	4.822	0.519

Supp. Table 13: Expression of Ten cmiRNA in OIR Treated Mice and Controls. The expression of the top 10 cmiRNA candidates identified in the laser-induced CNV study are shown. The expression was investigated using qRT-PCR, and the expression was normalized to the mean expression on day 0, the data from separate experiments were normalized separately. Significance was investigated using a student t-test. Significantly dysregulated cmiRNA, and the corresponding p-values are shown in bold. The prefix of each cmiRNA is mmu-mir. The mean expression and standard deviation are shown. The standard deviation is abbreviated as SD.

cmiRNA	Control		Treated		p-value
	mean	SD	mean	SD	
mir-20a-5p	1.220	0.710	0.710	0.275	**0.002**
mir-30a-5p	1.163	0.601	0.601	0.401	**0.007**
mir-30e-5p	1.199	0.740	0.740	0.407	**0.014**
mir-92a-3p	1.158	0.586	0.586	0.264	**0.001**
mir-140-3p	1.142	0.564	0.564	0.685	0.527
mir-191-5p	1.193	0.675	0.675	0.378	**0.047**
mir-298-5p	1.127	0.487	0.487	0.245	**0.0002**
mir-449a-5p	1.086	0.417	0.417	0.326	**0.005**
mir-486a-5p	1.162	0.589	0.589	0.316	**0.0003**
mir-674-5p	1.136	0.498	0.498	0.321	**0.001**

9. References

1. Darwin C. On the Origin of Species by Means of Natural Selection. In: Darwiniana. 1859. p. 7–50.

2. Li JQ, Welchowski T, Schmid M, Mauschitz MM, Holz FG, Finger RP. Prevalence and incidence of age-related macular degeneration in Europe: a systematic review and meta-analysis. Br J Ophthalmol [Internet]. 2020 Aug;104(8):1077–84. Available from: https://bjo.bmj.com/lookup/doi/10.1136/bjophthalmol-2019-314422

3. Lyda W, Eriksen N, Krishna N. Studies of Bruch's membrane. Flow and permeability studies in a Bruch's membrane-choroid preparation. Am J Ophthalmol [Internet]. 1957 Nov 1 [cited 2021 Jan 14];44(5):362–70. Available from: http://www.sciencedirect.com/science/article/pii/0002939457931331

4. Swaroop A, Chew EY, Rickman CB, Abecasis GR. Unraveling a multifactorial late-onset disease: From genetic susceptibility to disease mechanisms for age-related macular degeneration. Annu Rev Genomics Hum Genet [Internet]. 2009 Sep;10(1):19–43. Available from: https://www.ncbi.nlm.nih.gov/pmc/articles/PMC3469316/

5. Fritsche LG, Fariss RN, Stambolian D, Abecasis GR, Curcio CA, Swaroop A. Age-related macular degeneration: Genetics and biology coming together. Annu Rev Genomics Hum Genet [Internet]. 2014;15:151–71. Available from: https://www.ncbi.nlm.nih.gov/pmc/articles/PMC4217162/

6. Flaxman SR, Bourne RRA, Resnikoff S, Ackland P, Braithwaite T, Cicinelli M V., et al. Global causes of blindness and distance vision impairment 1990–2020: a systematic review and meta-analysis. Lancet Glob Heal [Internet]. 2017;5(12):e1221–34. Available from: https://www.sciencedirect.com/science/article/pii/S2214109X17303935?via%3Dihub

7. Khan KN, Mahroo OA, Khan RS, Mohamed MD, McKibbin M, Bird A, et al. Differentiating drusen: Drusen and drusen-like appearances associated with ageing, age-related macular degeneration, inherited eye disease and other pathological processes. Prog Retin Eye Res [Internet]. 2016;53:70–106. Available from: https://www.sciencedirect.com/science/article/abs/pii/S1350946216300246?via%3Dihub

8. Curcio CA, Johnson M, Huang JD, Rudolf M. Aging, age-related macular degeneration, and the response-to-retention of apolipoprotein B-containing lipoproteins. Prog Retin Eye Res [Internet]. 2009;28(6):393–422. Available from: http://dx.doi.org/10.1016/j.preteyeres.2009.08.001

9. Crabb JW, Miyagi M, Gu X, Shadrach K, West KA, Sakaguchi H, et al. Drusen proteome analysis: An approach to the etiology of age-related macular degeneration. Proc Natl Acad Sci U S A [Internet]. 2002;99(23):14682–7. Available from: https://www.ncbi.nlm.nih.gov/pmc/articles/PMC137479/

10. Mullins RF, Russell SR, Anderson DH, Hageman GS. Drusen associated with aging and age-related macular degeneration contain proteins common to extracellular deposits associated with atherosclerosis, elastosis, amyloidosis, and dense deposit disease. FASEB J [Internet]. 2000 May;14(7):835–46. Available from: http://www.ncbi.nlm.nih.gov/pubmed/10783137

11. Mcleod DS, Grebe R, Bhutto I, Merges C, Baba T, Lutty G a. Relationship between RPE and choriocapillaris in age-related macular degeneration. Investig Ophthalmol Vis Sci [Internet]. 2009;50(10):4982–91. Available from: https://www.ncbi.nlm.nih.gov/pmc/articles/PMC4829357/

12. Owsley C, McGwin G, Jackson GR, Kallies K, Clark M. Cone- and rod-mediated dark adaptation impairment in age-related maculopathy. Ophthalmology [Internet]. 2007 Sep [cited 2015 Jul 28];114(9):1728–35. Available from: http://www.sciencedirect.com/science/article/pii/S0161642006016733

13. Bhutto I, Lutty G. Understanding age-related macular degeneration (AMD): relationships between the photoreceptor/retinal pigment epithelium/Bruch's membrane/choriocapillaris complex. Mol Aspects Med [Internet]. 2012 Aug [cited 2015 May 14];33(4):295–317. Available from: http://www.sciencedirect.com/science/article/pii/S0098299712000453

14. Holz FG, Strauss EC, Schmitz-Valckenberg S, Van Lookeren Campagne M. Geographic atrophy: Clinical features and potential therapeutic approaches. Ophthalmology [Internet]. 2014;121(5):1079–91. Available from: http://dx.doi.org/10.1016/j.ophtha.2013.11.023

15. Grassmann F, Fauser S, Weber BHFF. The genetics of age-related macular degeneration (AMD) – Novel targets for designing treatment options? Eur J Pharm Biopharm [Internet]. 2015 May [cited 2016 Aug 12];95:194–202. Available from: https://www.sciencedirect.com/science/article/abs/pii/S0939641115002271?via%3Dihub

16. Sarks SH. New vessel formation beneath the retinal pigment epithelium in senile eyes. Br J Ophthalmol [Internet]. 1973;57(12):951–65. Available from: https://www.ncbi.nlm.nih.gov/pmc/articles/PMC1215217/

17. Grossniklaus HE, Green WR. Choroidal neovascularization. Am J Ophthalmol [Internet]. 2004 Mar [cited 2015 Sep 1];137(3):496–503. Available from: http://www.sciencedirect.com/science/article/pii/S0002939403011309

18. Freund KB, Ho I-V, Barbazetto I a, Koizumi H, Laud K, Ferrara D, et al. Type 3 neovascularization: the expanded spectrum of retinal angiomatous proliferation. Retina [Internet]. 2008;28(2):201–11. Available from: https://journals.lww.com/retinajournal/Abstract/2008/02000/TYPE_3_NEOVASCULARIZATION__The_Expanded_Spectrum.2.aspx

19. Balasubramanian SA, Krishna Kumar K, Baird PN. The role of proteases and inflammatory molecules in triggering neovascular age-related macular degeneration: basic science to clinical relevance. Transl Res [Internet]. 2014 Sep [cited 2015 Sep 1];164(3):179–92. Available from: http://www.sciencedirect.com/science/article/pii/S1931524414001297

20. Wong T, Chakravarthy U, Klein R, Mitchell P, Zlateva G, Buggage R, et al. The Natural History and Prognosis of Neovascular Age-Related Macular Degeneration. Ophthalmology [Internet]. 2008 Jan [cited 2015 Sep 1];115(1):116-126.e1. Available from: http://www.sciencedirect.com/science/article/pii/S0161642007002333

21. Mavija M, Alimanovic E, Jaksic V, Kasumovic S, Cekic S, Stamenkovic M. Therapeutic Modalities of Exudative Age-related Macular Degeneration. Med Arch [Internet]. 2014;68(3):204. Available from: http://www.scopemed.org/?mno=161092

22. Folkman J, Merler E, Abernathy C, Williams G. Isolation of a tumor factor responsible for angiogenesis. J Exp Med [Internet]. 1971;133(2):275–88. Available from: https://rupress.org/jem/article/133/2/275/5989/ISOLATION-OF-A-TUMOR-FACTOR-RESPONSIBLE-FOR

23. Feigin I, Allen LB, Lipkin L, Gross SW. The endothelial hyperplasia of the cerebral blood vessels with brain tumors, and its sarcomatous transformation. Cancer [Internet]. 1958;11(2):264–77. Available from: https://pubmed.ncbi.nlm.nih.gov/13511345/

24. Shima DT, Adamis AP, Ferrara N, Yeo KT, Yeo TK, Allende R, et al. Hypoxic induction of endothelial cell growth factors in retinal cells: identification and characterization of vascular endothelial growth factor (VEGF) as the mitogen. Mol Med [Internet]. 1995;1(2):182–93. Available from: https://www.ncbi.nlm.nih.gov/pmc/articles/PMC2229943/

25. Kwak N, Okamoto N, Wood JM, Campochiaro PA. VEGF is major stimulator in model of choroidal neovascularization. Investig Ophthalmol Vis Sci [Internet]. 2000;41(10):3158–64. Available from: https://iovs.arvojournals.org/article.aspx?articleid=2123593

26. Day S, Acquah K, Lee PP, Mruthyunjaya P, Sloan FA. Medicare costs for neovascular age-related macular degeneration, 1994-2007. Am J Ophthalmol [Internet]. 2011 Dec [cited 2015 Sep 2];152(6):1014–20. Available from: http://www.sciencedirect.com/science/article/pii/S0002939411004107

27. McKibbin M, Ali M, Bansal S, Baxter PD, West K, Williams G, et al. CFH, VEGF and HTRA1 promoter genotype may influence the response to intravitreal ranibizumab therapy for neovascular age-related macular degeneration. Br J Ophthalmol [Internet]. 2012;96(2):208–12. Available from: https://bjo.bmj.com/content/96/2/208.long

28. Rosenfeld PJ, Shapiro H, Tuomi L, Webster M, Elledge J, Blodi B. Characteristics of patients losing vision after 2 years of monthly dosing in the phase III ranibizumab clinical trials. Ophthalmology [Internet]. 2011 Mar [cited 2015 Sep 2];118(3):523–30. Available from: http://www.sciencedirect.com/science/article/pii/S0161642010007475

29. Hunter A, Spechler PA, Cwanger A, Song Y, Zhang Z, Ying GS, et al. DNA methylation is associated with altered gene expression in AMD. Invest Ophthalmol Vis Sci. 2012;53(4):2089–105.

30. Thornton J, Edwards R, Mitchell P, Harrison R a, Buchan I, Kelly SP. Smoking and age-related macular degeneration: a review of association. Eye [Internet]. 2005;19(9):935–44. Available from: https://www.nature.com/articles/6701978

31. Edwards AO, Lee SJ, Fridley BL, Tosakulwong N. Density of common complex ocular traits in the aging eye: Analysis of secondary traits in genome-wide association studies. PLoS One [Internet]. 2008;3(6):2–8. Available from: https://journals.plos.org/plosone/article?id=10.1371/journal.pone.0002510

32. Frederick PA, Kleinman ME. The Immune System and AMD. Curr Ophthalmol Rep [Internet]. 2014;2(1):14–9. Available from: https://doi.org/10.1007/s40135-013-0037-x

33. Klein ML, Mauldin WM, Stoumbos VD. Heredity and Age-Related Macular Degeneration: Observations in Monozygotic Twins. Arch Ophthalmol [Internet]. 1994 Jul 1;112(7):932–7. Available from: https://doi.org/10.1001/archopht.1994.01090190080025

34. Heiba IM, Elston RC, Klein BE, Klein R. Sibling Correlations and Segregation Analysis of Age-Related Maculopathy : The Beaver Dam Eye Study lbrahim. Genet Epidemiol [Internet]. 1994;11(1):51–67. Available from: http://www.ncbi.nlm.nih.gov/pubmed/8013888

35. Fisher SA, Abecasis GR, Yashar BM, Zareparsi S, Swaroop A, Iyengar SK, et al. Meta-analysis of genome scans of age-related macular degeneration. Hum Mol Genet [Internet]. 2005 Aug 1;14(15):2257–64. Available from: http://academic.oup.com/hmg/article/14/15/2257/551757/Metaanalysis-of-genome-scans-of-agerelated-macular

36. Klein RJ, Zeiss C, Chew EY, Tsai JY, Sackler RS, Haynes C, et al. Complement factor H polymorphism in age-related macular degeneration. Science (80-) [Internet]. 2005;308(5720):385–9. Available from: https://science.sciencemag.org/content/308/5720/385.long

37. Grassmann F, Cantsilieris S, White SJ, Richardson AJ, Hewitt AW, Vote BJ, et al. Multiallelic copy number variation in the complement component 4A (C4A) gene is associated with late-stage age-related macular degeneration (AMD). J Neuroinflammation [Internet]. 2016;1–9. Available from: http://dx.doi.org/10.1186/s12974-016-0548-0

38. Gold B, Merriam JE, Zernant J, Hancox LS, Taiber AJ, Cramer K, et al. Variation in factor B (BF) and complement component 2 (C2) genes is associated with age-related macular degeneration. Nat Genet [Internet]. 2010;38(4):458–62. Available from: https://www.nature.com/articles/ng1750

39. Lars G. Fritsche1,†, Wilmar Igl2,†, Jessica N. Cooke Bailey3,†, Felix Grassmann4,†, Sebanti Sengupta1,†, Jennifer L. Bragg-Gresham1, 5, Kathryn P. Burdon6, Scott J. Hebbring7, Cindy Wen8, Mathias Gorski2, Ivana K. Kim9, David Cho10, Donald Zack11, 12, 13, and IMH. A large genome-wide association study of age-related macular degeneration highlights contributions of rare and common variants. Nat Genet [Internet]. 2016;48(2):134–43. Available from: https://www.nature.com/articles/ng.3448

40. Rudnicka AR, Jarrar Z, Wormald R, Cook DG, Fletcher A, Owen CG. Age and gender variations in age-related macular degeneration prevalence in populations of European ancestry: A meta-analysis. Ophthalmology [Internet]. 2012;119(3):571–80. Available from: http://dx.doi.org/10.1016/j.ophtha.2011.09.027

41. Velilla S, García-Medina JJ, García-Layana A, Dolz-Marco R, Pons-Vázquez S, Pinazo-Durán MD, et al. Smoking and age-related macular degeneration: review and update. J Ophthalmol [Internet]. 2013/12/04. 2013;2013:895147. Available from: https://pubmed.ncbi.nlm.nih.gov/24368940

42. Vingerling JR, Hofman A, Grobbee DE, de Jong PTVM. Age-Related Macular Degeneration and Smoking: The Rotterdam Study. Arch Ophthalmol [Internet]. 1996 Oct 1;114(10):1193–6. Available from: https://doi.org/10.1001/archopht.1996.01100140393005

43. R Klein, B E Klein, K L Linton DLD. The Beaver Dam Eye Study: the relation of age-related maculopathy to smoking. Am J Epidemiol [Internet]. 1993; Available from: https://academic.oup.com/aje/article/137/2/190/138360

44. Klein R, Cruickshanks KJ, Nash SD, Krantz EM, Nieto FJ, Huang GH, et al. The prevalence of age-related macular degeneration and associated risk factors. Arch

Ophthalmol [Internet]. 2010;128(6):750–8. Available from: https://jamanetwork.com/journals/jamaophthalmology/fullarticle/425802

45. Smith W, Mitchell P, Leeder SR. Smoking and Age-Related Maculopathy: The Blue Mountains Eye Study. Arch Ophthalmol [Internet]. 1996 Dec 1;114(12):1518–23. Available from: https://doi.org/10.1001/archopht.1996.01100140716016

46. Group A-REDSR. Risk factors associated with age-related macular degeneration. A case-control study in the age-related eye disease study: Age-Related Eye Disease Study Report Number 3. Ophthalmology [Internet]. 2000 Dec;107(12):2224–32. Available from: https://pubmed.ncbi.nlm.nih.gov/11097601

47. Tuo J, Ross RJ, Reed GF, Yan Q, Wang JJ, Bojanowski CM, et al. The HtrA1 Promoter Polymorphism, Smoking, and Age-related Macular Degeneration in Multiple Case-control Samples. Ophthalmology [Internet]. 2008;115(11):1891–8. Available from: https://www.sciencedirect.com/science/article/pii/S0161642008004934?via%3Dihub

48. Chu J, Zhou CC, Lu N, Zhang X, Dong FT. Genetic variants in three genes and smoking show strong associations with susceptibility to exudative age-related macular degeneration in a Chinese population. Chin Med J (Engl) [Internet]. 2008;121(24):2525–33. Available from: https://journals.lww.com/cmj/Fulltext/2008/12020/Genetic_variants_in_three_genes_and_smoking_show.11.aspx

49. Lee SJ, Kim NR, Chin HS. LOC387715/HTRA1 polymorphisms, smoking and combined effects on exudative age-related macular degeneration in a Korean population. Clin Experiment Ophthalmol [Internet]. 2010 Oct 1;38(7):698–704. Available from: https://doi.org/10.1111/j.1442-9071.2010.02316.x

50. Berber P, Grassmann F, Kiel C, Weber BHF. An Eye on Age-Related Macular Degeneration: The Role of MicroRNAs in Disease Pathology. Mol Diagnosis Ther [Internet]. 2017;21(1):31–43. Available from: https://www.ncbi.nlm.nih.gov/pmc/articles/PMC5250647/

51. Gemenetzi M, Lotery AJ. The role of epigenetics in age-related macular degeneration. Eye [Internet]. 2014;28(12):1407–17. Available from: http://dx.doi.org/10.1038/eye.2014.225

52. Weinhold B. Epigenetics: the science of change. Environ Health Perspect [Internet]. 2006;114(3):160–7. Available from: https://www.ncbi.nlm.nih.gov/pmc/articles/PMC1392256/

53. Oliver VF, Jaffe AE, Song J, Wang G, Zhang P, Branham KE, et al. Differential DNA methylation identified in the blood and retina of AMD patients. Epigenetics [Internet]. 2015;10(8):698–707. Available from: https://www.ncbi.nlm.nih.gov/pmc/articles/PMC4622056/

54. Gemenetzi M, Lotery AJ. Epigenetics in age-related macular degeneration: new discoveries and future perspectives. Cell Mol Life Sci [Internet]. 2020;77(5):807–18. Available from: https://doi.org/10.1007/s00018-019-03421-w

55. Deutsche Stiftung Organtransplantation. Jahresbericht organspende und transplantation in deutschland [Internet]. 2019. Available from: https://www.dso.de/organspende/statistiken-berichte/jahresbericht

56. Gesetz über die Spende, Entnahme und Übertragung von Organen und Geweben

(Transplantationsgesetz - TPG) [Internet]. 1997. Available from: https://www.gesetze-im-internet.de/tpg/

57. Pennesi ME, Neuringer M, Courtney RJ. Animal models of age related macular degeneration. Mol Aspects Med [Internet]. 2012;33(4):487–509. Available from: https://www.ncbi.nlm.nih.gov/pmc/articles/PMC3770531/

58. Tobe T, Ortega S, Luna JD, Ozaki H, Okamoto N, Derevjanik NL, et al. Targeted disruption of the FGF2 gene does not prevent choroidal neovascularization in a murine model. Am J Pathol [Internet]. 1998 Nov [cited 2015 Sep 2];153(5):1641–6. Available from: http://www.sciencedirect.com/science/article/pii/S0002944010657537

59. Lambert V, Lecomte J, Hansen S, Blacher S, Gonzalez M-LA, Struman I, et al. Laser-induced choroidal neovascularization model to study age-related macular degeneration in mice. Nat Protoc [Internet]. 2013 Nov;8(11):2197–211. Available from: http://dx.doi.org/10.1038/nprot.2013.135

60. Smith LEH, Wesolowski E, McLellan A, Kostyk SK, D'Amato R, Sullivan R, et al. Oxygen-induced retinopathy in the mouse. Investig Ophthalmol Vis Sci [Internet]. 1994;35(1):101–11. Available from: https://iovs.arvojournals.org/article.aspx?articleid=2160821

61. Liegl R, Priglinger C, Ohlmann A. Induction and Readout of Oxygen-Induced Retinopathy. In: Methods in Molecular Biology [Internet]. 2019. p. 179–91. Available from: https://pubmed.ncbi.nlm.nih.gov/30324445/

62. Connor KM, Krah NM, Dennison RJ, Aderman CM, Chen J, Guerin KI, et al. Quantification of oxygen-induced retinopathy in the mouse: A model of vessel loss, vessel regrowth and pathological angiogenesis. Nat Protoc [Internet]. 2009;4(11):1565–73. Available from: https://www.nature.com/articles/nprot.2009.187

63. Rotschild T, Nandgaonkar BN, Yu K, Higgins RD. Dexamethasone Reduces Oxygen Induced Retinopathy in a Mouse Model. Pediatr Res [Internet]. 1999;46(1):94–100. Available from: https://doi.org/10.1203/00006450-199907000-00016

64. Sharma J, Barr SM, Geng Y, Yun Y, Higgins RD. Ibuprofen improves oxygen-induced retinopathy in a mouse model. Curr Eye Res [Internet]. 2003;27(5):309–14. Available from: https://www.tandfonline.com/doi/abs/10.1076/ceyr.27.5.309.17222

65. Yoshida S. Role of MCP-1 and MIP-1alpha in retinal neovascularization during postischemic inflammation in a mouse model of retinal neovascularization. J Leukoc Biol [Internet]. 2003;73(1):137–44. Available from: https://pubmed.ncbi.nlm.nih.gov/12525571/

66. Ntumba K, Akla N, Paul Oh S, Eichmann A, Larrivée B. BMP9/ALK1 inhibits neovascularization in mouse models of agerelated macular degeneration. Oncotarget [Internet]. 2016;7(35):55957–69. Available from: https://www.oncotarget.com/article/11182/text/

67. Kiel C, Berber P, Karlstetter M, Aslanidis A, Strunz T, Langmann T, et al. A circulating microRNA profile in a laser-induced mouse model of choroidal neovascularization. Int J Mol Sci [Internet]. 2020;21(8):1–18. Available from: https://www.ncbi.nlm.nih.gov/pmc/articles/PMC7216141/

68. Shweiki D, Itin A, Soffer D, Keshet E. Vascular endothelial growth factor induced by hypoxia may mediate hypoxia-initiated angiogenesis. Nature [Internet].

1992;359(6398):843–5. Available from: https://www.nature.com/articles/359843a0

69. Saishin Y, Saishin Y, Takahashi K, Silva RLE, Hylton D, Rudge JS, et al. VEGF-TRAPR1R2 suppresses choroidal neovascularization and VEGF-induced breakdown of the blood-retinal barrier. J Cell Physiol [Internet]. 2003;195(2):241–8. Available from: https://pubmed.ncbi.nlm.nih.gov/12652651/

70. Heier JS, Brown DM, Chong V, Korobelnik JF, Kaiser PK, Nguyen QD, et al. Intravitreal aflibercept (VEGF trap-eye) in wet age-related macular degeneration. Ophthalmology [Internet]. 2012;119(12):2537–48. Available from: https://pubmed.ncbi.nlm.nih.gov/23084240/

71. Rosenfeld PJ, Rich RM, Lalwani GA. Ranibizumab: Phase III Clinical Trial Results. Ophthalmol Clin [Internet]. 2006 Sep 1;19(3):361–72. Available from: https://doi.org/10.1016/j.ohc.2006.05.009

72. Sone H, Kawakami Y, Kumagai AK, Okuda Y, Sekine Y, Honmura S, et al. Effects of intraocular or systemic administration of neutralizing antibody against vascular endothelial growth factor on the murine experimental model of retinopathy. Life Sci [Internet]. 1999;65(24):2573–80. Available from: https://pubmed.ncbi.nlm.nih.gov/10619365/

73. Campbell K. Intensive oxygen therapy as a possible cause of retrolental fibroplasia; a clinical approach. Med J Aust [Internet]. 1951;2(2):48–50. Available from: https://pubmed.ncbi.nlm.nih.gov/14874698/

74. Hellström A, Smith LEH, Dammann O. Retinopathy of prematurity. Lancet [Internet]. 2013;382(9902):1445–57. Available from: https://pubmed.ncbi.nlm.nih.gov/23782686/

75. Kornerup T. Studies in Diabetic Retinopathy. Acta Med Scand [Internet]. 1955 Jan 12;153(2):81–101. Available from: https://doi.org/10.1111/j.0954-6820.1955.tb18208.x

76. Avila MP, Weiter JJ, Jalkh AE, Trempe CL, Pruett RC, Schepens CL. Natural History of Choroidal Neovascularization in Degenerative Myopia. Ophthalmology [Internet]. 1984 Dec 1 [cited 2019 Dec 16];91(12):1573–81. Available from: https://pubmed.ncbi.nlm.nih.gov/6084222/

77. Chau FY, Wallace D, Vajaranant T, Herndon L, Lee P, Challa P, et al. Osteogenesis Imperfecta and the Eye. Osteogenes Imperfecta A Transl Approach to Brittle Bone Dis [Internet]. 2013 Jan 1 [cited 2019 Dec 16];289–303. Available from: https://doi.org/10.1016/B978-0-12-397165-4.00031-9

78. Desjarlais M, Rivera JC, Lahaie I, Cagnone G, Wirt M, Omri S, et al. MicroRNA expression profile in retina and choroid in oxygen-induced retinopathy model. PLoS One [Internet]. 2019;14(6):1–24. Available from: https://pubmed.ncbi.nlm.nih.gov/31188886/

79. Zhang LS, Zhou Y Di, Peng YQ, Zeng HL, Yoshida S, Zhao TT. Identification of altered microRNAs in retinas of mice with oxygen-induced retinopathy. Int J Ophthalmol [Internet]. 2019;12(5):739–45. Available from: https://pubmed.ncbi.nlm.nih.gov/31131231/

80. Djuranovic S, Nahvi A, Green R. miRNA-mediated gene silencing by translational repression followed by mRNA deadenylation and decay. Science (80-) [Internet]. 2012;336(6078):237–40. Available from: https://pubmed.ncbi.nlm.nih.gov/22499947/

81. He L, Hannon GJ. MicroRNAs: Small RNAs with a big role in gene regulation. Nat Rev

Genet [Internet]. 2004;5(7):522–31. Available from: https://pubmed.ncbi.nlm.nih.gov/15211354/

82. Lee RC, Feinbaum RL, Ambros V. The C. elegans heterochronic gene lin-4 encodes small RNAs with antisense complementarity to lin-14. Cell [Internet]. 1993;75(5):843–54. Available from: https://pubmed.ncbi.nlm.nih.gov/8252621/

83. Wightman B, Ha I, Ruvkun G. Posttranscriptional regulation of the heterochronic gene lin-14 by lin-4 mediates temporal pattern formation in C. elegans. Cell [Internet]. 1993;75(5):855–62. Available from: https://pubmed.ncbi.nlm.nih.gov/8252622/

84. Chalfie M, Horvitz HR, Sulston JE. Mutations that lead to reiterations in the cell lineages of C. elegans. Cell [Internet]. 1981;24(1):59–69. Available from: https://pubmed.ncbi.nlm.nih.gov/7237544/

85. Ambros V, Horvitz HR. Heterochronic mutants of the nematode Caenorhabditis elegans. Science (80-) [Internet]. 1984;226(4673):409–16. Available from: https://pubmed.ncbi.nlm.nih.gov/6494891/

86. Ruvkun G, Giusto J. The Caenorhabditis elegans heterochronic gene lin-14 encodes a nuclear protein that forms a temporal developmental switch. Nature [Internet]. 1989;338(6213):313–9. Available from: https://pubmed.ncbi.nlm.nih.gov/2922060/

87. Chim SSC, Shing TKF, Hung ECW, Leung TY, Lau TK, Chiu RWK, et al. Detection and characterization of placental microRNAs in maternal plasma. Clin Chem [Internet]. 2008;54:482–90. Available from: http://www.clinchem.org/content/54/3/482.full

88. Zen K, Zhang CY. Circulating MicroRNAs: A novel class of biomarkers to diagnose and monitor human cancers. Med Res Rev [Internet]. 2012;32(2):326–48. Available from: https://pubmed.ncbi.nlm.nih.gov/22383180/

89. Vickers KC, Palmisano BT, Shoucri BM, Shamburek RD, Remaley AT. MicroRNAs are transported in plasma and delivered to recipient cells by high-density lipoproteins. Nat Cell Biol [Internet]. 2011;13(4):423–35. Available from: https://pubmed.ncbi.nlm.nih.gov/21423178/

90. Zernecke A, Bidzhekov K, Noels H, Shagdarsuren E, Gan L, Denecke B, et al. Delivery of microRNA-126 by apoptotic bodies induces CXCL12-dependent vascular protection. Sci Signal [Internet]. 2009;2(100):ra81. Available from: https://pubmed.ncbi.nlm.nih.gov/19996457/

91. Wang K, Zhang S, Weber J, Baxter D, Galas DJ. Export of microRNAs and microRNA-protective protein by mammalian cells. Nucleic Acids Res [Internet]. 2010;38(20):7248–59. Available from: http://nar.oxfordjournals.org/content/38/20/7248.full.pdf+html

92. Lin JB, Moolani H V., Sene A, Sidhu R, Kell P, Lin JB, et al. Macrophage microRNA-150 promotes pathological angiogenesis as seen in age-related macular degeneration. JCI insight [Internet]. 2018;3(7):1–17. Available from: https://pubmed.ncbi.nlm.nih.gov/29618664/

93. Litwińska Z, Sobuś A, Łuczkowska K, Grabowicz A, Mozolewska-Piotrowska K, Safranow K, et al. The Interplay Between Systemic Inflammatory Factors and MicroRNAs in Age-Related Macular Degeneration. Front Aging Neurosci [Internet]. 2019;11(October):1–13. Available from: https://pubmed.ncbi.nlm.nih.gov/31695606/

94. Bär C, Thum T, De Gonzalo-Calvo D. Circulating miRNAs as mediators in cell-to-cell communication. Epigenomics [Internet]. 2019;11(2):111–3. Available from:

https://pubmed.ncbi.nlm.nih.gov/30638052/

95. Valadi H, Ekstrom K, Bossios A, Sjostrand M, Lee JJ, Lotvall JO. Exosome-mediated transfer of mRNAs and microRNAs is a novel mechanism of genetic exchange between cells. Nat Cell Biol [Internet]. 2007 Jun;9(6):654–9. Available from: http://dx.doi.org/10.1038/ncb1596

96. Wahlgren J, Karlson TDL, Brisslert M, Vaziri Sani F, Telemo E, Sunnerhagen P, et al. Plasma exosomes can deliver exogenous short interfering RNA to monocytes and lymphocytes. Nucleic Acids Res [Internet]. 2012;40(17). Available from: https://pubmed.ncbi.nlm.nih.gov/22618874/

97. Bang C, Batkai S, Dangwal S, Gupta SK, Foinquinos A, Holzmann A, et al. Cardiac fibroblast-derived microRNA passenger strand-enriched exosomes mediate cardiomyocyte hypertrophy. J Clin Invest [Internet]. 2014;124(5):2136–46. Available from: https://pubmed.ncbi.nlm.nih.gov/24743145/

98. Thomou T, Mori MA, Dreyfuss JM, Konishi M, Sakaguchi M, Wolfrum C, et al. Adipose-derived circulating miRNAs regulate gene expression in other tissues. Nature [Internet]. 2017;542(7642):450–5. Available from: http://dx.doi.org/10.1038/nature21365

99. Lawrie CH, Gal S, Dunlop HM, Pushkaran B, Liggins AP, Pulford K, et al. Detection of elevated levels of tumour-associated microRNAs in serum of patients with diffuse large B-cell lymphoma. Br J Haematol [Internet]. 2008;141(March):672–5. Available from: https://pubmed.ncbi.nlm.nih.gov/18318758/

100. Mitchell PS, Parkin RK, Kroh EM, Fritz BR, Wyman SK, Pogosova-Agadjanyan EL, et al. Circulating microRNAs as stable blood-based markers for cancer detection. Proc Natl Acad Sci U S A [Internet]. 2008;105(30):10513–8. Available from: https://pubmed.ncbi.nlm.nih.gov/18663219/

101. Ramírez-Salazar EG, Carrillo-Patiño S, Hidalgo-Bravo A, Rivera-Paredez B, Quiterio M, Ramírez-Palacios P, et al. Serum miRNAs miR-140-3p and miR-23b-3p as potential biomarkers for osteoporosis and osteoporotic fracture in postmenopausal Mexican-Mestizo women. Gene [Internet]. 2018;679(4809):19–27. Available from: https://doi.org/10.1016/j.gene.2018.08.074

102. Gu WJ, Zhang C, Zhong Y, Luo J, Zhang CY, Zhang C, et al. Altered serum microRNA expression profile in subjects with heroin and methamphetamine use disorder. Biomed Pharmacother [Internet]. 2020;125(August 2019):109918. Available from: https://doi.org/10.1016/j.biopha.2020.109918

103. Divi SN, Markova DZ, Fang T, Guzek R, Kurd MF, Rihn JA, et al. Circulating miR-155-5p as a Novel Biomarker of Lumbar Degenerative Disc Disease. Spine (Phila Pa 1976) [Internet]. 2019;1. Available from: https://pubmed.ncbi.nlm.nih.gov/31770330/

104. Cheng P, Wang J. The potential of circulating microRNA-125a and microRNA-125b as markers for inflammation and clinical response to infliximab in rheumatoid arthritis patients. J Clin Lab Anal [Internet]. 2020;34(8):1–8. Available from: https://pubmed.ncbi.nlm.nih.gov/32281166/

105. Fujii R, Yamada H, Munetsuna E, Yamazaki M, Ohashi K, Ishikawa H, et al. Associations of circulating microRNAs (miR-17, miR-21, and miR-150) and chronic kidney disease in a Japanese population. J Epidemiol [Internet]. 2020;30(4):177–82. Available from: https://pubmed.ncbi.nlm.nih.gov/30905898/

106. Martins-Ferreira R, Chaves J, Carvalho C, Bettencourt A, Chorão R, Freitas J, et al. Circulating microRNAs as potential biomarkers for genetic generalized epilepsies: a three microRNA panel. Eur J Neurol [Internet]. 2020;27(4):660–6. Available from: https://pubmed.ncbi.nlm.nih.gov/31746515/

107. Finkel RS, Mercuri E, Darras BT, Connolly AM, Kuntz NL, Kirschner J, et al. Nusinersen versus Sham Control in Infantile-Onset Spinal Muscular Atrophy. N Engl J Med [Internet]. 2017;377(18):1723–32. Available from: https://pubmed.ncbi.nlm.nih.gov/29091570/

108. Lacerra G, Sierakowska H, Carestia C, Fucharoen S, Summerton J, Weller D, et al. Restoration of hemoglobin A synthesis in erythroid cells from peripheral blood of thalassemic patients. Proc Natl Acad Sci U S A [Internet]. 2000;97(17):9591–6. Available from: https://pubmed.ncbi.nlm.nih.gov/10944225/

109. Friedman KJ, Kole J, Cohn JA, Knowles MR, Silverman LM, Kole R. Correction of aberrant splicing of the cystic fibrosis transmembrane conductance regulator (CFTR) gene by antisense oligonucleotides. J Biol Chem [Internet]. 1999;274(51):36193–9. Available from: https://pubmed.ncbi.nlm.nih.gov/10593905/

110. Wilton SD, Lloyd F, Carville K, Fletcher S, Honeyman K, Agrawal S, et al. Specific removal of the nonsense mutation from the mdx dystrophin mRNA using antisense oligonucleotides. Neuromuscul Disord [Internet]. 1999;9(5):330–8. Available from: https://pubmed.ncbi.nlm.nih.gov/10407856/

111. Grassmann F, Schoenberger PGA, Brandl C, Schick T, Hasler D, Meister G, et al. A Circulating MicroRNA Profile Is Associated with Late-Stage Neovascular Age-Related Macular Degeneration. PLoS One [Internet]. 2014 Jan;9(9):e107461. Available from: http://www.ncbi.nlm.nih.gov/pubmed/25203061

112. Hurteau GJ, Spivack SD, Brock GJ. Potential mRNA degradation targets of hsa-miR-200c, identified using informatics and qRT-PCR. Cell Cycle [Internet]. 2006;5(February 2015):1951–6. Available from: http://www.ncbi.nlm.nih.gov/pubmed/16929162

113. Szemraj M, Oszajca K, Szemraj J, Jurowski P. MicroRNA expression analysis in serum of patients with congenital hemochromatosis and age-related macular degeneration (AMD). Med Sci Monit [Internet]. 2017;23:4050–60. Available from: https://pubmed.ncbi.nlm.nih.gov/28827515/

114. Romano GL, Platania CBM, Drago F, Salomone S, Ragusa M, Barbagallo C, et al. Retinal and circulating miRNAs in age-related macular degeneration: An in vivo animal and human study. Front Pharmacol [Internet]. 2017;8(MAR):1–10. Available from: https://pubmed.ncbi.nlm.nih.gov/28424619/

115. Szemraj M, Bielecka-Kowalska A, Oszajca K, Krajewska M, Goś R, Jurowski P, et al. Serum MicroRNAs as Potential Biomarkers of AMD. Med Sci Monit [Internet]. 2015;21:2734–42. Available from: https://pubmed.ncbi.nlm.nih.gov/26366973/

116. Ulańczyk Z, Sobuś A, Łuczkowska K, Grabowicz A, Mozolewska-Piotrowska K, Safranow K, et al. Associations of microRNAs, angiogenesis-regulating factors and CFH Y402H polymorphism—an attempt to search for systemic biomarkers in age-related macular degeneration. Int J Mol Sci [Internet]. 2019;20(22). Available from: https://pubmed.ncbi.nlm.nih.gov/31731799/

117. Ertekin S, Yildirim Ö, Dinç E, Ayaz L, Balci Fidanci Ş, Tamer L. Evaluation of circulating miRNAs in wet age-related macular degeneration. Mol Vis [Internet].

2014;20(July):1057–66. Available from: https://pubmed.ncbi.nlm.nih.gov/25221421/

118. Ménard C, Rezende FA, Miloudi K, Wilson A, Tétreault N, Hardy P, et al. MicroRNA signatures in vitreous humour and plasma of patients with exudative AMD. Oncotarget [Internet]. 2016;7(15):19171–84. Available from: https://pubmed.ncbi.nlm.nih.gov/27015561/

119. Ren C, Liu Q, Wei Q, Cai W, He M, Du Y, et al. Circulating miRNAs as potential biomarkers of age-related macular degeneration. Cell Physiol Biochem [Internet]. 2017;41(4):1413–23. Available from: https://pubmed.ncbi.nlm.nih.gov/28315863/

120. Elbay A, Ercan Ç, Akbaş F, Bulut H, Ozdemir H. Three new circulating microRNAs may be associated with wet age-related macular degeneration. Scand J Clin Lab Invest [Internet]. 2019;79(6):388–94. Available from: https://pubmed.ncbi.nlm.nih.gov/31277558/

121. Blasiak J, Watala C, Tuuminen R, Kivinen N, Koskela A, Uusitalo-Järvinen H, et al. Expression of VEGFA-regulating miRNAs and mortality in wet AMD. J Cell Mol Med [Internet]. 2019;23(12):8464–71. Available from: https://pubmed.ncbi.nlm.nih.gov/31633290/

122. Elshelmani H, Wride MA, Saad T, Rani S, Kelly DJ, Keegan D. Identification of novel serum microRNAs in age-related macular degeneration. Transl Vis Sci Technol [Internet]. 2020;9(4):1–13. Available from: https://pubmed.ncbi.nlm.nih.gov/32818115/

123. Friedländer MR, Chen W, Adamidi C, Maaskola J, Einspanier R, Knespel S, et al. Discovering microRNAs from deep sequencing data using miRDeep. Nat Biotechnol [Internet]. 2008;26(4):407–15. Available from: http://www.ncbi.nlm.nih.gov/pubmed/18392026

124. R Development Core Team. R: A Language and Environment for Statistical Computing [Internet]. Vienna, Austria; 2010. Available from: https://www.r-project.org/

125. Langmead B, Salzberg SL. Fast gapped-read alignment with Bowtie 2. Nat Methods [Internet]. 2012;9(4):357–9. Available from: https://pubmed.ncbi.nlm.nih.gov/22388286/

126. Robinson MD, Oshlack A. A scaling normalization method for differential expression analysis of RNA-seq data. Genome Biol [Internet]. 2010;11(3):R25. Available from: https://pubmed.ncbi.nlm.nih.gov/20196867/

127. Johnson WE, Li C, Rabinovic A. Adjusting batch effects in microarray expression data using empirical Bayes methods. Biostatistics [Internet]. 2007;8(1):118–27. Available from: https://pubmed.ncbi.nlm.nih.gov/16632515/

128. Pinheiro J, Bates D, DebRoy S, Sarkar D, EISPACK, Heisterkamp S, et al. Linear and Nonlinear Mixed Effects Models Description. Vol. version 3., R package. 2017. p. 1–336.

129. Ploner AM, Dunkler D, Southworth H, Heinze G. The logistf Package Title Firth's bias reduced logistic regression [Internet]. 2006. Available from: http://www.meduniwien.ac.at/msi/biometrie/programme/fl/index.html

130. Untergasser A, Nijveen H, Rao X, Bisseling T, Geurts R, Leunissen JAM. Primer3Plus, an enhanced web interface to Primer3. Nucleic Acids Res [Internet]. 2007;35(SUPPL.2):71–4. Available from: https://pubmed.ncbi.nlm.nih.gov/17485472/

131. Silva J, García V, Zaballos Á, Provencio M, Lombardía L, Almonacid L, et al. Vesicle-related microRNAs in plasma of nonsmall cell lung cancer patients and correlation with survival. Eur Respir J. 2011;37(3):617–23.

132. Atella V, Piano Mortari A, Kopinska J, Belotti F, Lapi F, Cricelli C, et al. Trends in age-related disease burden and healthcare utilization. Aging Cell [Internet]. 2019;18(1):1–8. Available from: https://pubmed.ncbi.nlm.nih.gov/30488641/

133. Fong JH. Disability incidence and functional decline among older adults with major chronic diseases. BMC Geriatr [Internet]. 2019;19(1):323. Available from: https://pubmed.ncbi.nlm.nih.gov/31752701/

134. Leung AKL, Sharp PA. MicroRNA Functions in Stress Responses. Mol Cell [Internet]. 2010;40(2):205–15. Available from: http://dx.doi.org/10.1016/j.molcel.2010.09.027

135. Patz A, Eastham A, Higginbotham DH, Kleh T. Oxygen studies in retrolental fibroplasia. II. The production of the microscopic changes of retrolental fibroplasia in experimental animals. Am J Ophthalmol [Internet]. 1953;36(11):1511–22. Available from: http://www.sciencedirect.com/science/article/pii/0002939453917796

136. Kim CB, D'Amore PA, Connor KM. Revisiting the mouse model of oxygen-induced retinopathy. Eye Brain [Internet]. 2016;8:67–79. Available from: https://pubmed.ncbi.nlm.nih.gov/27499653/

137. Berger J, Bhandari V. Animal models of bronchopulmonary dysplasia. Am J Physiol Cell Mol Physiol [Internet]. 2014 Oct 10;307(12):L936–47. Available from: https://doi.org/10.1152/ajplung.00159.2014

138. Ratner V, Slinko S, Utkina-Sosunova I, Starkov A, Polin RA, Ten VS. Hypoxic Stress Exacerbates Hyperoxia-Induced Lung Injury in a Neonatal Mouse Model of Bronchopulmonary Dysplasia. Neonatology [Internet]. 2009;95(4):299–305. Available from: https://www.karger.com/DOI/10.1159/000178798

139. Freeman BA, Topolosky MK, Crapo JD. Hyperoxia increases oxygen radical production in rat lung homogenates. Arch Biochem Biophys [Internet]. 1982;216(2):477–84. Available from: https://pubmed.ncbi.nlm.nih.gov/6287935/

140. Li Z, Choo-Wing R, Sun H, Sureshbabu A, Sakurai R, Rehan VK, et al. A potential role of the JNK pathway in hyperoxia-induced cell death, myofibroblast transdifferentiation and TGF-β1-mediated injury in the developing murine lung. BMC Cell Biol [Internet]. 2011;12(1):54. Available from: https://doi.org/10.1186/1471-2121-12-54

141. Stahl A, Chen J, Sapieha P, Seaward MR, Krah NM, Dennison RJ, et al. Postnatal Weight Gain Modifies Severity and Functional Outcome of Oxygen-Induced Proliferative Retinopathy. Am J Pathol [Internet]. 2010;177(6):2715–23. Available from: http://www.sciencedirect.com/science/article/pii/S0002944010629008

142. Anand S, Cheresh DA. Emerging Role of Micro-RNAs in the Regulation of Angiogenesis. Genes and Cancer [Internet]. 2011;2(12):1134–8. Available from: https://pubmed.ncbi.nlm.nih.gov/22866204/

143. Zhang L, Zhou M, Qin G, Weintraub NL, Tang Y. MiR-92a regulates viability and angiogenesis of endothelial cells under oxidative stress. Biochem Biophys Res Commun [Internet]. 2014;446(4):952–8. Available from: https://pubmed.ncbi.nlm.nih.gov/24650666/

144. Doebele C, Bonauer A, Fischer A, Scholz A, Reiss Y, Urbich C, et al. Members of the

microRNA-17-92 cluster exhibit a cell-intrinsic antiangiogenic function in endothelial cells. Blood [Internet]. 2010;115(23):4944–50. Available from: https://pubmed.ncbi.nlm.nih.gov/20299512/

145. Bonauer A, Carmona G, Iwasaki M, Mione M, Koyanagi M, Fischer A, et al. MicroRNA-92a controls angiogenesis and functional recovery of ischemic tissues in Mice. Science (80-) [Internet]. 2009 Jun;324(5935):1710–3. Available from: https://pubmed.ncbi.nlm.nih.gov/19460962/

146. Gallant-Behm CL, Piper J, Dickinson BA, Dalby CM, Pestano LA, Jackson AL. A synthetic microRNA-92a inhibitor (MRG-110) accelerates angiogenesis and wound healing in diabetic and nondiabetic wounds. Wound Repair Regen [Internet]. 2018;26(4):311–23. Available from: https://pubmed.ncbi.nlm.nih.gov/30118158/

147. Murata K, Ito H, Yoshitomi H, Yamamoto K, Fukuda A, Yoshikawa J, et al. Inhibition of miR-92a enhances fracture healing via promoting angiogenesis in a model of stabilized fracture in young mice. J Bone Miner Res [Internet]. 2014;29(2):316–26. Available from: https://pubmed.ncbi.nlm.nih.gov/23857760/

148. Zhang Q, Yu N, Yu BT. MicroRNA-298 regulates apoptosis of cardiomyocytes after myocardial infarction. Eur Rev Med Pharmacol Sci [Internet]. 2018;22(2):532–9. Available from: https://pubmed.ncbi.nlm.nih.gov/29424914/

149. Sun H, Zhong D, Wang C, Sun Y, Zhao J, Li G. MiR-298 Exacerbates Ischemia/Reperfusion Injury Following Ischemic Stroke by Targeting Act1. Cell Physiol Biochem [Internet]. 2018;48(2):528–39. Available from: https://www.karger.com/DOI/10.1159/000491810

150. Hawke K, van Driel ML, Buffington BJ, McGuire TM, King D. Homeopathic medicinal products for preventing and treating acute respiratory tract infections in children. Cochrane Database Syst Rev [Internet]. 2018 [cited 2021 Apr 12]; Available from: www.cochranelibrary.com

151. Peckham EJ, Cooper K, Roberts ER, Agrawal A, Brabyn S, Tew G. Homeopathy for treatment of irritable bowel syndrome. Cochrane Database Syst Rev [Internet]. 2019;2019(9). Available from: www.cochranelibrary.com

152. Coulter MK, Dean ME. Homeopathy for attention deficit/hyperactivity disorder or hyperkinetic disorder. Cochrane Database of Systematic Reviews. 2007.

153. Cucherat M, Haugh MC, Gooch M, Boissel JP. Evidence of clinical efficacy of homeopathy. A meta-analysis of clinical trials. Vol. 56, European Journal of Clinical Pharmacology. 2000.

154. Linde K, Clausius N, Ramirez G, Melchart D, Eitel F, Hedges L V., et al. Are the clinical effects of homoeopathy placebo effects? A meta-analysis of placebo-controlled trials. Lancet. 1997 Sep 20;350(9081):834–43.

155. DeStefano F, Shimabukuro TT. The MMR Vaccine and Autism. Annu Rev Virol [Internet]. 2019;6:585–600. Available from: https://pubmed.ncbi.nlm.nih.gov/30986133/

156. Espinosa-Heidmann DG, Suner IJ, Catanuto P, Hernandez EP, Marin-Castano ME, Cousins SW. Cigarette Smoke–Related Oxidants and the Development of Sub-RPE Deposits in an Experimental Animal Model of Dry AMD. Invest Ophthalmol Vis Sci [Internet]. 2006;47(2):729–37. Available from: https://doi.org/10.1167/iovs.05-0719

157. Cousins SW, Espinosa-Heidmann DG, Alexandridou A, Sall J, Dubovy S, Csaky K. The Role of Aging, High Fat Diet and Blue Light Exposure in an Experimental Mouse Model for Basal Laminar Deposit Formation. Exp Eye Res [Internet]. 2002;75(5):543–53. Available from: http://www.sciencedirect.com/science/article/pii/S0014483502920476

158. Espinosa-Heidmann DG, Suner I, Hernandez EP, Frazier WD, Csaky KG, Cousins SW. Age as an independent risk factor for severity of experimental choroidal neovascularization. Investig Ophthalmol Vis Sci [Internet]. 2002;43(5):1567–73. Available from: https://pubmed.ncbi.nlm.nih.gov/11980875/

159. Suñer IJ, Espinosa-Heidmann DG, Marin-Castano ME, Hernandez EP, Pereira-Simon S, Cousins SW. Nicotine Increases Size and Severity of Experimental Choroidal Neovascularization. Invest Ophthalmol Vis Sci [Internet]. 2004;45(1):311–7. Available from: https://doi.org/10.1167/iovs.03-0733

160. Espinosa-Heidmann DG, Malek G, Mettu PS, Caicedo A, Saloupis P, Gach S, et al. Bone Marrow Transplantation Transfers Age-Related Susceptibility to Neovascular Remodeling in Murine Laser-Induced Choroidal Neovascularization. Invest Ophthalmol Vis Sci [Internet]. 2013;54(12):7439–49. Available from: https://doi.org/10.1167/iovs.13-12546

10. List of Abbreviations

Abbreviation	Meaning
AMD	Age-related Macular Degeneration
ARMS2	Age-related Maculopathy Susceptibility 2
ASO	Antisense Oligonucleotides
bp	Base Pairs
BPD	Bronchopulmonary Dysplasia
C. elegans	*Caenorhabditis elegans*
CNV	Choroidal Neovascularization
cmiRNA	Circulating MicroRNA
cDNA	Complementary Deoxyribonucleic Acid
DNA	Deoxyribonucleic Acid
E. coli	Escherichia Coli
Et al.	Et aliter (and others)
gaAMD	Geographic Atrophy AMD
GSTM1	Glutathione S-Transferase Isoform mu1
GSTM5	Glutathione S-Transferase Isoform mu5
HDL	High Density Lipoprotein
MIP-1α	Macrophage Inflammatory Protein-1α
µl	Microliter
miRNA	MicroRNA
ml	Milliliter
MCP-1	Monocyte Chemotactic Protein-1
nAMD	Neovascular AMD
NGS	Next Generation Sequencing
dNTP	Nucleosidtriphosphate
OIR	Oxygen-Induced Retinopathy
P	Postnatal
PBMC	Peripheral Blood Mononuclear Cell
PBNC	Peripheral Blood Nuclear Cell
qRT-PCR	Quantitative Reverse Transcription Polymerase Chain Reaction
RPE	Retinal Pigment Epithelium
ROP	Retinopathy of Prematurity
RISC	RNA-induced Silencing Complex
RPM	Rotations Per Minute
SD	Standard Deviation
siRNA	Short Interfering RNA
TMM	Trimmed Mean of M-values
VEGF	Vascular Endothelial Growth Factor
U-Test	Wilcoxon-Mann-Whitney-Test

11. List of Figures

12. List of Tables

13. Eidesstattliche Erklärung

Ich erkläre hiermit, dass ich die vorliegende Arbeit ohne unzulässige Hilfe Dritter und ohne Benutzung anderer als der angegebenen Hilfsmittel angefertigt habe. Die aus anderen Quellen direkt oder indirekt übernommenen Daten und Konzepte sind unter Angabe der Quelle gekennzeichnet. Insbesondere habe ich nicht die entgeltliche Hilfe von Vermittlungs- bzw. Beratungsdiensten (Promotionsberater oder andere Personen) in Anspruch genommen. Niemand hat von mir unmittelbar oder mittelbar geldwerte Leistungen für Arbeit erhalten, die im Zusammenhang mit dem Inhalt der vorgelegten Dissertation stehen. Die Arbeit wurde bisher weder im In- noch im Ausland in gleicher oder ähnlicher Form einer anderen Prüfungsbehörde vorgelegt.

Regensburg, den 7.7.21

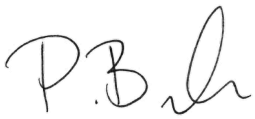

Patricia Berber

14. Acknowledgements

I would like to express my sincere gratitude to my supervisor, Prof. Dr. Weber, for giving me the opportunity to do research, and providing invaluable guidance throughout the completion of this project. Thank you for sharing your knowledge and drive, and for giving me the time I needed to produce a dissertation I am proud of.

Furthermore, I would like to express my appreciation and gratitude for the guidance and support I received from Dr. Felix Grassmann. Your enthusiasm and our stimulating discussions helped shape this experience. Thank you for your confidence in me.

I would also like to thank Christina Kiel, without whom this work would not have been possible (and a lot less fun).

I wish to thank Dr. Marcus Karlstetter, Dr. Alexander Aslanidis and Albert Caramoy who performed the laser treatment under the supervision of Prof. Dr. Langmann, and PD Dr. Andreas Ohlmann who performed the OIR treatment. This project would not have been possible without your help - thank you!

Finally, I need to say thank you to my best friend, my partner, and my husband Andreas. Life taught me that ambitious girls are less desirable. Thank you for showing me the opposite.